MODELLING OF AN ORGANIC RANKINE CYCLE SOLAR-THERMAL POWER PLANT

OLUMUYIWA YINUS ODUFUWA

Dissertation submitted in fulfilment of the requirements for the degree

MAGISTER TECHNOLOGIAE:

ENGINEERING: MECHANICAL

in the

Department of Mechanical and Mechatronics Engineering
Faculty of Engineering and Information Technology

at the

Central University of Technology, Free State

Supervisor: Mr T. Ngonda, PrEng, MEng
Co-supervisor: Dr J.A. Strauss, PhD
Co-supervisor: Prof. M.A.E Kaunda, PrEng, PhD

BLOEMFONTEIN
October 2016

DECLARATION WITH REGARDS TO INDEPENDENT WORK

I, OLUMUYIWA YINUS ODUFUWA, student number [redacted], do hereby declare that this research project submitted to the Central University of Technology, Free State, for the degree MAGISTER TECHNOLOGIAE: ENGINEERING: MECHANICAL, is my independent work; and complies with the Code of Academic Integrity, as well as other relevant policies, procedures, rules and regulations of the Central University of Technology, Free State; and has not been submitted before to any institution by myself or any other person in fulfilment of the requirements for the attainment of any qualification.

_____ _____

SIGNATURE OF STUDENT **DATE**

ACKNOWLEDGEMENTS

I give thanks to God Almighty for guidance towards completion of the study.

I also thank my family and friends for their support and endurance during the study.

I also acknowledge the efforts of my supervisors, Dr K. kusakana and Dr B. P. Numbi and my mentor Prof. F. Emuze for guidance and motivation provided during the study. I am grateful to colleagues and other individuals for their contribution and support during the study.

Lastly, I thank the Central University of Technology, Free State for the opportunity given to conduct this research wok.

ABSTRACT

The purpose of this research is to present a comprehensive numerical model for the conversion of solar energy from sunlight to target mechanical energy of the Organic Rankine Cycle. The terminal processes include intermediate conversion of solar energy to thermal energy in the collector, and from thermal to mechanical work at the turbine. The model also incorporates thermal energy storage.

Organic Rankine cycles have unique properties that are well suited for solar power generation. The thermodynamic potential of a varying Organic Rankine Cycle's working fluids and configurations is analysed. Also, a specific thermodynamic model for STORC power plants is developed in Matlab Simulink ® software and presented. The methodology was implemented based on an existing plant design, which demonstrates opportunities for further optimisation and usability of current design practice.

The model has the following elements: the first element is the solar resources model which sources the insolation energy and meteorological input at an instance of time for a specific location to the system. The second element is the solar collector model that accepts output from the solar resources model and presents the output of exit temperature of the collector fluid, the collector efficiency and the useful heat energy gained. The third element is the fluid transfer and storage model that shows the retention and regulation of system heat and temperature from the inlet to the outlet. The last item is the Organic Rankine Cycle model that presents the performance for the expected output power required with a varying fluid and configuration property diagram.

Based on the study outcome, the integrated model was created to analyse the variations in geographic, geometrical properties with thermo-physical properties for a specific period of the possible power output from the plant. Case studies on the sensitivity and performance analysis show that the plant will provide more power and higher efficiencies with a larger aperture width of the collector than to the length of the collector. Furthermore, power outputs are higher for elevated and high Direct Normal Irradiance (DNI) locations than those locations with lower elevation and DNI. The report also discusses other results from the analysis of the effect on the model performance.

Keywords: Energy, Organic Rankine Cycle, Solar Collectors, Heat transfer, sensitivity and performance analysis

TABLE OF CONTENTS

LIST OF FIGURES

LIST OF TABLES

NOMENCLATURE

ε	Surface emittance (with subscript r and c is applicable to receiver and glass cover respectively)
ϵ	Emissivity
A	Area, m^2
A_{abs}	Absorptivity
A_{total}	Total fluid-solid heat transfers surface area in a packed-bed storage tank
Abs	Absorber
A_c	Cross-sectional area, m^2
Amb	Ambient
A_s/A_c	Surface area exposed to heat transfer,m^2
A_{sf}	Solar field area,m^2
Bi	Biot Number
C	Specific heat, *kJ/kg-K*
Cd	Condenser
Col	Collector
CR	Solar collector concentration ratio
D	Diameter, m
D_{co}	Glass cover outside diameter
D_{ro}	Receiver outside diameter (if subscript is “ri”, consider the inside diameter)
ED	Energy density, kW/m^3
Ev	Evaporator
Ex	Exhaust
Exp	Expander
F	Ratio of resistance to fluid-solid heat transfer and environmental losses
F'	Heat removal factor
F''	Collector flow factor
F_R	Solar collector performance factor
h_k	Heat transfer coefficient, W/m^2-K
h	Specific enthalpy(if it is uppercase it applies to enthalpy without kg in the unit, *J/kg*
h_{tf}	Heat transfer fluid
h_v	Volumetric heat transfer coefficient, W/m^3-K

h_w	Wind loss coefficient
Hx	Heat exchanger
k	Thermal conductivity (with subscript r,c and eff is for receiver, glass cover and effective respectively), *W/m-K*
L	Length (collector length), *m*
Liq	Liquid
$\dot{m}$	Mass flow rate (with subscript WF applies to the working fluid),*kg/s*
m	Mass, *kg*
M	Heat capacity per loss
n	Number of nodes
n_i	Molar fraction
η	Efficiency (with subsript “col” means collector efficiency)
N_{rot}/N	Rotating speed, *rpm*
NTU	*NTU fluid*, storage system heat transfer parameter
NTU_{fluid}	Storage fluid heat transfer parameter
NTU_{solid}	Storage solid heat transfer parameter
NTU_{sum}	Total fluid-solid nodal heat transfer parameter
Nu	Nusselt number
Opt	Optical
P	Pressure, *Pa*
P	Density, kg/m^3 (if Δ “delta” at the front, it implies difference)
ρ_r	Reflectivity
σ	Stefan Boltzman’s constant
Pinch	Pinch point value, *K*
Pp	Pump
Pr	Prandtl number
$\dot{Q}_r$	Energy transfer rate, *kW*
$\dot{Q}_r$	Heat power, *W*
Q	Linear heat flux, *W/m*
Q_{loss}	Heat loss (with repect to the medium if numbered)
Q_u	Useful energy gain, *kW*

R	Fluid-solid storage system capacitance ratio
R/r	Ratio
$R_{axial\ conduction}$	Resistance to axial conduction, *K/W*
Re	Reynolds' number
Rec	Recuperator
RPM	Rotational speed (Revolution Per Minute)
$R_{losses/R}$	Resistance to environmental losses, *K/W*
R_g	McMaster regression (subscrip 1 implies 1st fan and 2 for 2nd fan)
S	Absorbed solar radiation, W/m^2
T	Temperature, *K*
T_a	Ambient temperature
t	Temperature, *C*
t_c	Thickness
T_{ci}	Glass cover inside temperature; K
T_{co}	Glass cover outside temperature; K
T/t	Time, *s*
T_{drop}	Temperature drop
T_f	Fluid temperature
T_h	High-temperature thermal resource
T_l	Low-temperature thermal resource
T_{sky}	Sky temperature
$\overline{T}$	Normalised temperature
Tot	Total
U	Heat transfer coefficient, $W/(m^2K)$
UA	Total power cycle heat exchanger conductance, *W/K*
U_L	Loss coefficient, W/m^2-*K*
μ	Dynamic viscosity
v	Velocity (or specific volume by context)
V	Volume, m^3
$\dot{V}$	Volume flow rate, m^3/s
V''	Volume flux, m^3/m^2-*s*
Vs	Swept volume, m^3
W	Work, *J*

W_dot	Power output, *W*
w	Specific work, *J/kg*
W	Width, *m*
X_w	Aperture width, *m*

LIST OF ACRONYMS

BFN	Bloemfontein
CPC	Compound Parabolic Collector
CSP	Concentrating Solar Power
CTC	Cylindrical Trough Collector
DNI	Direct Normal Irradiance
EES	Engineering Equation Solver
ETC	Evacuated Tube Collector
FPC	Flat-Plate collector
GRT	Graaf - Reinet
HCE	Heat Collecting Element
HFC	Heliostat Field Collector
HTF	Heat Transfer Fluid
HVAC	Heat Ventilation and Air Conditioning
LFR	Linear Fresnel Reflector
µCSP	micro Concentrating Solar Power
ORC	Organic Rankine Cycle
PDR	Parabolic Dish Reflector
PCM	Phase Change Material
PSA	Plataforma Solar de Almeria
PTC	Parabolic Trough Collector
RPM	Revolution Per Minute (rotational speed)
SAURAN	South African Universities Radiometric Network
SAWS	South African Weather Service
SCAs	Solar Collector Assemblies
SEGS	Solar Electric Generating System
STG	Solar Turbine Group
STORC	Solar-Thermal Organic Rankine Cycle

STORES	Solar Trough Organic Rankine Electricity System
VAN	Vanrhynsdorp
WF	Working Fluid

CHAPTER 1

INTRODUCTION

1.1 BACKGROUND

There is a high demand for alternative modes of energy provision to reduce the potential for negative environmental impact. Addressing the problem of sustainable energy supply is one of the major engineering challenges of the 21st century (Katayama and Tamaura, 2005). One potential approach to this challenge is the development of renewable energy technology through a dedicated research effort. The outcome of the efforts includes exploration of biomass utilisation, waste heat recovery, the wind and solar energy, among others (Mendelsohn, Lowder, and Canavan, 2012). Among these alternative sources, renewable energy sources provide economical, safe and renewable energy technologies and create opportunities for sustainability of power generation (Resch et al., 2014).

Moreover, renewable technologies have only recently achieved mass adoption. Similar to conventional energy technologies, there is a need to check and prove the reliability of the application. One way of hastening the adoption of these technologies is to limit the amount of field testing and field optimisation by using numerical models to optimise the technologies. Modelling of the specific renewable energy technology, such as the Organic Rankine Cycle (ORC), reduces the cost of testing and optimisation by providing tools for the evaluation and optimisation of existing and proposed ORC plants (Orosz et al., 2013).

Thermal power generation is a proven technology with several hundreds of plants in operation. Current large-scale systems rely on traditional steam-based Rankine cycles for power production. Most of these plants develop megawatts of electricity. On the other hand, ORC power plants are more compact and less costly than traditional steam cycle power plants and can better exploit lower temperature thermal resources. ORC plants develop kilowatts of electricity. ORC usage permits solar-

thermal power generation to become more flexible in construction and is a resourceful means of replacing traditional fuels (Daggubati, 2014).

While ORC has great potential, it has received limited attention from the solar energy research community. Although solar-thermal power generation has the potential to play a major role in future energy markets, the ability to capture and store the energy creates a fundamental limitation. The capacity to store large amounts of high-temperature thermal energy enables the delivery of solar-thermal power independent of variation in insolation (insolation is the amount of solar radiation per given area). Storage can be used to make output mimic grid demand, compensate for variation in radiation levels throughout the day, or provide 24-hour on-demand solar-thermal power (Karaki et al., 2011). McMahan (2006:26) notes that, if the flexibility provided by thermal energy storage is achieved efficiently and at a low cost, it has the potential to increase the economic viability and overall market share of solar power generation.

1.2 AIM AND OBJECTIVES

The aim of this research is to build a comprehensive numerical model for the conversion of energy from sunlight into heat in the solar collectors; to transfer heat in the storage system to the ORC via heat exchangers; and to acquire full operation of the ORC cycle - including heat rejection - via air condensers. Model predictions will be validated using experimental data collected from an available operational research prototype of solar-thermal ORC plant, one of this which is in Lesotho, built by STG International (Stginternational.org, 2015). The model will possibly be made available as a stand-alone executable programme through a suitable web-based host after future development.

The primary objective of this research project was to provide a tool, in the form of a computer simulation and modelling capability, possibly optimising the performance of a solar-thermal ORC plant in the medium output category. The secondary objective of the research was to determine whether it would be possible to incorporate all components of an ORC solar-thermal power plant system into one numerical model

that could be used to analyse the whole system energy conversion processes from a solar resource to a power output for the generation of electricity.

1.3 APPROACH

To accomplish the aim and objective of the research, the following tasks were performed:

1. A comprehensive review and synthesis of publications relevant to the research topic was undertaken, with a focus on the principles and fundamentals of energy conversion.

2. Information on thermo-physical parameters derived from the literature review was used for the equation based quasi-steady state modelling that was implemented in Matlab Simulink ™.

3. Data was collected from an experimental solar-thermal ORC power plant model that was designed and installed in Lesotho by Matt Orosz's team from MIT and combined with published data from other similar power stations.

4. Experimental results were compared with model outputs. Discrepancies were considered as intervention points for model revision before publication.

1.4 CONTRIBUTION OF THE STUDY

Previous modelling works on solar-thermal ORC systems, particularly at the initial stage of the research project, have typically focused on one aspect or component of the system (e.g. collectors, or power cycles). This research project entailed a comprehensive modelling effort integrating all critical components of a solar ORC power plant system. This stage of modelling has gained higher interest among recent researchers.

1.5 LIMITATIONS OF THE STUDY

The study was conducted with the following limitations to minimise the complexity of the project and its duration:

The project consisted of equation-based modelling of the basic engineering and thermodynamic principles of solar-thermal ORC, while the electrical and certain special mechanical aspects of the system (e.g. stress analysis of the material components) were not considered. Specific economic modelling was also ignored due to limited information on the costs of components of an ORC plant, to avoid the presentation of invalid facts in this dissertation.

1.6 DISSERTATION LAYOUT

- Chapter 1 of the dissertation presents an introduction of the Solar- Thermal Organic Rankine Cycle (STORC). The primary and secondary objectives of the study are explained, as well as the contribution of the research to the engineering body of knowledge. The limitations of the research work are provided, as well as the research approach.
- Chapter 2 of the dissertation focuses on the compilation of the outcome of the literature review on the STORC. It also presents information on the benefits and development of the models.

- Chapter 3 presents the action taken towards implementation of the study. It explains the methods involved and procedures before the study.
- Chapter 4 describes the thermodynamic principles and numerical analysis of the components that make up each model of the Solar-Thermal ORC power plant. It entails a presentation of the numerical and thermodynamic analyses by providing mathematical equations and expressions and technical descriptions of each subsystem.
- Chapter 5 presents the Matlab Simulink ™ model description and results of the components of the STORC plants and energy source.
- Chapter 6 provides results and a comparison of the results with other models of power plants. It also focuses on the validations for the entire model.
- Chapter 7 presents the conclusion and recommendations based on the research findings.

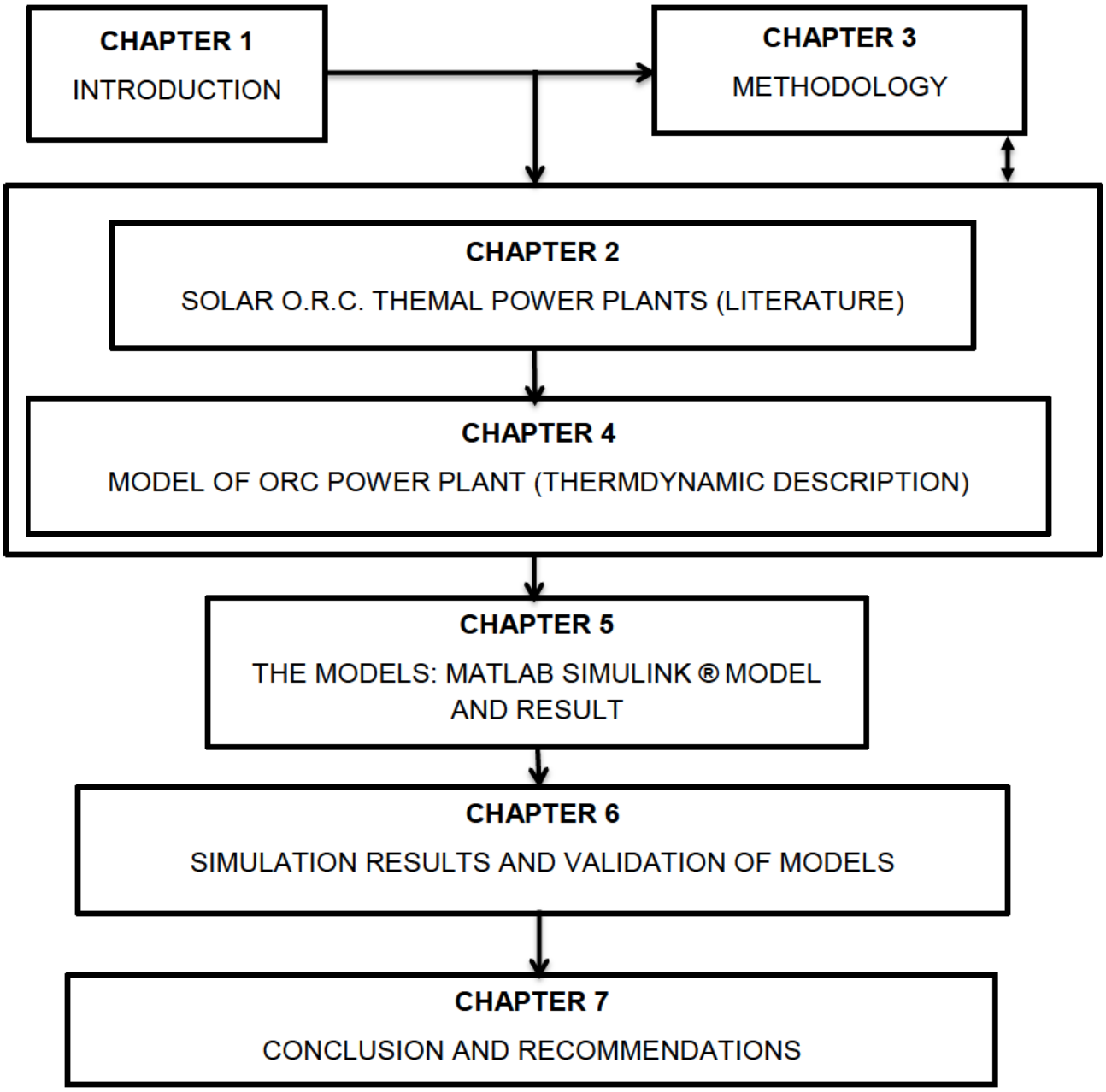

Figure 1.1 Layout of the dissertation.

CHAPTER 2

SOLAR-THERMAL O.R.C. POWER PLANTS

2.1 INTRODUCTION

Modelling requires a thorough understanding of the concepts, principles and methods needed to create reliable and realistic components of the system of interest. The chapter focuses on the outcome of the literature review on the STORC power plant technology. The chapter also presents information on the benefits of research and development of Solar-Thermal ORC power plant models and components.

2.2 TECHNICAL DESCRIPTION OF THE SOLAR-THERMAL ORC POWER PLANT

Figure 2.1 describes the operation and functions of the Solar ORC components and their function. The figure was taken from the STG International website and presents a summary of the working principle of the plant in Lesotho (Orosz, 2012).

The energy source of the STORC power plant is the sun. The solar collectors, depending on the type and applications, transform the focused solar radiation energy received through the Heat Collecting Element (HCE) to useful heat energy of the transport medium (Heat Transfer Fluid) (Kalogirou, 2009). The collector type in the schematic presentation is the parabolic trough type. It operates as a single axis and tubular absorber. The fluid transports the energy to the solar-thermal storage facility, a vertically placed cylindrical tank containing some materials with high heat capacity and Heat Transfer Fluid (HTF). The solar-thermal plant stores thermal energy and stabilises the temperature changes, to provide the ORC part of the plant with a stable thermal source (Orosz, 2012).

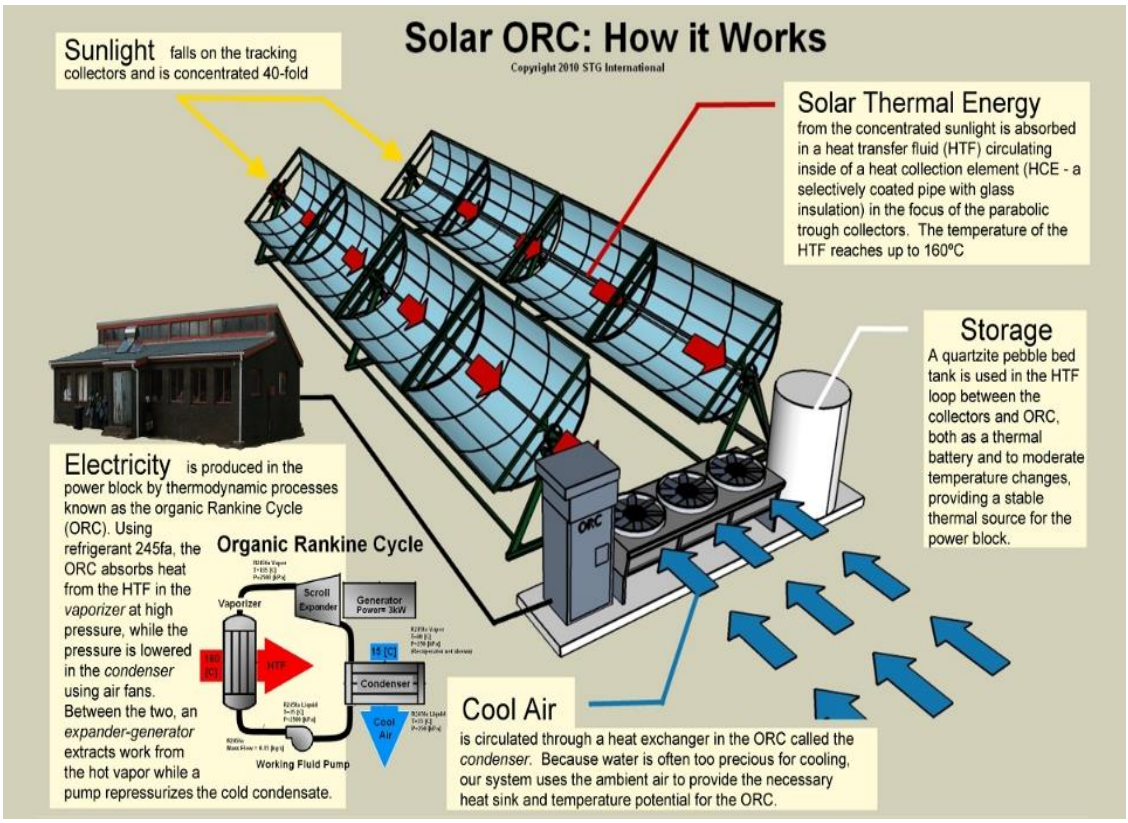

Figure 2.1 Schematic presentation of an Organic Rankine Cycle Solar-Thermal Plant (Orosz, 2012).

The ORC part of the plant with transport fluid (Working Fluid) converts the thermal energy into mechanical work through a Rankine Cycle thermodynamic system. The generator transforms the work output of the turbine into electricity (Li, 2013).

2.2.1 OVERVIEW FROM THE PLANT SITE VISIT

The following photos (see Figures 2.2 to 2.5) were taken during the visit to the small scale Solar- thermal ORC plant.

Figure 2.2 Photo of the parabolic trough collectors

Figure 2.3 Photo of the white solar-thermal storage tank.

Figure 2.4 ORC engine.

Figure 2.5 Air condenser side view with the three air fans at the top.

2.2.2 WORKING PRINCIPLE

This part of the report further describes STORC power plant technology based on general investigations on ORC plants .

Solar collectors: These are composed of four parabolic troughs, each four metres in length, connected in series to a single-axis drive mechanism along the troughs. Two pairs of the parabolic trough are joined in such a way that rotational movement is possible along an axis with the aid of a chain-sprocket mechanism powered by a motor geared system. The plant has a drive mechanism for a solar tracking system, which allows each of four pairs of the solar collector assemblies to move independently. Tracking allows controlling of the temperature of the heat-transfer fluid (HTF), as one or numbers of the Solar Collector Assemblies (SCAs) can be taken off during operation, to assist in the efficient control of the solar input. On each parabolic trough

is a set of four aluminium sheets of 1.25 x 3.05 x 0.01 metres, bent into a parabolic shape with the reflective side facing upwards, and riveted to the base of the trough on a galvanised steel sheet of the same dimensions. The adhesive foam insulation on the collector aperture between the aluminium sheets and the galvanised steel sheets provides rigidity to the structure as well as heat retention around the surface. Each of the parabolic troughs focuses incoming sunlight onto an absorber pipe Heat Collecting Element (HCE) located at the trough's focal line. The HCE are layers of steel pipes, solar-selective painting (with high absorbance of radiation in the solar energy spectrum, and low emitting in the long-wave energy-spectrum) and glass tubes (Pyrex). The assembly is linked together with Teflon at each joint to form a continuous loop through which a heat-transfer fluid (glycol compound, the anti-freeze fluid used in automotive radiators) circulates (Macedo-Valencia et al., 2014). During operation the system pumps heat HTF through this array from the sun's rays striking the pipes, reaching up to 350 ºC (depending on the type of fluid) on complete circulation. The HTF then passes through a heat exchanger where it transfers its heat to the Working Fluid (WF) of the STORC. The HTF exits the heat exchanger at a much cooler temperature, then recirculates for further heat input. The construction of the Solar Collector Assemblies (SCAs) for concentrating solar power requires core competencies such as welding, pipe coupling, and basic fabrication and capabilities (Winter, Sizmann and Vant-Hull, 2012).

ORC engine: The ORC engine utilises the heat transferred to the working fluid via the heat exchanger. A simple model of the engine has four main stages. First, as the working fluid is heated (in the vaporiser); it vaporises to form a pressurised gas. This gas is expanded through a series of "**expanders**" (turbines), converting the fluid flow energy to mechanical work. Coupled to the turbines are regenerators and generators for heat recycling and electricity generation. In this configuration, the outputs of the ORC are electricity and hot water (co-generation); additional components could provide air-conditioning as well by way of an absorption chiller design. The ORC engine is constructed using standard and modified parts, which reduces the cost of the system and increases the availability of initial materials and replacements.

Small-scale engine design requires only simplified components that are easily replaced and serviced (Kaczmarczyk, Ihnatowicz and Żywica, 2015).

Solar storage system: To meet demand peaks, a fully functional storage system was utilised to prevent the effect of the inherent change in the electrical output of the solar ORC plant. This advantage is useful to both predictable and unpredictable variations such as the influence of time and weather. The storage system is a cylindrical steel tank 2.2 metres high and with a circumference of 3.7 metres. Inside the reservoir are the inlet and the outlet for the heat-transfer fluid (HTF) with sieve containers to allow proper intake and delivery of the HTF. Alongside the tanks are two copper pipes, 10 millimetres in diameter, that are linked from the top to the bottom, and another two from the middle of the tank to the top of the reservoir. The four copper pipes extend outwards to the top of the storage tank to sense the conditions at different regions of the reservoir. The tank also has a steel bar of 50 x 8 millimetres in width and thickness joined to the body at the middle for rigidity and maintenance purposes (Johannes et al., 2005).

The following conceptual choice for the storage system meets cost-benefit requirements: Steel storage material, which has a high density (per unit mass and volume), is affordable and widely available. Heat-transfer fluid is automobile anti-freeze (a Glycol compound) with a good heat-transfer quality and the storage medium of quartzite sand (Orosz, 2012).

Single-tank stratified systems and concrete systems have obvious cost advantages over the two-tank systems. They offer both a reduction in equipment size (number of tanks), and the use of an inexpensive packing material allows for reduced HTF inventory. As a result of these advantages, direct and indirect single-tank systems utilising secondary filler material were chosen for the storage system (Mather, Hollands and Wright, 2002).

Condenser: The system utilises an air-cooled heat exchanger. The compartment dimension is from a 2.4-metre long shell and copper pipe tube of 40.8 m long. At the

top, the compartment is divided into three parts with a four-vane fan of 0.56 metres on each to circulate the air. A fin thickness of 0.2 metres is also present between the fan and the tube. The main purpose of this condenser is to recirculate heat from one medium to the other at a controllable rate (Orosz, 2012).

2.3 SOLAR-THERMAL TECHNOLOGIES

Solar technology is one of a portfolio of renewable technologies suitable for addressing the global energy generation issue. Its main advantage is the unlimited nature and abundance of the energy source, the sun. Solar ORC is a potentially reliable technology that can be used to exploit low-temperature thermal sources which might not be viably exploited by other technologies (Kane et al., 2003). The solar – thermal ORC power plant can exhibit a relatively high availability through thermal storage. The ORC power block allows some thermodynamic benefits such as lower evaporation temperature, higher viscosity, lower pressures and a smaller isentropic exponent leading to reduced dimensions of the vapour conducting equipment, and higher molar mass which reduces the circumferential speed and thus mechanical loads (Incropera and DeWitt, 1981).

Solar energy is free and widely distributed in this region. The utilisation of solar energy in the place of fossil fuels is also beneficial to reducing global warming and minimising environmental pollution caused by sulphur and nitrogen oxides (Prinn et al., 2005). These potential advantages justify research in the development of solar energy technologies that includes various aspects of technology, such as manufacturing techniques, material selection, and simulation of performance. For Solar ORC technology, the analytical part will involve multi-physics modelling of various components that make up the units of the system. Modelling helps with the accurate prediction of the outputs and efficient optimisation of the performance of the plant (Steinmann, Eck, and Laing, 2005).

2.4 STUDIES ON SOLAR THERMAL ORC TECHNOLOGIES

Studies in solar ORC technology initially started as a response to increasing the cost of energy from hydrocarbon and hydropower installations. Negative environmental impacts of the conventional power generation technologies provide another reason for researchers to seek alternative technologies for power generation (Rasul, 2013). Peterson and Davidson (1977) conducted research on solar ORC technology back in the 1970s. Their device had low-efficiency rates and also utilised refrigerants with high pollution capacities (Peterson and Davidson, 1977). Since then, further studies have been conducted with improved performance, and resulting in less pollution. Wolpert and Riffat (1996) provided designs of a more efficient ORC producing less pollution. The potential for performance enhancement of applicable models was identified, and also considered was the design of an ORC pipe and other key components of the plants. The first set of practical design evolved from the early development of macro-concentrating solar power technology (DeMeo and Galdo, 1997). McMahan's (2006) analytical studies on component optimisation and fluid selection provided evidence of better engine opportunities.

Orosz (2012) conducted research for a doctorate study on small-scale electricity, heating and cooling provision for a pilot clinic in Lesotho. The research contributed to the improvement of a Micro-Concentrating Solar power (µCSP) plant. Application of the knowledge of optimisation and economization concerning solar power analysis is essential to the construction of a Solar-Thermal ORC power plant. Modification and adoption of parts of the plant provided a means for utilising available devices from Heat Ventilation and Air Conditioning (HVAC) component types based in Southern Africa. From the research recommendations provided, opportunities exist for further research on the µCSP technology in Southern Africa. Orosz's (2012) modified and adopted the HVAC scroll compressor with reversed operation. The reversed scroll compressor design replaced the ORC expander part of the plant. He also modelled the plant implemented in Engineering Equation Solver (EES) providing an executable programme for multiple purposes. Kane et al. (2003) presented a hybrid of ORC and a diesel engine for electricity generation. The concept provides electricity and other

utilities to remote settlement. The ORC part of the plant uses the hermetic scroll expander to transmit torque to the generator. Furthermore, the technology utilises Concentrating Solar Power (CSP) with the aid of a specific sun-tracking collector. The plant could operate both during the night and during cloudy periods. The concept provided a reasonable performance device for power generation. A laboratory test of load capacities for varying thermal supply validates the performance of the plant. McMahan (2006) conducted a study on the design and optimisation of the Solar-Thermal ORC power plants. He analysed and developed the models of Organic Rankine cycles and packed-bed stratified (thermocline) thermal energy storage systems. These models provided a low-cost context for analysing the design and optimisation (both economic and engineering) of solar-thermal technologies. The study focused on the ORC engine and thermal storage models. MchMahan did not include studies on solar resources and solar collectors. The results from thermal storage aspects of McMahan's study provided some useful developmental tools for thermal storage applications. He also did an analytical study on the ORC Cycle with a focus on design considerations, configurations and fluids used in the power plant.

Forristall (2003) researched heat transfer analysis and modelling of a parabolic trough solar receiver implemented in EES. He described the development, validation and use of a heat transfer model implemented in EES. The model determines the performance of a parabolic trough solar collector's linear receiver, also called a HCE. Furthermore, he discussed the heat transfer and thermodynamic equations, optical properties, and parameters used in the model inputs and outputs. Inputs include collector and HCE geometry, optical properties, heat transfer fluid (HTF) properties, HTF inlet temperature and flow rate, solar insolation, wind speed, and ambient temperature. Outputs include collector efficiency, HTF outlet temperature, heat gain, and heat and optical losses. Modelling assumptions and limitations are also discussed, along with recommendations for model improvement, hence quite useful for the modelling of the collectors in the general National Renewable Energy Laboratory.

Quoilin (2007) did an experimental study titled “modelling of a low-temperature Rankine cycle for small scale cogeneration”. The study was carried out on an ORC recovering heat from the hot air at a temperature ranging from 150 to 200°C. The expander used for this study was a volumetric scroll expander. The working fluid selected was R123 because of its high efficiency in ORC applications. Quoilin achieved an increase in the effectiveness of the cycle and the output shaft power by improving the test bench during the testing period. He investigated the limits of the Rankine cycle by modifying some parameters of the trial bench (hot air source temperature, expander rotational speed, refrigerant charge). He discovered that the refrigerant charge has tremendous importance in the behaviour of the cycle and also reported the optimal value required to maximise the performances of the ORC. A model of each component of the cycle was presented and validated. The whole cycle was simulated, enabling him to understand the behaviour of the cycle under different working conditions. The model was then used to optimise the cycle, starting from the basic case to realistic improvement aimed at evaluating the system’s potential. He finally proposed several improvements for the test bench that could be beneficial for future studies. The above study also created a tool for further analysis of the ORC power plant.

Wolpert and Riffat (1996) conducted a study into solar-powered Rankine systems for domestic applications. They described the solar-powered Rankine system, giving emphasis to a computer model which calculates the optimum features (solar collector size and efficiency and power output) of the electricity-generation phase of the system. They based their analysis on the weather conditions for the UK and Mexico City, and computer simulations were made using metrological data for both latitudes. They were able to propose the collector area for a given annual power output under similar conditions. They also discovered that the required collector area could be reduced by increasing the efficiency of the turbine and feed pump.

Prabhu (2006) researched a Solar Trough Organic Rankine Electricity System (STORES). He focused on the initial stage of STORC power plant optimisation and economics. A summary of his study includes the following;

- Development of optimised ORC power cycle for integration with a parabolic trough solar field.
- Conceptual design and cost estimate for a 10 MW STORC system.
- Conducting a performance and economic assessment of pilot and specific STORC plants.
- Conducting a preliminary evaluation of the STORC market potential.
- Identifying the next steps towards a demonstration or early commercial STORC project.

From the above research, the STORC concept proved to be successful. Reflective research effort helped with a demonstration of the STORC power plant.

2.5 SOLAR RADIATION RESOURCE

Various solar resource validated models are available (Zhang et al., 2014) and appropriate ones are discussed in this section of the report. Time step models are useful for prediction and optimisation of power plant operation (Ciolkosz, 2009).

Duffie and Beckmann (2006) developed a quasi-steady state model on solar resources based on total radiation arriving at an inclined surface and axis tracking surfaces. Their model applies to all radiation models. A related study was done to accurately estimate solar radiation components using several mathematical equations with the appropriate theoretical method and a computer program (Al-Mohamad, 2004).

Stine and Geyer (2001) presented the Hottel clear day model which is a state transient model for collectors at any orientation, whether fixed, single-axis or double-axis tracking, and hourly insolation output on aperture for a day. The model is also applicable for the determination of solar systems' performance.

Hodge (2010) presented the solar resources model implemented in Mathcad. The model focuses on the sun path development and the solar energy database. Insolation on the flat plate and CSP collectors were established by utilising the information provided in a database.

Kuehn, Ramsey, Threlkeld and Threlkeld (1998) presented a steady-state model of the American Society of Heating, Refrigerating and Air-Conditioning Engineers' (ASHRAE) clear day model for determining the estimated insolation on flat and inclined surfaces. The model applies to building structures exposed to solar insolation. The ASHRAE model was also adjusted to determine the beam, diffuse and ground-reflected solar radiation components for Ryadh (Al-Sanea, Zedan and Al-Ajlan, 2004)

Bird and Hulstrom (1981), using the clear sky model, reported a comprehensive analysis of data from the mathematical energy model utilising the meteorological data and numerical analysis to determine the solar irradiance. Bird's model was proved to be accurate, the easiest to implement and broader in its application (Bi et al., 2013). A clear sky model was also applied to the evaluation of enhancement events of total solar irradiance during cloudy conditions at a particular location (Piedehierro et al., 2014).

Given the geometrical coordinates of a place (such as latitude, longitude and daylight savings) and the meteorological data and other climate data, computation of possible solar radiation obtainable from a location is possible (George, Wilcox and Anderberg, 2008; Meyer, 2013). Studies show that monthly mean hourly (MMH) values of direct irradiance can be correlated with the clearness index K_t of a particular location (Pérez-Burgos et al., 2014). Furthermore, Huang, J., Troccoli, A. and Coppin, P. (2014) analysed solar resources by the comparison of four approaches to modelling of the daily variability of solar irradiance using meteorological records. The comparison shows the reliability of weather data in predicting solar irradiance.

Another approach to the estimation of real-time solar radiation was presented using satellite images, where beam, diffuse, and global components were evaluated in real time for all sky conditions (Alonso-Montesinos, Batlles and Bosch, 2015). A statistical

approach to bi-model short-term solar irradiance prediction using support vector regressors also resulted in a useful outcome (Cheng, Yu and Lin, 2014).

Reliable online data are also available for validation purposes (Tukiainen, 2014).

Weather data is also available from the South African Weather Service (SAWS) database, but there is no provision for any form of solar radiation data (Weathersa.co.za, 2016).

The study focuses on the South African weather, and reliable data is available on a database of the Southern African Universities Radiometric Network (SAURAN) (Brooks et al., 2015).

2.6 SOLAR-THERMAL COLLECTORS

Solar thermal collectors vary depending on the application thereof. Types of collectors are categorised based on their motion, design, absorber type, and concentration ratio (aperture area to the receiver area of the collector). The types are described in Table 2.1.

Table 2.1 Types of solar collectors (Kalogirou, 2009).

Motion	**Collector type**	**Absorber type**	**Concentration Ratio**	**Indicative temperature range (°C)**
Stationary	Flat-Plate Collector (FPC)	Flat	1	30-80
	Evacuated Tube Collector(ETC)	Flat	1	50-200
	Compound Parabolic Collector (CPC)	Tubular	1-5	60-240
Single-axis tracking			5-15	60-300
	Linear Fresnel Reflector(LFR)	Tubular	10-40	60-250
	Cylindrical Trough Collector (CTC)	Tubular	15-50	60-300
	Parabolic Trough Collector (PTC)	Tubular	10-85	60-400
Double-axis tracking	Parabolic Dish Reflector (PDR)	Point	60-2000	100-1500
	Heliostat Field Collector (HFC)	Point	300-1500	150-2000

The property state of the fluid in circulation at each point is critical in the analysis of energy transfer in the collector system. Thermo-physical parameters of the materials were also required for proper analysis of the system (Mokhtaria et al., 2007).

2.6.1 RELATED STUDIES ON COLLECTORS

Studies showed the applicability of collectors to solar thermal power plant technologies (Gauché, von Backstrὸm and Brent, 2013)

Forristall (2003) undertook a substantial amount of research work on the modelling of PTCs implemented in the Engineering Equation Solver. He focused on the development, validation of a heat transfer models for PTCs in one-dimensional and transient two-dimensional model.

Kalogirou (2009) presented both the optical and thermodynamic analysis of different types of collectors which include fixed and axis tracking types. The model presented was based on both transient and quasi-steady states. A thermal storage component does not appear in the model. The model was implemented in f-chart.

Duffie and Beckman (2006) analyse the transient and quasi-static state models for different types of collectors by given consideration to the effect on other components of the plant (i.e. effect on storage for load variations on the plant).

Hefni (2014) presented a dynamic model of a linear parabolic trough solar power plant and a model of a Solar Hybrid Combined-Cycle Power Plant with a linear Fresnel field. The model was implemented in ThermoSysPro ^{TM}. The study considered the state transient model which was developed and other components of the power plant. The model applies to modelling power plants with different sources of energy.

Orosz (2012) presented a state transient model of the PTCs adopting the Forristall (2003) model in the EES as executable programme. The model was also modified to meet the specifications of a solar power plant in Lesotho.

Colomer, G., Chiva, J., Lehmkuhl, O. and Oliva, A. (2014), in the advanced computational fluid dynamics and heat transfer numerical modelling, provided a useful result applicable to validation of solar tower receivers.

A study shows that wind effect also contributes to the functionality of the solar collectors (Mier-Torrecilla, Herrera and Doblaré, 2014)

Particle effect on heat transfer fluid was also modelled showing an improvement in the heat transfer coefficient (Flamant et al., 2014).

2.6.2 PARABOLIC TROUGH COLLECTORS (PTCs)

Utilisation of the energy from sunlight requires means to efficiently and widely capture radiation from its source (Mier-Torrecilla, Herrera and Doblaré, 2014). At night, study shows that the cooling effect on the collector is also important (Voorthuysen and Roes, 2014). PTCs operate both on molten salt and packed bed thermal storage (Marcotte and Manning, 2014). PTCs also function effectively on steam and qualify the technology as a reasonable candidate for its intended purpose (Mason and Reitze, 2014; Alguacil et al., 2014).

The second largest capacity plant is the Solar Electric Generating System (SEGS), located in Southern California, with an output of 354 MW. SEGS I has an output capacity of 14 MW, while SEGS II –SEGS VII also provide an output capacity of up to 30 MW, and SEGS VIII and IX net solar production of electricity up to 140 MWh. There is also an experimental plant at Plataforma Solar de Almeria (PSA), in Southern Spain (Thefraserdomain.typepad.com, 2005).

PTC modelling involves thermodynamic analysis considering the thermo-physical properties, geometric parameters and other factors that determine the output of the collector unit of the power plant. Sequences of mathematical equations, relation properties and parameters were used to evaluate the required output and losses in the collector (Lemos, Neves-Silva and Igreja, n.d.).

The efficiency, output temperature and heat gain value were determined for assessment of the collector unit. Verification and validation were obtained by comparing the data extracted from existing plants and models (Soenke Holger, 2011).

Solar-thermal collectors are radiation-absorber and heat-exchanger devices. They absorb the solar radiation and transform it into energy in a Heat Transfer Fluid (HTF) in the receiver. The receiver analysis for optimisation was also done (Zavattoni et al., 2014). The HTF transports the heat energy to the required destination. The performance of the collector requires an analytical knowledge of heat transfers,

thermodynamics, optical properties and all parameters involved in the input and output of the model (Kalogirou, 2009). Kalogirou's study (2009) also revealed the assumptions, limitations and future recommendations related to the model. The first part of the model focuses on the one-dimensional model of the PTCs (for short receivers), while the other part relies on the two-dimensional model of the PTCs (for long receivers) (Kalogirou, 2009). Three-dimensional related model and simulation of heat transfer and turbulent flow in a Receiver tube of solar parabolic trough done by Ghadirijafarbeigloo, S., Zamzamian, A. and Yaghoubi, M. (2014), will be useful for compared validations

2.7 SOLAR-THERMAL STORAGE

Storage of the solar energy is required to stabilise the periodic fluctuations in the radiation for the solar plant system. Stability in temperature and energy is mostly achieved by stratification and increasing the heat capacity of the system (Maithani, Patil and Saini, 2013). Reasonable performance could be achieved in the system taking into consideration the relative function of the components of the system (Regin, Solanki and Saini, 2008; Karaki et al., 2011).

There are various types of solar thermal storage technology implemented in a CSP plant (Marcotte and Manning, 2014). Two common types are molten salt and packed bed thermal storage. The molten salt has proved to be successful in some instances (Tyner and Wasyluk, 2014; Montero et al., 2014).The packed bed type of thermal storage is mostly applicable to the study of solar-thermal storage and reviews of related studies are provided in this section. The first case is the experimental and numerical investigation of the solid particle thermal energy storage unit by Benmansour, A., Hamdan, M. and Bengeuddach, A. (2006). They use a two-dimensional separate phase formulation to develop a numerical analysis of the transient response of a cylindrical packed bed thermal energy storage system.The system is randomly packed with spheres having uniform sizes and encapsulates the paraffin wax as a Phase Change Material (PCM), with air as a working fluid flowing through the bed. The numerical and experimental outcomes show the solution to fluid

energy equation analysis property and the geometrical parameter is valid for fluids of various Prandtl and Reynolds numbers. Secondly, Bindra, H., Bueno, P., Morris, J. and Shinnar, R. (2013) , investigated thermal analysis and exergy evaluation of packed bed thermal storage systems.They showed that, for packed beds, sensible heat storage systems can provide much higher energy recovery than phase change material (PCM) storage systems under similar high-temperature storage conditions. A third case is a study on the influence of the accuracy of thermal property data of a phase change material on the results of a numerical model of packed bed latent heat storage with spheres. The study outcome confirmed the hypothesis relating to the important role that the PCM's thermal properties play, especially during slow running processes, which are characteristic for the specific application (Arkar and Medved, 2005). The similar predictive study also shows reasonable results (Singh, Saini and Saini, 2009).

Fourthly, on the application of packed bed thermal energy storage model, Opitz, F. and Treffinger, P. (2014) provided a generalised approach and experimental validation. They showed that packed bed thermal energy storage simulation without the necessity to apply measured data for model calibration or to apply specific heat transfer correlations with the restricted application, establishes the possibility to integrate the same pattern within plant models of larger scale without increasing the simulation time drastically. The validity of models was proven with data sets taken from two different experiments reported in their literature.

The last case of the related study of packed bed thermal energy storage is an experimentally validated model which is validated on modelling a Biot number analysis and the thermal capacities of the solid and fluid medium (Anderson et al., 2015).

Modelling allows cost and performance analysis to verify the viability of solar thermal storage capacity (Strasser and Selvam, 2014). A useful study on economic analysis of a hybrid energy storage system based on liquid air and compressed air, also encourages the use of solar thermal technologies (Pimm, Garvey and Kantharaj, 2015). Load requirements, capacity and condition of the source of energy to the system determine the expectation of the system (Allen, 2015).

Analysis of the geometric capacity and rate of charging and discharging provide a reasonable tool towards system optimisation (Wei et al., 2005; Li et al., n.d.).

Studies have been done on storage ability to retain the required thermal energy (Kere et al., 2014). Modelling required a reasonable understanding of the mathematical relation describing the energy retention of the system (Kumar and Shukla, 2015). The major characteristics of the solar-thermal storage are (Tian and Zhao, 2013):

- Capacity per unit volume and dimensional considerations (Cheng, 2011)
- Operating temperature range
- Means of heat addition and removal by measuring the temperatures
- Temperature stratification in the storage unit
- Power requirements for heat addition and withdrawal in the system
- Means of thermal loss control

Materials used in thermal storage need consideration for optimisation purposes (Avila-Marin, Alvarez-Lara and Fernandez-Reche, 2014).

2.8 ORGANIC RANKINE CYCLE (ORC)

The operation of the Simple Rankine Cycle still applies to an Organic Rankine Cycle (ORC). The difference is based on the transport fluid in the system (Saleh et al., 2007). The ORC uses a high molecular mass organic fluid which allows heat recovery from a low-temperature source such as industrial waste heat and solar-thermal collectors. The low-temperature heat is converted into mechanical energy using an expander. The further modification also includes the use of a hematic scroll compressor in reverse as the expander for economic and performance purposes in application to solar and biomass energy technology (Yang and Yeh, 2015). The working fluid is utilised at the expander region for transport to work output areas, and studies show the relevance of this aspect of the ORC.

An experimental investigation of the performance of a hermetic screw-expander ORC by Hsu, S., Chiang, H. and Yen, C. (2014) demonstrated from the study results that a scroll expander ORC could operate with a broad range of heat sources and heat sinks with satisfactory cycle efficiency.

Oudkerk, J., Quoilin, S., Declaye, S., Guillaume, L., Winandy, E. and Lemort, V. (2013) evaluated the energy performance of an ORC-based micro combined heat and power system involving a hermetic scroll expander. They found that increasing the maximum inlet temperature and using two scroll expanders in series, relatively increases the overall electrical efficiency.

Further study of the application of a scroll expander (Jradi, M., Li, J., Liu, H. and Riffat, S. 2014) in micro-scale ORC-based combined heat and power system using a novel scroll expander, showed the range of maximum electric power generated by the expander under an approximate pressure differential. The expander's isentropic efficiency was estimated at the peak operating conditions with a state of no working fluid leakage.

Performance study of Zhang, Y. (2015) on a Single-screw expander in an ORC System showed that under the same heat resource, the expander ratio of a single-screw expander increases with the increase of torque and dryness.On the other hand, it decreases with the increase of back pressure; the volume efficiency decreased with increases in torque and dryness. The total efficiency of single-scroll expander decreased with increases of back pressure and dryness, and with an increase of torque, it increased at first and then decreased after the reaching the maximum.

Empirical models for a screw expander based on experimental data from ORC system testing, predicted screw expander power output using two models: the polytropic exponent model and the isentropic model in the work output percentage range of experimental values (Krishna Avadhanula, V. and Lin, C. 2014).

Experimental investigation of a scroll expander for an ORC done by Ali Tarique, M., Dincer, I. and Zamfirescu, C. (2014) experimentally showed the relationship between the inlet pressure, the volume flow rate and the volume ratio value under the tested

conditions. They investigated minimum start states to generate electricity from the scroll expander. The isentropic efficiency of the scroll expander was estimated, and the electrical efficiency achieved by this system was determined at the specific pressure supply.

In conclusion, the study focuses on ORC that incoporates solar-thermal collectors. The component varies according to the required application. Some of the plant uses the air condenser due to variations in the available water source which is dependent on site-specific conditions for given water constraints faced by the regions.

The thermodynamic analysis follows the first law of the thermodynamics of non-flow and steady flow processes for the components of the system. Property changes with the process occurring in each unit are systematically analysed (Moran et al., 2011). The analysis also required an understanding of heat transfer in the system (Incropera, 2013). Analysis of the evaporators, condensers and most components follows the principle of energy flow (Moran et al., 2011).

2.9 HEAT TRANSFER FLUIDS AND WORKING FLUIDS

Heat transfer fluid and working fluid effects are paramount to the modelling and analysis of ORC (Bao and Zhao, 2013). A case study was done on working fluids for low-temperature ORCs considering the efficiency and pinch analysis for different cycle configuration and variable property states (Saleh et al., 2007). Optimum design criteria for an ORC using low-temperature geothermal heat sources also required comparisons for working fluid (Madhawa Hettiarachchi et al., 2007). Another study was done by Tchanche, B., Lambrinos, G., Frangoudakis, A. and Papadakis, G. (2011) and required the consideration of variation in working fluid effects on ORC applications. Manente, G., Toffolo, A., Lazzaretto, A. and Paci, M. (2013) considered Isobutane and R134a as working fluid in their ORC off-design model for the search of the optimal control strategy. Khennich, M. and Galanis, N. (2012) also studied the optimal design of ORC Systems with a Low-Temperature Heat Source considering

R134a and R141b as the working fluid. Studies that involve a wide range of working fluid comparisons also include:

An efficiency optimisation potential in supercritical ORC by Schuster, A., Karellas, S. and Aumann, R. (2010).

Also, Astolfi, M., Romano, M., Bombarda, P. and Macchi, E. (2014) studied the thermodynamic optimisation of binary ORC power plants for the exploitation of medium–low-temperature geothermal sources. While some studies relate the working fluid variation to output parameters of the system, others focus on specific working fluid for a system. Bracco, R., Clemente, S., Micheli, D. and Reini, M. (2013) experimentally tested and modelled some parts of a domestic-scale STORC power plant.

Bamgbopa, M. and Uzgoren, E. (2013) focused on the numerical analysis of an organic Rankine cycle under steady and variable heat input, and both used R245fa as the working fluid in the system.

Studies have proved that the choice of transport fluid is relevant to performance optimisation of the system (Liu, Chien and Wang, 2004; Le et al., 2014).

A thermodynamic properties data for a vast number of working fluid is also available for modelling (Webbook.nist.gov, 2013).

2.10 CONCLUSION

Information gathered during the literature review provided a useful tool for further research into the modelling of the STORC power plant. Inputs and outputs from previous and recent studies conducted apply to modelling, analysis and validation of the ORC power plant. Knowledge of thermodynamics and engineering was gathered from reviews and applied regarding the modelling of the CSP plant technology on STORC. Valid thermo-physical parameters are available from an experimental set-up and numerical models of related technology, a useful tool for validation. STORC technology, require effective research efforts to optimise the components of the power

plant. Challenges of electricity generation could be managed with the contribution of STORC power plant technology.

CHAPTER 3

SOLAR-THERMAL ORC MODELS

3.1 INTRODUCTION

The approach to initiate the models involves a review of literature and gathering of field information. The review of literature involves numerical equations based on thermophysical analysis of components of the STORC power plant. Gathering of information requires visits to the existing STORC power plant. Reliable parameters of the power plant are available from related plants and results mentioned in the literature.

3.2 FIELD INFORMATION

The existing Solar-thermal ORC power plant is a utility for a pilot health clinic located in the Berea (T.Y) District of Lesotho, approximately 100 kilometres from Maseru. The Pilot Clinic serves 50 to 80 patients each day and has a permanent live-in staff of two to three nurses. The system currently installed at Pilot Clinic to provide 18-24 kWh of energy, along with 200-300 litres of hot water per day. These resources allow nurses to extend clinic working hours and improve services to patients.

A visit to the plant site permits the gathering of information on the dimensional parameters and technical specifications.

The study task involves the sourcing of further information by communicating with researchers and employees working with the plant. On the other hand, information from some existing facilities around the globe was gathered to obtain a useful parameter for model testing and validation. Inquiry considers experimental and operational reports applicable to the power plant model. Comparison and validation of models at different stages of modelling are made possible from data obtained.

3.3 MODELLING SOFTWARE

The proposed plan required Engineering Equation Solver (EES) for the model, which has the advantage of transient state modelling, simultaneous equation solving and built-in thermodynamic properties sourcing for different materials and fluids. At a later stage, a collective decision to model the plant leads to the use of Microsoft Excel ™. The Microsoft Excel ™ modelling focused more on steady state and quasi-static analysis. Instead of the built-in capabilities and thermodynamic properties of EES, it required sourcing of the valid thermodynamic tables for specifications in spreadsheet format and applying the lookup function to obtain the required values. The modelling challenges occurred with Microsoft Excel ™, which led to a further solution. Finally, the knowledge and experience resulted in the creation of a model implemented in Matlab Simulink ® with the add-on. The Thermolib Software ® was also used. The choice also allows easier variation in system configurations, initial conditions and working fluids.

3.4 COMPARISON AND VALIDATION

Validations were obtained by utilising the option based on comparisons to other validated research results, where this was available, and also by using parameters and outputs available from the research outcomes. The study considered the validity of parametric information and utilised the most reliable data. The report finally discusses the difference in values from the model output and those taken from other research and project outputs.

3.5 PLANT SPECIFICATIONS

Table 3.1 Information below describes the design specification of the Lesotho plant (Stginternational.org, 2015)

Thermal Input	• Direct Sunlight
	  ○ 800-1000 W/m^2, peak
	  ○ 400-600 W/m^2, nominal
	• 50-70% thermal collector efficiency

Collector Thermal Output	• 650 W/m^2 peak thermal output • 150º C maximum temperature • 70 m^2 array = 40 kW thermal, nominal

ORC Heat and Power Outputs	• 3 kW electrical / 23 kW thermal (co-generation mode)
	  ○ up to 15% thermal-electric efficiency
	  ○ 2-10% solar-electric efficiency
	• 48V DC output (battery charging)
	• 220 V AC inverter
	• 300 Litres hot water / day

3.6 TECHNICAL APPROACHES TO MODELLING THE ORC TECHNOLOGIES

Thermo-physical analysis of the components utilising input variables and experimental data from test plant/operational plants provided the necessary tools for the modelling. Numerical equations for each component and connecting variables for system integration allowed the modelling of the whole system. Components were modelled relatively, depending on the configuration of the plant. The different approaches - from the energy source to the output part - are discussed in the next section.

The system source of energy

Measured insolation for various locations is available on the weather database of the SAURAN (Sauran.net, 2016). The Direct Normal Irradiance (DNI) for the site applies to a system with parabolic trough collectors. They measure the DNI by means of a tracking device. The recorded DNI from the measuring instrument is available at a different time interval, from minutes, to hourly and daily. A weather station also records the temperatures, barometric pressure and relative humidity at the required time. Each site has the measuring instrument mounted in a suitable position. These data are the input parameters to the solar collector sub-system. Table 3.2 shows the main parameters and measuring instrument;

Table 3.2 Important parameters of the weather station

Measurement:	**Instrument:**
Direct normal irradiance in [W/m^2]	Kipp & Zonen CHP1 on a SOLYS tracker
Air temperature in [°C]	Campbell Scientific CS215 sensor
Barometric pressure in [mbar]	Vaisala PTB110 sensor
Relative humidity in [%]	Campbell Scientific CS215 sensor

Based on the case study the data were taken from three locations for 2015 hourly data. The first is that of Bloemfontein (Latitude: -29.11074°, Longitude: 26.1850°) with an elevation of 1491 m. The second is that of Graaff-Reinet (Latitude: -32.48547°, Longitude: 24.58582°) with an elevation of 660 m. The third is that of Vanrhynsdorp (Latitude: -31.61748°, Longitude: 18.73834°) with an elevation of 130 m. A case study will compare the output parameters for different seasons of the year. The output will be based specifically on one day (24 hours) in two seasons (specifically first of January and July) in South Africa. The comparison allows for ranking of the location based on the available insolation that could be the input source of energy per location. From literature, the air temperature, DNI, and wind speed and are the most sensitive factors for energy input.

Extraction of useful energy

The parabolic trough collector was modelled based on its common use. Thermal analysis of the parabolic trough collector model focuses on (a) radiative heat losses and gains, convective heat losses and gains, and coefficient of heat losses at surfaces and interfaces; and (b) conductive heat losses through support structures. The model also considers the linearized radiative energy loss coefficients on components of the HCE and the energy loss coefficient on the receiver area. Useful energy gain, outlet

temperature and collector efficiency were the output from the solar-thermal collectors considering the thermal analysis.

The retention and storage of heat energy and fluid in the system

The model treated the thermal storage as a liquid tank, available in Thermolib TM. The capacity of the tank, fluid other parameters were the input according to system requirements.

Conversion of heat to useful mechanical work

The ORC part of the power plant is modelled almost similarly to a simple Rankine Cycle but required further consideration of the additional components of the system. The energy and flow properties from the collector storage unit of the plant are the input parameter to the ORC part of the plant. Energy balance with regard to each component of an ORC depending on the configurations, was analysed. Output properties at a state from one component were used as an input properties state to the next component. This part of the plant was easily implemented in Thermolib TM.

3.7 EXPERIMENTAL DATA PARAMETERS AND VALIDATIONS

Validation of the model involves the use of input and output parameters from the available plants for power generation for educational, commercial or experimental purposes. Research models from previous studies also provided some valid inputs and results to validate model results.

The main input parameters considered to determine the energy source are the DNI, wind speed and atmospheric temperature and pressures. The output parameters of the solar resources are the values of the input parameter at a specific location and time as required for further computations.

For the collector model, the input parameters are those from the resources, the geometrical dimension (length of the collector, aperture width, diameter and thickness of the glass envelope and receiver) and thermo-physical properties (considering the heat transfer medium; specific heat, thermal conductance, dynamic viscosity, density,

temperatures). Significant output parameters are the heat gain rate, the outlet temperature of the fluid, the rate of heat losses, and collector efficiency (Forristall, 2003). The model also includes assumptions in some cases of negligible factors and complicated situations (examples are types of flow between the HTF and absorber assumed as uniform flow, while the temperature is assumed bulk temperature). The assumptions cause a slight alteration in the output results.

The solar storage model input parameters are the tank mass, initial temperature, mass flow rate, type of fluid in the system. The outputs are the fluid rate of enthalpy, mass flow rate, temperature, pressure, entropy, and specific heat.

The model accounted for energy flow from the thermal storage to the vaporiser and other components (turbine, condenser, pump) flowing back to the thermal storage, while at the same time producing work at the expander (Orosz, 2012 and Quoilin, 2007).

3.8 CONCLUSIONS

Accuracy, flexibility and simplicity were seriously considered regarding the choice of techniques and approach adopted for the Solar-thermal ORC models. The model accounted for output discrepancies on model perfection. The outputs also included rankings, performance, efficiencies, statistical analysis, and sensitivity studies.

CHAPTER 4

MODELLING THE STORC POWER PLANT

4.1 INTRODUCTION

The power plant transforms available energy from solar irradiance into other forms such as heat and work in the components of the power plants. Thermodynamically, energy is transformed using a device that minimises losses as much as possible. When modelling the power, one plant considers the thermodynamic analysis of each component that transforms energy. This chapter presents the description, theories and equations relative to the operation of the components of the solar-thermal ORC power plant.

4.2 OBTAINING THE HOURLY RESOURCES REQUIRED FOR INPUT

The function of the model is mainly to look for the required value from the given set of data as shown in the flow chart in Figure 4.1. The model requires accurate meteorological data the as input parameter. Table 4.1 shows a sample of the data collected for the model. The main requirement in this part of the model is to read the specific meteorological data at the particular hour of a given day for the location of interest. This variable at the instance of the hour is the output to the collector model.

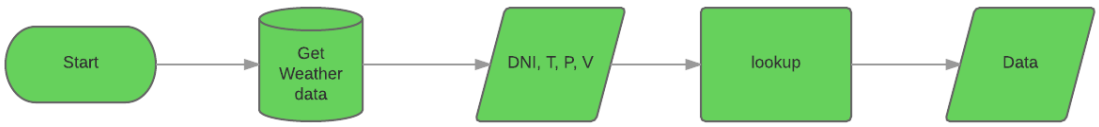

Figure 4.1 Lookup hourly parameter flow chart

Table 4.1 Meteorological data for collector input.

		DNI_CHP1			Air_Temp			BP			WS		
		W/m^2			Deg C			mbar			meters/second		
		Avg			Avg			Avg			WVc		
HN	DATE&TIME	BFN	GRT	VAN	BFN	GRT	VAN	BFN	GRT	VAN	BFN	GRT	VAN
	1-Jan												
1	1/1/2015 0:00	0	0	0	19.81	17.65	18.09	853	936	996	2.47	4.03	4.8
2	1/1/2015 1:00	0	0	0	19.8	17.08	18.09	853	936	996	1.758	3.545	4.789
3	1/1/2015 2:00	0	0	0.000121	18.93	16.67	18.06	853	936	996	1.419	2.222	3.582
4	1/1/2015 3:00	0	0	0	18.57	16.37	18.21	853	935	995	1.502	2.37	2.959
5	1/1/2015 4:00	0	0	0.000242	19.07	16.4	18.24	853	935	994	2.833	2.336	1.398
6	1/1/2015 5:00	0	0	0	18.89	15.86	18.32	853	935	994	3.503	2.012	1.505
7	1/1/2015 6:00	108.919	0	0	18.26	15.06	18.44	853	936	995	2.98	0.639	2.529
8	1/1/2015 7:00	658.728	2.48577	0.057756	19.65	16.92	18.55	854	936	996	2.712	0.62	2.38
9	1/1/2015 8:00	863.781	142.828	0.401603	20.93	18.6	19.15	855	936	997	4.014	0.522	2.238
10	1/1/2015 9:00	872.391	955.333	0.685522	22.28	21.52	20.05	855	936	997	4.853	0.787	1.943
11	1/1/2015 10:00	838.303	1016.46	0.947328	23.5	24.36	21.35	854	935	997	6.667	0.686	1.916
12	1/1/2015 11:00	741.312	1047.65	62.7941	24.68	27.03	22.17	854	935	997	6.756	0.976	2.382
13	1/1/2015 12:00	213.782	1063.45	848.887	25.33	29.16	23.62	854	934	996	6.124	1.947	3.717
14	1/1/2015 13:00	402.63	1061.81	989.812	26.66	31.02	25.79	854	933	996	6.486	2.823	3.904
15	1/1/2015 14:00	640.775	1058.89	998.234	27.68	32.97	27.87	853	933	995	6.011	3.097	5.303
16	1/1/2015 15:00	518.025	1041.35	970.059	27.82	33.95	28.42	852	932	994	5.385	3.128	7.276
17	1/1/2015 16:00	679.149	995.374	919.385	27.77	34.54	27.82	852	931	994	5.338	3.889	7.876
18	1/1/2015 17:00	876.21	950.025	836.678	28.09	34.77	27.49	852	931	994	3.88	4.792	8.59
19	1/1/2015 18:00	662.612	873.022	679.113	28.75	34.57	26.43	851	931	993	2.695	4.037	8.33
20	1/1/2015 19:00	500.332	632.443	241.199	27.22	33.95	25.48	852	932	994	2.821	4.168	8.66
21	1/1/2015 20:00	32.5952	87.0415	0.000242	24.62	28.09	23.16	852	933	994	2.461	8.26	9.69
22	1/1/2015 21:00	0	0	0	22.51	25.72	21.06	853	934	995	2.341	7.435	9.01
23	1/1/2015 22:00	0	0	0	21.05	24.3	20.01	854	935	996	2.365	6.811	7.712
24	1/1/2015 23:00	0	0	0	19.32	22.88	19.35	854	935	996	2.961	5.683	7.291

4.3 POSSIBLE HEAT ENERGY FROM THE SOURCE

Solar collectors could be of a stationary or concentrating type. The model considers a PTC which is a concentrating type of solar collector. Concentrating collectors utilise a concave reflective surface to focus the radiation from the sunlight to a smaller receiving area. The application of geometric surfaces increases the solar radiation flux. PTCs use a structural trough that has a parabolic reflective surface.

PTCs are single-axis tracking with a tubular absorber. Designs and operations achieve a concentration ratio from 10-85, and an indicative temperature range of 60- 400 °C.

This type of collector is capable of delivering high temperatures and has excellent efficiency with high performance. Lighter design and low-cost technology are possible with the PTCs. Figure 4.2 shows a photograph of the collector used with the plant.

Figure 4.2 Parabolic reflectors (photo taken at Lesotho plant in the Berea district).

4.3.1 DESCRIPTION OF THE PARABOLIC TROUGH COLLECTORS

Below is a description of the major components of Parabolic Trough Collectors (PTCs).

i) Parabolic reflector

Parabolic reflectors are highly reflective surfaces made by bending sheets into a parabolic shape. The reflective surface has a Miro aluminium reflector with an area of about 75 m^2. The sheet of metal requires an accurate structural body to attain the position. The plant uses a single-axis tracking PTC. The reflector reflects the sun's rays and focuses them on a receiver tube, increasing the solar radiation flux.

ii) Heat collecting element (HCE)

The heat collecting element model comprises a tube with a high surface-absorbing capability enveloped in a glass tube. Modelling considers an air filled annulus between the receiver tube and glass tube.

iii) Absorber tube

The modelling considers stainless steel receiver tubes which are usually coated with a black selective outside coating to achieve absorptive properties. The selective coating has high absorptivity for radiation in the solar energy spectrum, and low emittance in the long wave energy spectrum to reduce thermal losses.

iv) Glass tube (envelope)

The model focused on degradation and heat losses occur on the absorber if the glass envelope in the HCE part of the collectors . Modelling considers high strength refractory glasses with high transmittance retention under high temperatures.

v) Other critical components of the collectors

The air-filled annulus reduces thermal losses and prevents deterioration of the selective coating. The modules incorporate a Teflon connector at each unit. The connectors allow absorber protrusion beyond the glass envelope to assemble a continuous receiver system. The points also create a space for HCE support brackets.

The heat-transfer fluid (HTF) present in the receiver tube transforms the solar radiation into thermal energy. It circulates and transports this heat energy in the system.

4.3.2 PTCs-WITH THE SINGLE-AXIS TRACKING COLLECTOR

The orientation of the reflector could be in an East-West (E-W) direction, tracking the sun from North to West, or in a North-South (N-S) direction, tracking the sun from East to West.

The advantage of the E-W is that it requires minor adjustment during the day; hence, full aperture always faces the sun at noon. Disadvantages involve reduced performance during the early and late hours of the day. Reduction in performance is due to large incidence angles (cosine loss). The above is the other way round case for the N-S-oriented collectors. The choice between these two relies specifically on the weather conditions of the location.

4.3.3 RELEVANT PARAMETERS FOR THE PTCs ANALYSIS

To implement a proper model for the PTCs, the parameters are discussed below.

i) COLLECTOR GEOMETRY

Information on the dimensions of the materials composed in the collectors was used to determine the sizing and shape factors for optimal design. PTCs require accuracy on the geometry of the structure to achieve the required optical and thermal performance. Optical performance relies greatly on the parabolic structure and other geometry that includes the length, width and the orientation of the components of the collector. Thermal analysis of heat transfer through the heat collecting elements requires the specific dimensions of the receiver and glass cover toward achieving the optimal heat gain and reduced energy losses. Modelling requires proper understanding of the processes and components of the collector for analysis.

ii) TEMPERATURE

The temperatures at specified points in the collector are a function of the insolation and the internal energy of the HTF. The analytical study provided the energy involved in different modes (convection, conduction and radiation) of heat transfer. The model must be capable of determining the outlet temperature, heat gains, heat losses and thermal efficiency.

iii) COLLECTOR FLUIDS THERMOPHYSICAL PROPERTIES

The thermophysical properties of the fluid (HTF, air and annulus medium; close to vacuum) were used to determine the property state of the fluid in different regions of the collector. These properties are the dynamic viscosity of air, wind/air speed, the thermal conductivity of air, mass flow rate of HTF, and pressure of the annulus.

iv) COLLECTOR MATERIAL PROPERTIES

Collector material properties include the physical properties of the material component of the collector. The known parameter includes the thermal conductivity and the heat-transfer coefficient. Thermal conductivity is available on the manufacturer specification data sheets. The model determines the heat-transfer coefficients using

Reynolds and Nusselt numbers relationships at a known dimension and thermo-physical properties of the medium of applications.

v) COLLECTORS REQUIRE RADIATION PARAMETERS

The model calculates the absorbed radiation per unit area of the aperture, glass cover surface emittance, receiver surface emittance and Stefan Boltzmann's constant. The absorbed radiation was taken from the solar resources model, while other radiations were available from the material data sheets.

vi) HEAT TRANSFER COEFFICIENT BETWEEN AIR AND GLASS

The model evaluates the thermal energy analysis from the surrounding air, a source of energy to the outer component of the HCE, which is the glass cover/envelope outer surface. The heat-transfer coefficient between the surrounding air and the glass cover was determined from dimensionless correlations applying the Reynolds number for flow regime, hence, computing the Nusselt number to account for the wind loss coefficient. The above is mathematically expressed in Equations 4.1, 4.2, 4.3 and 4.4 (Duffie and Beckman, 2013).

$$\mathrm{Re} = \frac{\rho V D_{co}}{\mu} \tag{4.1}$$

$$Nu = 0.40 + 0.54\,Re^{0.52} \; if \;\; 0.1 < Re < 1000 \tag{4.2}$$

$$Nu = 0.3\,Re^{0.6} \; if \;\; 1000 < Re < 50000 \tag{4.3}$$

$$h_w = \frac{Nu\,k}{D_{co}} \tag{4.4}$$

vii) FIRST ESTIMATION OF HEAT LOSS (GLASS COVER TO AIR)

At this stage, the analysis considers the heat loss between the glass cover and the surrounding air. Hence the value of the initial glass cover outside temperature is the same as the ambient temperature of the receiver temperature. The Equation 4.5 was used to find the heat loss using the measured value for the glass cover is outside temperature (Duffie and Beckman, 2013).

$$Q_{loss1} = \pi D_{co} h_w \left(T_{co} - T_a\right) + \varepsilon_c L \sigma D_{co} \left(T_{co}^4 - T_{sky}^4\right) \quad (4.5)$$

viii) GLASS COVER INSIDE TEMPERATURE

The process of estimating the outside glass cover temperature required calculating the glass cover's inside temperature. The expression in Equation 4.6 was used to determine the receiver glass cover's inside temperature (Duffie and Beckman, 2013).

$$T_{ci} = T_{co} + \frac{Q_{loss1}\left(D_{co} / D_{ci}\right)}{2\pi L k_c}.; \; D_{ci} = D_{co} - 2t_c \quad (4.6)$$

ix) SECOND ESTIMATION OF HEAT LOSS (RECEIVER TO GLASS COVER)

The heat loss between the receiver and the glass cover was estimated using Equations 4.7 and 4.8 (Duffie and Beckman, 2013). If the heat loss value of the second estimation is the same as that of the first estimation, and if the value of the outside glass cover is correct, the model computes the target outputs. If the values of both estimations are different, another set of iterations determines the right estimate of the outside cover temperature.

$$Q_{loss\,21} = \frac{\pi L \sigma D_{ro} \left(T_{ro}^4 - T_{ci}^4\right)}{\frac{1}{\varepsilon_r} + \frac{\left(1+\varepsilon_r\right)}{\varepsilon_r}\left(\frac{D_{ro}}{D_{ci}}\right)} \quad P < 1.33kPa \quad (4.7)$$

$$Q_{loss\,22} = \frac{2\pi L k_{eff}}{In\left(D_{ci}/D_{co}\right)}\left(T_r - T_{ci}\right) + Q_{loss\,21} \quad P \geq 1.33kPa \quad (4.8)$$

x) LOSS COEFFICIENT (BASED ON RECEIVER AREA)

The loss coefficient at the receiver was estimated using the expression in the Equation 4.9 (Duffie and Beckman, 2013). The area of the receiver was calculated considering the outside diameter.

$$U_L = \frac{Q_{loss,n}}{A_r\left(T_r - T_a\right)}; A_r = \pi D_{ro} \quad (4.9)$$

xi) COLLECTOR EFFICIENCY FACTOR AND HEAT REMOVAL FACTOR

The efficiency of the collector relies on the material properties and dimensions. The expression to consider the effects was presented in Equation 4.10, where the receiver's thickness determines the receiver's inside diameter (Duffie and Beckman, 2013).

$$F' = \frac{1/U_L}{\frac{1}{U_L} + \frac{D_{ro}}{h_{f,ri}} + \left(\frac{D_{ro}}{2k_r} In \frac{D_{ro}}{D_{ri}}\right)}, \; D_{ri} = D_{ro} - 2t_r \tag{4.10}$$

Other effects due to the heat capacity of the material and the heat loss effects are referred to as the heat removal factor; F_R and this was estimated using Equation 4.13.The M in Equation 4.11 considered the heat capacity per area loss and the F'' in Equation 4.12 determined the removal of heat at the flow of fluid, termed as the collector flow factor.

$$M = \frac{\dot{m}C_p}{F'U_L A_r} \tag{4.11}$$

$$F'' = M\left[1 - \exp(-1/M)\right] \tag{4.12}$$

$$F_R = F'' \times F' \tag{4.13}$$

xii) COLLECTOR OUTPUTS

The major outputs required from the collector models are the collector useful heat gain, determined using Equation 4.14 (Kalogirou, 2009); Equations 4.15 and 4.16 are used for relative temperatures computations and the exit temperature of the HTF was computed using Equation 4.17. The collector efficiency was estimated using Equation 4.18 (Duffie and Beckman, 2013).

$$Q_u = F_R A_a \left[S - \frac{A_r}{A_a} U_L (T_r - T_a) \right]; \; A_a = (x_w - D_{c\,o}) \tag{4.14}$$

$$\Delta T = \frac{Q_u}{\dot{m} C_p} \tag{4.15}$$

$$\overline{T}_{ro} - \overline{T}_f = Q_u \left[\frac{1}{\pi D_{ro} L h_{f,ri}} + \frac{\ln\left(D_{ro} / D_{ri} \right)}{2\pi L k_r} \right]; \; T_{drop} = \overline{T}_{ro} - \overline{T}_f \tag{4.16}$$

$$T_{f,exit} = T_f - \Delta T \tag{4.17}$$

$$\eta_{col} = \left(Q_u / S A_a \right) \times 100 \tag{4.18}$$

In general, modelling utilises the analysis and the appropriate sequence of mathematical equations for the thermal collectors.

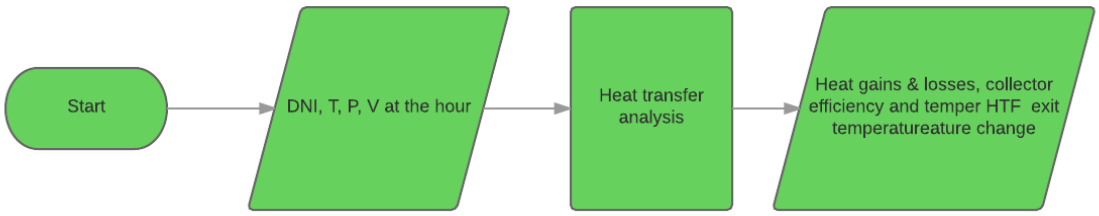

Figure 4.3 The solar-thermal collector process

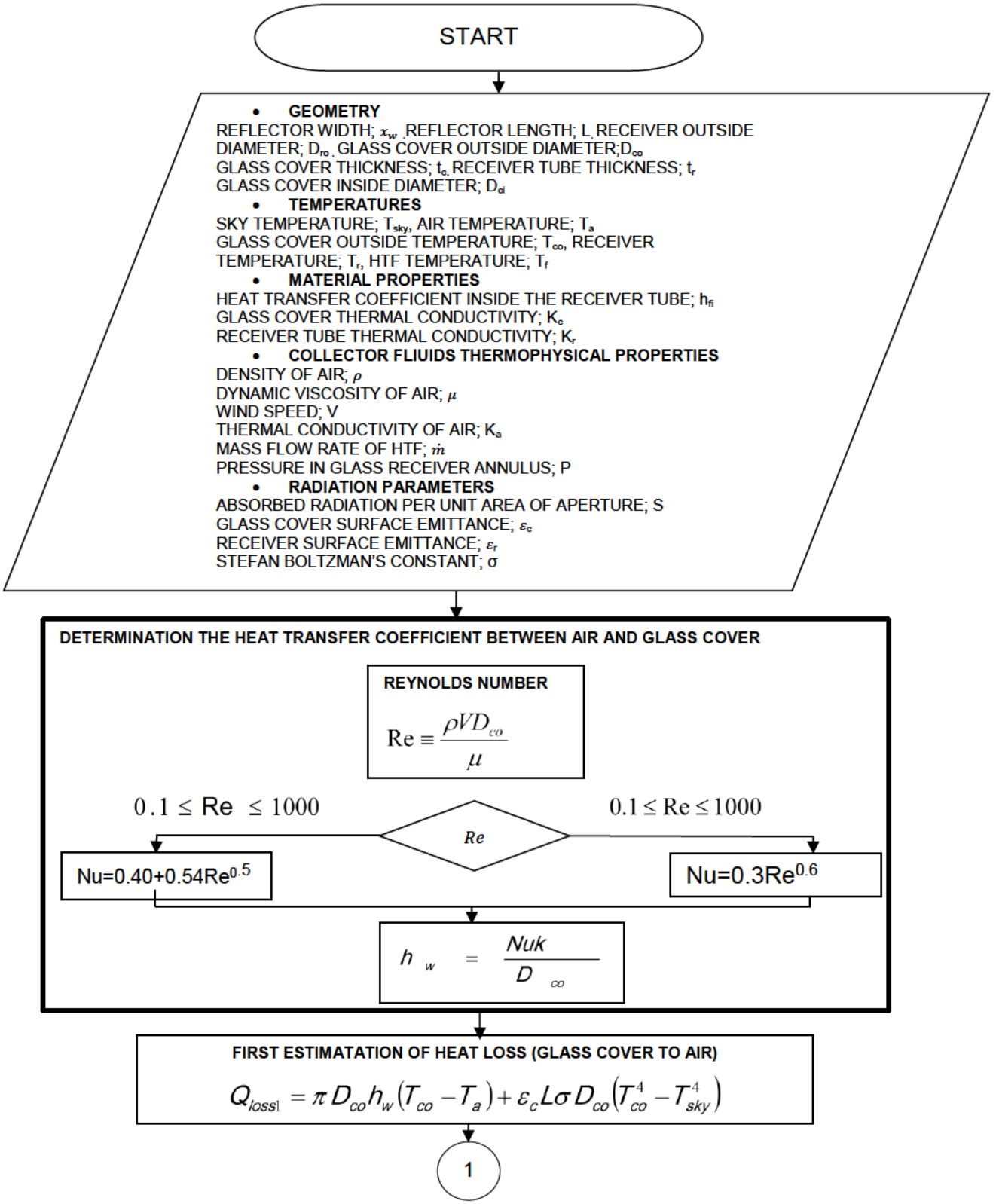

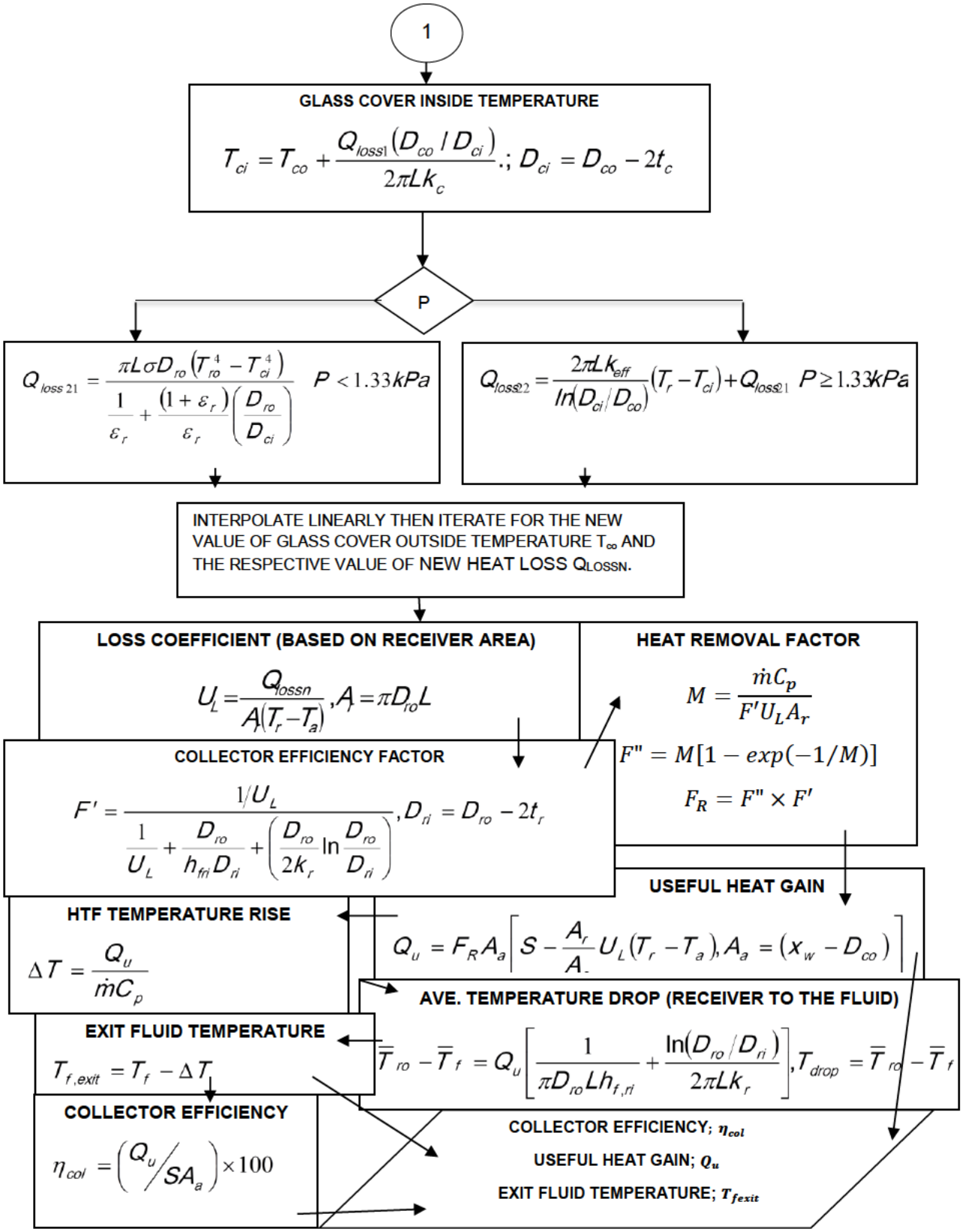

Figure 4.4 A flow chart of the steps of mathematical analysis and procedure to model the collector

4.4 SOLAR-THERMAL STORAGE

4.4.1 INTRODUCTION

Modelling of the solar-thermal storage involves the analysis of a liquid storage tank at constant pressure, assuming that the tank is adiabatic and mechanical work on the environment is negligible. Input parameter includes the mean atmospheric pressure for the day which has a small hourly change. The most important function of the storage is the ability to retain heat and store working and heat transfer fluid.

4.4.2 THERMAL STORAGE DESCRIPTION

Photos and sketches as presented in Figure 4.5 and 4.6 conveniently describe the thermal storage and pictures of the solar-thermal storage unit from the Lesotho plant.

Figure 4.5 Photo of the thermal storage unit (white cylindrical tank)

Figure 4.6 Schematic presentation of the solar-thermal storage unit

4.4.3 THERMAL STORAGE MODEL

When analysing the thermal storage model, consider the main parameters and the state properties of fluid in the tank and also the physical properties of the solid particle for packed bed storage. State properties of fluid element employed in the system at the input, output, stored and overflow stages at a point in time were estimated based on the mass and energy balance. Presented below is a mathematical approach to the thermal storage model using the Euler and Crank Nicholson method was shown in Equation 4.19 to 4.23 and 4.24 to 4.27 respectively (Ketkar and Reddy, 2003).

i) Euler method

Applying one dimensional transient heat transfer with boundary and initial conditions considered as shown in Figure 4.7.

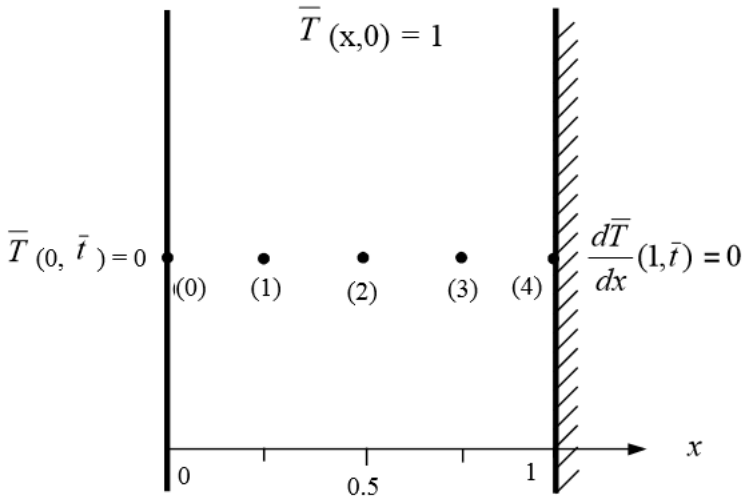

Figure 4.7 Finite difference nodal arrangement for temperature distribution

$$\overline{T}_1^{(i+1)} = \overline{T}_1^{(i)} + \frac{1}{(\Delta x)^2}(\overline{T}_0^{\,i} - 2\overline{T}_1^{\,i} + \overline{T}_2^{\,i})\Delta\bar{t} \qquad (4.19)$$

$$\overline{T}_2^{(i+1)} = \overline{T}_1^{(i)} + \frac{1}{(\Delta x)^2}(\overline{T}_1^{\,i} - 2\overline{T}_2^{\,i} + \overline{T}_3^{\,i})\Delta\bar{t} \qquad (4.20)$$

$$\overline{T}_3^{(i+1)} = \overline{T}_1^{(i)} + \frac{1}{(\Delta x)^2}(\overline{T}_2^{\,i} - 2\overline{T}_3^{\,i} + \overline{T}_4^{\,i})\Delta\bar{t} \qquad (4.21)$$

$$\overline{T}_4^{(i+1)} = \overline{T}_1^{(i)} + \frac{1}{(\Delta x)^2}\left(2\overline{T}_3^{i} + \overline{T}_4^{i}\right)\Delta t \tag{4.22}$$

$\overline{T}$, x and $\bar{t}$ are the normalised temperature, distance and time.

Where, $\overline{T}_0$,$\overline{T}_1$,$\overline{T}_2$,$\overline{T}_3$,and $\overline{T}_4$ are the normalized temperatures at nodes 0, 1, 2, 3, and 4 respectively.

$$p = \frac{\Delta\bar{t}}{(\Delta x)^2} \tag{4.23}$$

Parameter *p* in Equation 4.23 considers the material properties of the system to achieve stability and accuracy.

Crank Nicholson method

The method uses average of the derivatives at the beginning and the end of time interval, which yields more accurate and faster results. The algebraic equations for the nodal temperatures is shown in Equations 4.24 to 4.27.

$$\overline{T}_1^{(i+1)} = \frac{1}{1+p}\left[(1-p)\overline{T}_1^{(i)} + \frac{p}{2}\left(\overline{T}_2^{i} + \overline{T}_2^{(i+1)}\right)\right] \tag{4.24}$$

$$\overline{T}_2^{(i+1)} = \frac{1}{1+p}\left[(1-p)\overline{T}_2^{(i)} + \frac{p}{2}\left(\overline{T}_2^{i} + \overline{T}_2^{(i+1)} + \overline{T}_3^{i} + \overline{T}_3^{(i+1)}\right)\right] \tag{4.25}$$

$$\overline{T}_3^{(i+1)} = \frac{1}{1+p}\left[(1-p)\overline{T}_2^{(i)} + \frac{p}{2}\left(\overline{T}_2^{i} + \overline{T}_2^{(i+1)} + \overline{T}_4^{i} + \overline{T}_4^{(i+1)}\right)\right] \tag{4.26}$$

$$\overline{T}_4^{(i+1)} = \frac{1}{1+p}\left[(1-p)\overline{T}_1^{(i)} + \frac{p}{2}\left(\overline{T}_2^{i} + \overline{T}_2^{(i+1)}\right)\right] \tag{4.27}$$

The next case comprises the modelling of the pebble (quartzite) bed that estimates the fluid outlet temperature over time at five nodes along the tank. Equation 4.28 was used to compute the temperature increment at a given node *N*, while Equation 4.29 was used to calculate the dimensionless time. The equation compares the capacity and the effect of solids in the thermal storage tanks (Allen, 2015).

$$T_i^+ = T_i - \frac{\Delta\theta L}{2\Delta x}\left(T_{i+1} - T_i\right) for, i = 1,\ldots,N \quad (4.28)$$

$$\theta = \frac{t\left(mC_\upsilon\right)_f}{(\rho C_\rho)_b(1-\varepsilon)AL} \quad (4.29)$$

The part mentioned above considered the effect of solid particles in the thermal storage tank. The next phase of the model considers the stratification. Equations 4.28 and 4.29 were used to estimate the bed outlet temperature based on the nodal consideration on the numbers of divisions of the segment of the thermal storage tank. The subscript "*b"* and "*f"* inequation 4.29 represents fluid and bed respectively (Bindra et al., 2013).

The next set of procedures are from Duffie and Beckman model. Due to the low temperature involved during the process, the procedure requires the Biot number and NTU criteria (Benmansour, Hamdan and Bengeuddach, 2006). The following sequences of equations are used to compute the Biot and NTU. The volumetric heat transfer coefficient, Equation 4.30 in W/m^3K, was first computed.

$$h_v = 650\left(G/D\right) \quad (4.30)$$

G is the mass velocity in kg/m^2s , V air velocity and ρ is air density as expressed in Equation 4.31.

$$G = V \times \rho \quad (4.31)$$

The equivalent diameter, D of solid pebbles to sphere form is computed with the expression in Equation 4.32.

$$D = \left(\frac{6m}{\pi\rho_r N}\right)^{\frac{1}{3}} \quad (4.32)$$

m is the mass of the optimised rocks/pebbles, ρ_r is the density of HTF determined from Equation 4.33

N is the number of pebbles per sample; D is the diameter of a spherical particle having the same volume.

$$\rho_r = \frac{m}{V(1-\in)} \tag{4.33}$$

V is the sample volume of the shape of quartzite stones.

While the void fraction, $\in$ is;

$$\in = \frac{m_f / \rho_f}{V} \tag{4.34}$$

Pressure drops in the relationship is expressed in equation 4.35 as:

$$\Delta p = \frac{LG_0^2}{\rho_f} \frac{(1-\in)\propto}{\in^{\frac{3}{2}}} \left(4.7 + 166 \frac{(1-\in)\propto}{\in^{\frac{3}{2}}} \frac{\mu}{G_0 D} \right) \tag{4.35}$$

$\propto$ is the shape factor (mostly ignored),

μ symbolises the dynamic viscosity of the fluid. The Equation 4.36 is applicable when $\propto$ and $\in$ are unknown.

$$\Delta p = \frac{LG_0^2}{\rho_f D} - \left(21 + 1750 \frac{\mu}{G_0 D} \right) \tag{4.36}$$

Considering the Thermolib mass and energy balance, the liquid storage tank input and output flow will be based on the Equations 4.37 and 4.38. Equation 4.37 is used to calculate the mass balance using the molar fraction (at an instance i) n_i and the molar flow rate $\frac{dn_i}{dt}$ (per time from inlet to outlet) of the fluid in the system. The energy

balance is done by considering the enthalpy rate at the inlet and the outlet and is mathematically expressed in Equation 4.38.

$$\frac{dn_i}{dt} = n_{i,in} - n_{i,out} \tag{4.37}$$

$$\frac{dH}{dt} = H_{in} - H_{out} \tag{4.38}$$

The boundary conditions were set at zero time so that all initial temperatures were the same. For the first node and the boundary condition set, all values were known; hence the new temperature was computed.

4.5. ORGANIC RANKINE CYCLE

4.5.1 INTRODUCTION

The model was treated as a Rankine cycle with organic fluid as the working fluid.

4.5.2 ORC ANALYSIS

STORC requires the thermal energy from the thermal storage for purposes mentioned earlier. The ORC section transforms the thermal energy through devices to mechanical work and heat energy providing power output for electricity and hot water (hot water is a case of cogeneration) respectively. The modelling was carried out based on the sequence of energy flow in the ORC components. The state properties of the HTF and WF at the inlet and outlet for each component were measured through energy balance and mass balance. The known state properties of flow were used to determine the energy gain and losses, efficiencies and performance of the components of the ORC as a unit.

Mathematical and thermo-physical parameters that are available for the components determine the output from each component of the ORC.

The study considers the sensitivity analysis of the variation of system output and performance based on different working fluid. The model would also allow a change

in configurations and sizes for performance optimisation. Property diagram comparisons with different configurations can also be used to screen the ORC systems. Figure 4.7 shows the flow diagram for the thermodynamic system considering the ORC parts.

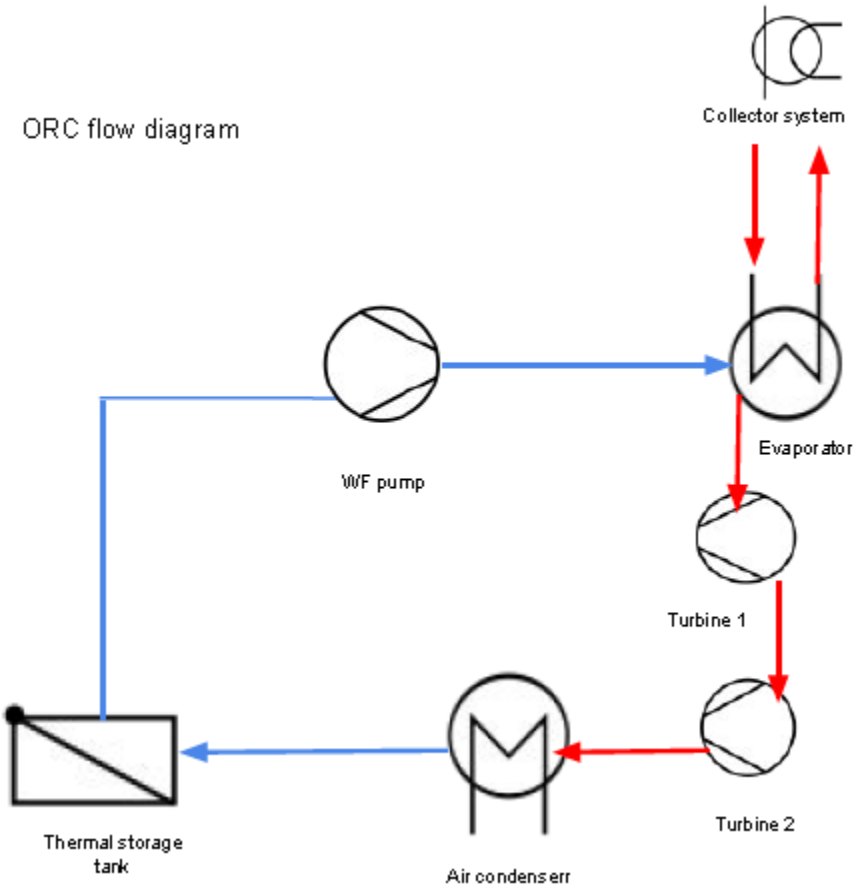

Figure 4.8 Components in an ORC with double-stage expansion and WF tank

The major components of the ORC are analysed and described below as a mathematical model for each element. Thermolib ® library was also used for the modelling (Simulation toolbox for the Design and Development of Thermodynamic Systems in MATLAB®/Simulink®, 2011).

i) Evaporator

Modelling was done based on a single adiabatic counter flow heat exchanger. The Number of Transfer Units (NTU) method is used to calculate the maximum possible heat transfer between flows. The same model applies to the preheater and recuperator if included in the system. Equation 4.39 was used to determine the output energy of the device (m_f is the mass of WF).

$$Energy = m_f(\Delta h) \tag{4.39}$$

The model utilises energy balance for effectiveness, which is the ratio of actual heat transfer to the maximum possible heat transfer and it is expressed in Equation 4.40 and used to determine the heat transfer rate.

$$\varepsilon = \frac{\dot{Q}}{\dot{Q}_{\max}} \quad or \quad \frac{h_{in} - h_{out}}{h_{in} - h_{out,\min}} \tag{4.40}$$

The effectiveness in cases of parallel flow, counter flow are cross flow are given in Equations 4.41, 4.42, and 4.43 respectively.

$$\varepsilon = \left(\frac{1-\exp(-N(1+C))}{1+C}\right) \tag{4.41}$$

$$\varepsilon = \left(\frac{1-\exp(-N(1-C))}{1-C\times\exp(-N(1-C))}\right) \tag{4.42}$$

$$\varepsilon = 1-\exp\left(\frac{\exp(-C\times N^{0.78})-1}{C\times N^{-0.22}}\right) \tag{4.43}$$

$$N = \frac{UA}{\dot{C}_{\min}}, \quad C = \frac{\dot{C}_{\min}}{\dot{C}_{\max}}, \quad \dot{C}_{\min} = \min(\dot{m}_1 c_{p1}, \dot{m}_2 c_{p2}), \quad \dot{C}_{\max} = \max(\dot{m}_1 c_{p1}, \dot{m}_2 c_{p2})$$

$$\dot{Q}_{\max} = \dot{C}_{\min}(T_{hi} - T_{ci}) \tag{4.44}$$

'UA' is the heat transfer rate between the flows, '*U*' the heat transfer coefficient and '*A*' the effective heat area between the flow. '*C*', '*c*' and 'm' represent the heat capacity, specific heat capacity and mass, respectively. Subscript '1' and '2' accounts for the states. Equation 4.44 determines the maximum heat transfer rate between flows. The heat exchange between the thermal mass and the environment is determined by Equation 4.45 be (Incropera, 2013).

$$\dot{Q}_{env} = K_{env} A_{env} \left(T_{TM} - T_{env} \right) \tag{4.45}$$

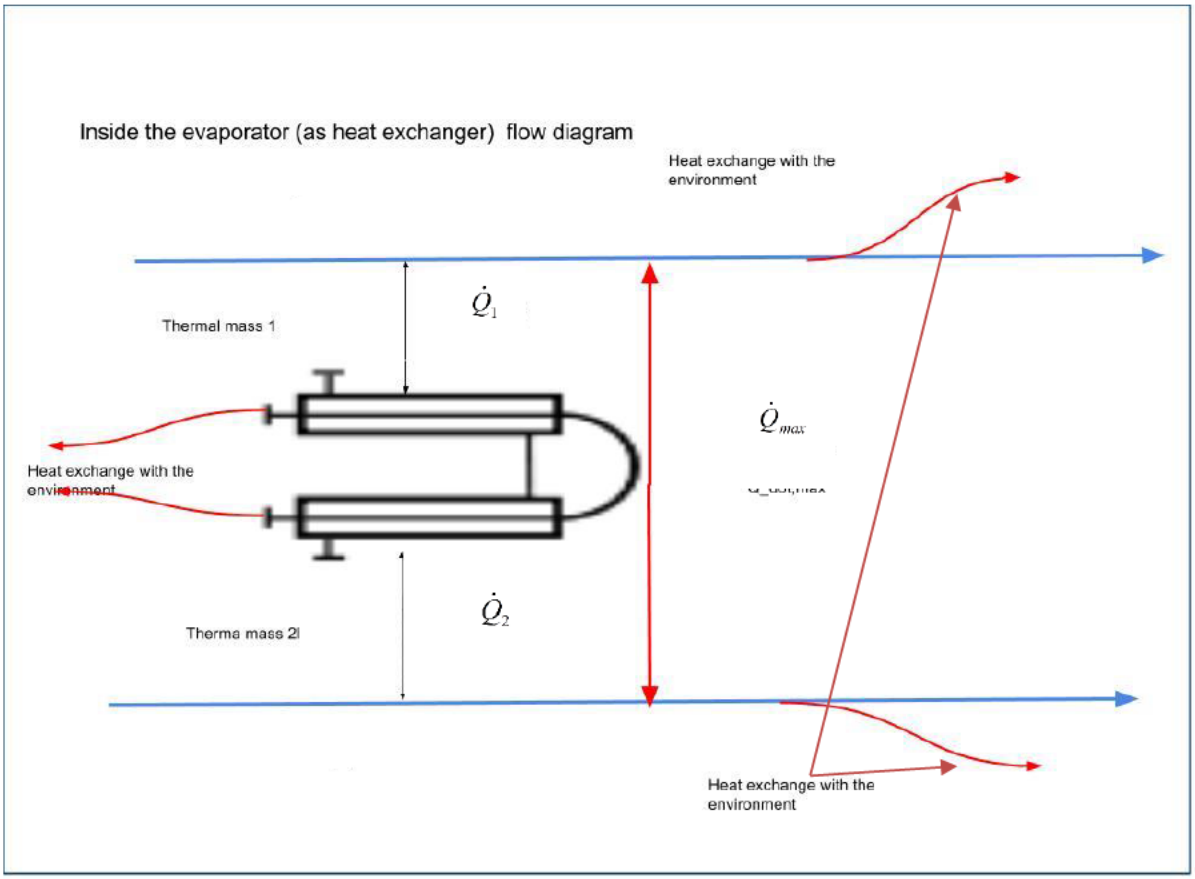

Figure 4.9 Internal representation of the evaporator modelled as heat exchanger

ii) Turbine

The pressure drop of the inlet fluid to the outlet produces mechanical work at a given isentropic efficiency. The model treats the turbine as an adiabatic expansion process with the gaseous flow. Equation 4.46 determines the turbine's isentropic efficiency:

$$\eta_{Turbine} = \frac{h_{in} - h_{out}}{h_{in} - h_{out\ s}} \tag{4.46}$$

The $h_{out,s}$ is the working fluid enthalpy at the turbine exit after an isentropic expansion.

The turbine could be operated as passive (constant mass flow) and active (mass flow depending on other variables) modes. The power output of the entire system is the turbine exit power output.

Turbine power is expressed in Equation 4.47 where, $\dot{m}_{WF}$ is the mass flow rate of the working fluid.

$$\dot{W}_{Turbine} = \dot{m}_{WF}\left(h_{in} - h_{out}\right) \tag{4.47}$$

iii) CONDENSER

The condenser was modelled as an air-cooled heat exchanger. The condenser model uses the same procedures as the evaporator, but the air is provided at the other flow on the fan specification. The volume ratio was also estimated based on McMaster regression from industrial fan power as expressed in Equations 4.48 and 4.49 below.

$$Rg_1 = 87.725 \times V_{AF} + 21.89 \tag{4.48}$$

$$Rg_2 = 225.37 \times A_{CD} \tag{4.49}$$

V_{AF} and A_{CD} represent volumetric air flow and area of the condenser respectively.

vi) PUMP MODEL

The required input power of the pump model was based on the first law analysis on a steady flow. The enthalpy at the inlet and outlet of the pump were measured, and the relative pump efficiency was used for analysis and expressed in Equation 4.50;

$$\eta_{pump} = \frac{h_{out,s} - h_{in}}{h_{out} - h_{in}} \tag{4.50}$$

The power input by the pump is expressed in Equation 4.51. where, $\dot{m}_{WF}$ is the mass flow rate of the working fluid.

$$\dot{W}_{pump} = \dot{m}_{WF}\left(h_{out} - h_{in}\right) \tag{4.51}$$

Another important aspect of the pump is the mass flow rate calculation. The mass flow rate could be imputed or determined from the pressure difference. The mathematical expression in Equation 4.52 evaluates volume flow expressed as the function of the head or pressure rise. Equation 4.53 was used to evaluate the head.

$$Q = f(Head) = \frac{\dot{m}}{\rho} \tag{4.52}$$

$$Head = \frac{\Delta p}{\rho g} \tag{4.53}$$

The isentropic efficiency of the pump is also determined from the relationship with the volumetric flow rate as expressed in Equation 4.54, and easily implemented with lookup. Other rotational speeds RPM are expressed in pump similarity laws and used to determine the pump flow rate. They are expressed mathematically in Equations 4.55, 4.56 and 4.57 where subscript 1 and 2 represent the particular model and head evaluated in Equation 4.53.

$$\eta = f(Q) \tag{4.54}$$

$$\frac{Q_1}{Q_2} = \frac{RPM_1}{RPM_2} \tag{4.55}$$

$$\frac{\Delta p_1}{\Delta p_2} = \left(\frac{RPM_1}{RPM_2} \right)^2 \tag{4.56}$$

$$\frac{Q}{RPM} = f\left(\frac{Head}{RPM^2} \right) \tag{4.57}$$

Two pumps were present in the STORC power plant, namely the heat-transfer fluid pump and the fluid-working fluid pump.

4.6 CONCLUSION

A summary of the principles of thermodynamics and numeric analysis was presented as follows:

- Estimation of the solar resources with regard to the location of interest.
- Determination of heat energy that could be produce for the PTC.
- Numerical analysis to estimate the amount of storage thermal energy.
- ORC energy balance considering the components (evaporator, turbine, pump and condenser).

The knowledge was used with some inbuilt function in Matlab Simulink and Thermolib to simulate the model as presented in the next chapter.

CHAPTER 5

MODEL SIMULATION AND RESULTS

This chapter presents Matlab Simulink models and the results from the STORC power plant component models integrated as a unit for the plant.

5.1. SOLAR RESOURCES MODEL

This part presents models relative to the solar resources.

5.1.1 MATLAB MODEL DESCRIPTION FOR THE RESOURCES

The n-dimensional lookup block was adopted to determine the DNI, atmospheric temperature, atmospheric pressure, wind speed and relative humidity at a specific hour of a chosen location of interest. The model allows the change of data for different places and times. The lookup block made it easier to read the different meteorological data at any location for 24 hours during the various seasons of the year. The user is only required to modify the lookup table data for the measured data of the location, and the periods and dates of the seasons of interest.

The Figure 5.1, Figure 5.2 and Figure 5.3 shows respectively the subsystem for getting inputs for the location and season of interest, the one-dimensional look-up block in Simulink and a sample of the n-dimensional lookup implementation for the model.

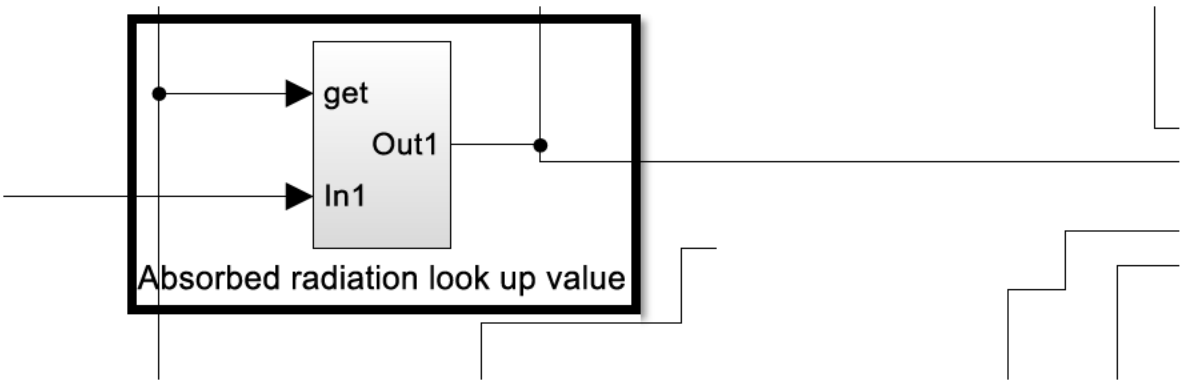

Figure 5.1 The main lookup block for absorbed radiation

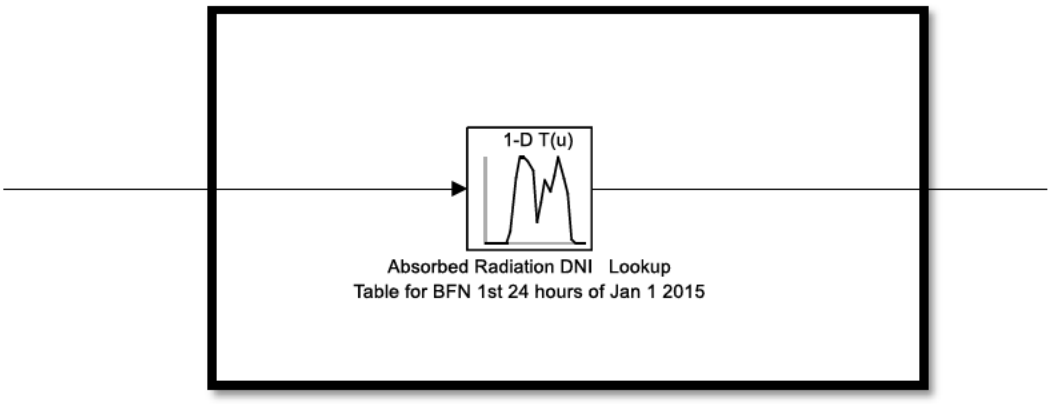

Figure 5.2 One-dimensional lookup block in Simulink

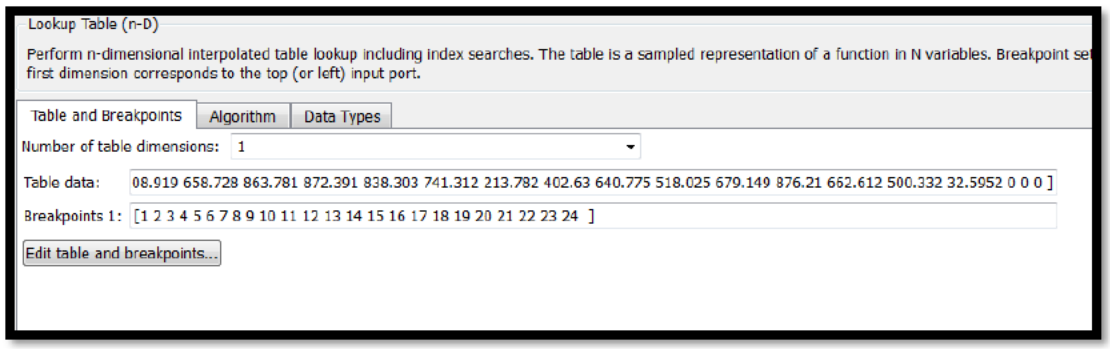

Figure 5.3 Table data and breakpoints of the one-dimensional lookup table

The input describes the position of an hour of the day synchronised with the Simulink run time. The other input is to indicate the location of interest. The switch block chooses the location and the season of the year. The implementation of the choices by the switch block and input time is shown in Figures 5. 4 and 5.5 respectively.

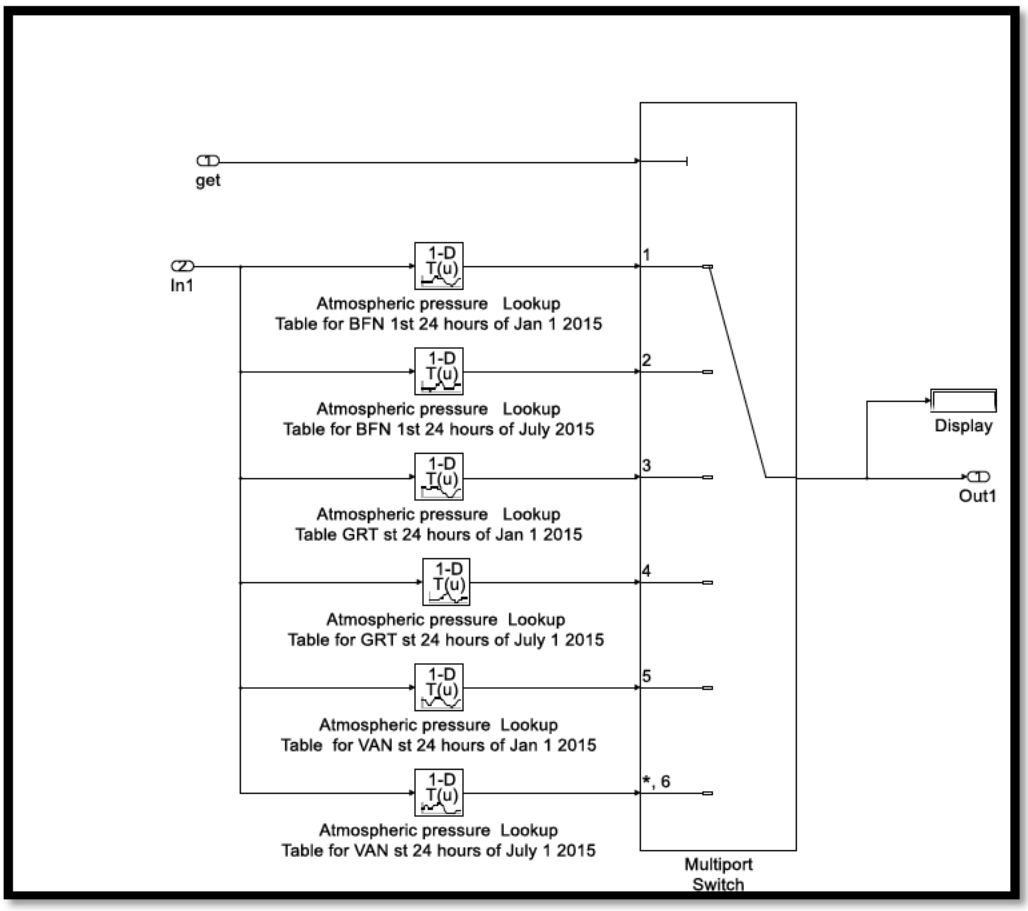

Figure 5.4 The multi-switch and lookup blocks applied in Simulink

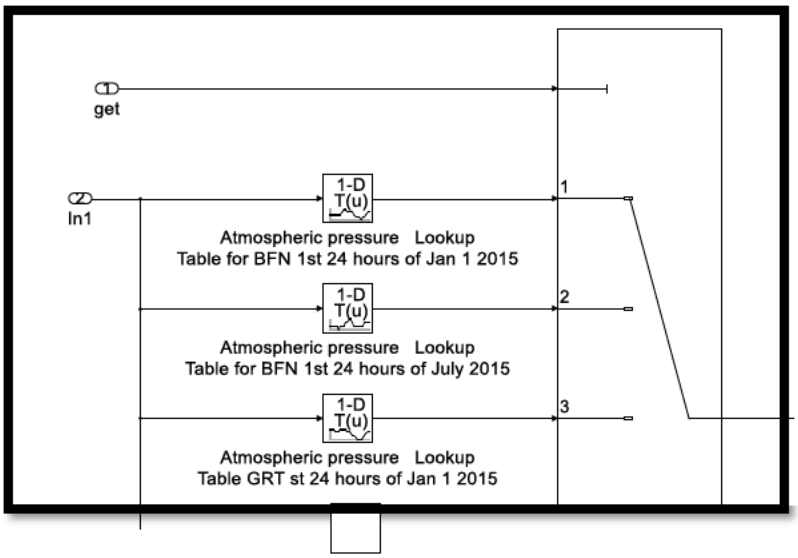

Figure 5.5 Atmospheric temperature lookup model

5.2. RESULTS FROM THE RESOURCES MODEL

The model results of the solar resources with reagards to the locations and time of the year was presented in this section.

5.2.1 RESULTS FROM THE RESOURCES MODEL CONSIDERING BLOEMFONTEIN'S WEATHER ON JANUARY 1, 2015

In this section, Bloemfontein's weather variations for the first 24 hours on January 1, 2015 is shown in Figure 5.6. The hourly DNI (in W/m^2) variations is plotted in the green curve of the Figure 5.6. The hourly wind speeds (in m/s) variations for 24 hours is plotted in the yellow line of the Figure 5.6. The hourly atmospheric temperture (in ˚C) variations for 24 hours is plotted in the blue line of the Figure 5.6. The hourly atmospheric pressure (in mBar) variations for 24 hours is plotted in red line of the Figure 5.6.

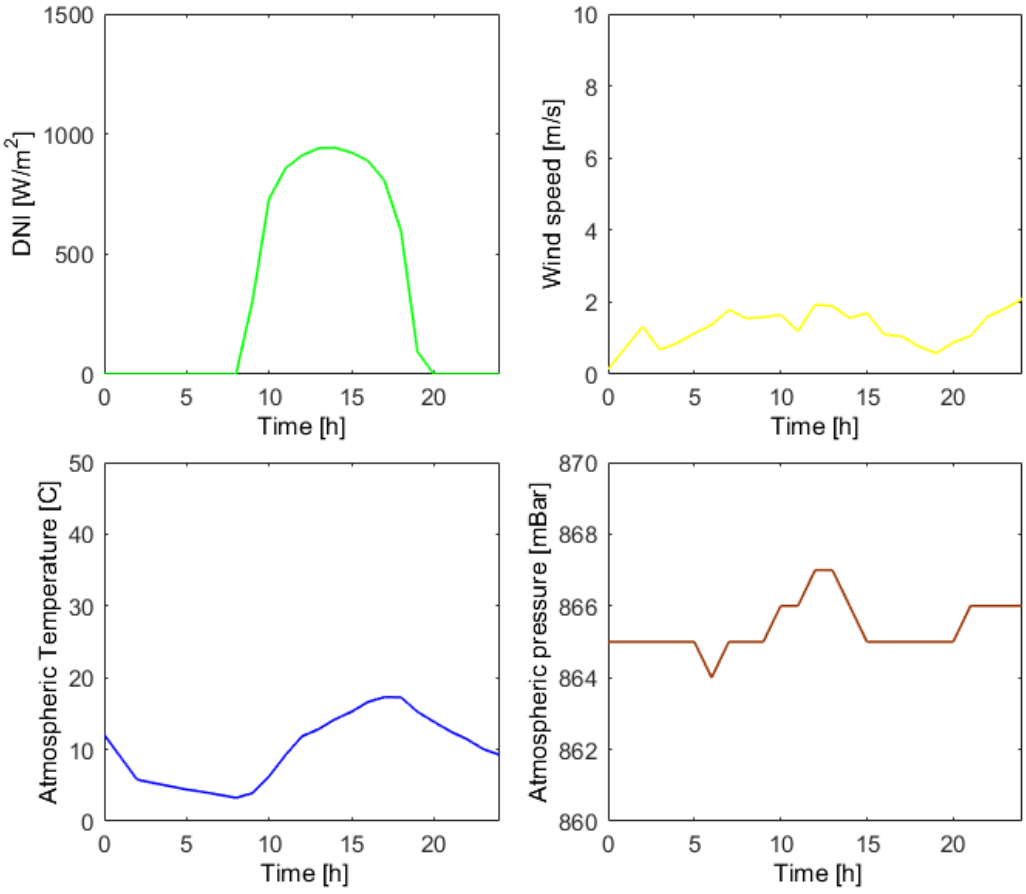

Figure 5.6 Bloemfontein's weather variation for the first 24 hours on January 1, 2015

Tables 5.1 shows the statistical analysis of outcomes, which are useful for validating the data source and provides further information on Bloemfontein's weather variations for the first 24 hours on January 1. The values and time of maximum, minimum, peak to peak, mean, median, and root mean square are presented. The mean DNI, of 353.033 W/m^2 as shown in Table 5.1 provides a useful information to energy input to the plant.

Table 5.1 The statistical analysis of the result in Figure 5.6

Statistics	DNI (W/m^2)		Air_Temp (° C)		WS (m/s)		BP (mbar)	
	Value	Time	Value	Time	Value	Time	Value	Time
Maximum	876.210	18	28.750	19	6.756	12	855.000	9
Minimum	0.000	0	18.260	7	1.419	3	851.000	19
Peak to peak	876.210		10.490		5.337		4	
Mean	353.033		22.915		3.790		853.145	
Median	323.189		22.249		3.102		855.000	
Root Mean Square	488.784		23.193		4.102		853.146	

5.2.2 RESULTS FROM THE RESOURCES MODEL CONSIDERING BLOEMFONTEIN'S WEATHER ON JULY 1, 2015

In this section, Bloemfontein's weather variations for the first 24 hours on July 1, 2015 is shown in Figure 5.7. The hourly DNI (in W/m^2) variations is plotted in the green curve of the Figure 5.7. The hourly wind speeds (in m/s) variations for 24 hours is plotted in the yellow line of the Figure 5.7. The hourly atmospheric temperture (in ℃) variations for 24 hours is plotted in the blue line of the Figure 5.7. The hourly atmospheric pressure (in mBar) variations for 24 hours is plotted in red line of the Figure 5.7.

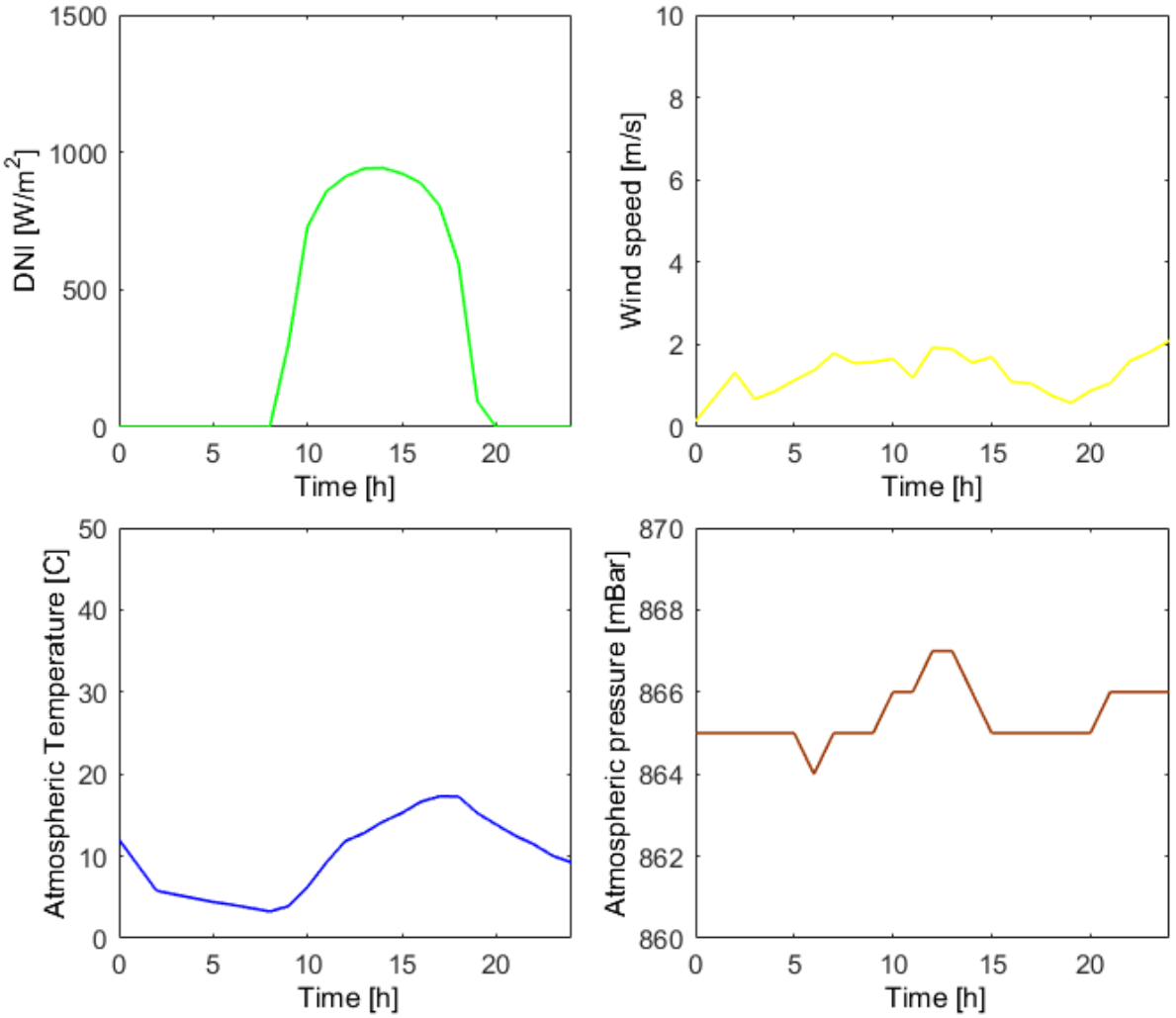

Figure 5.7 Bloemfontein's weather variation for the first 24 hours on July 1, 2015

Tables 5.2 shows the statistical analysis of outcomes, which are useful for validating the data source and provides further information on Bloemfontein's weather variations for the first 24 hours on July 1. The values and time of maximum, minimum, peak to peak, mean, median, and root mean square are presented. Mean DNI of 330.156 W/m^2, which smaller than value 353.033 W/m^2 of 1 Janualry indication a characteristic difference. July is in the winter period for Bloemfontein and comparing the weather data with that of January in summer period of the year shows a sensible reliability of the data.

Table 5.2 The statistical analysis of the result in Figure 5.7

Statistics	DNI (W/m^2)		Air_Temp (° C)		WS (m/s)		BP (mbar)	
	Value	Time	Value	Time	Value	Time	Value	Time
Maximum	942.023	14	17.300	17	2.096	24	867.000	12
Minimum	0.000	0	3.258	8	0.139	0	864.000	6
Peak to peak	943.023		14.042		1.975		3	
Mean	330.516		9.958		1.285		865.395	
Median	0.000		10.298		1.325		865.000	
Root Mean Square	519.202		10.986		1.356		865.395	

5.2.3 RESULTS FROM THE RESOURCES MODEL CONSIDERING GRAAF-REINET'S WEATHER ON JANUARY 1, 2015

In this section, Graaf-Reinet's weather variations for the first 24 hours on January 1, 2015 is shown in Figure 5.8. The hourly DNI (in W/m^2) variations is plotted in the green curve of the Figure 5.8. The hourly wind speeds (in m/s) variations for 24 hours is plotted in the yellow line of the Figure 5.8. The hourly atmospheric temperture (in ℃) variations for 24 hours is plotted in the blue line of the Figure 5.8. The hourly atmospheric pressure (in mBar) variations for 24 hours is plotted in red line of the Figure 5.8.

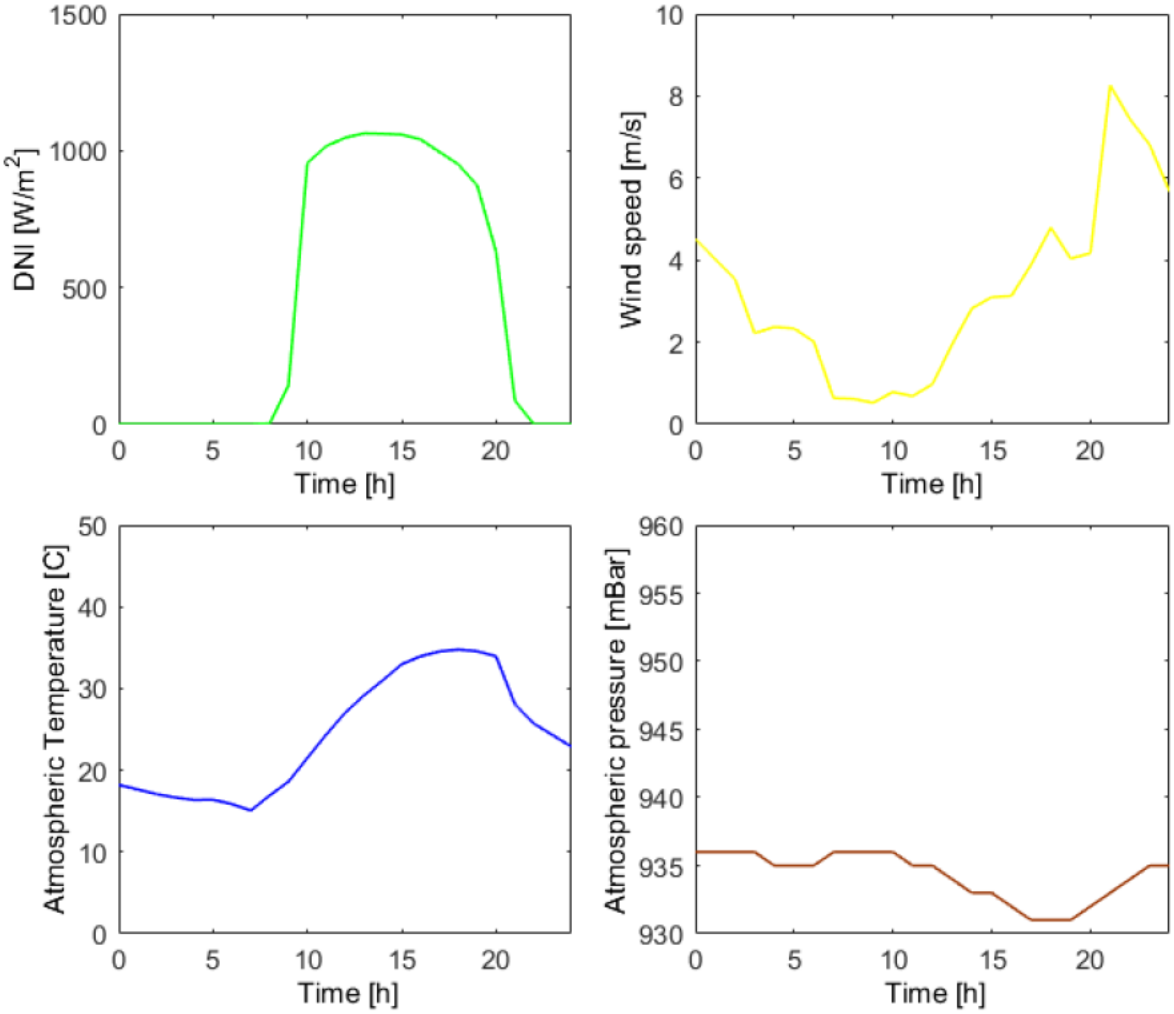

Figure 5.8 Graaf-Reinet's weather variation for the first 24 hours on January 1, 2015

Tables 5.3. shows the statistical analysis of outcomes, which are useful for validating the data source and provides further information on Graaf-Reinet's weather variations for the first 24 hours on January 1

Table 5.3 The statistical analysis of the result in Figure 5.8

Statistics	DNI (W/m^2)		Air Temp (° C)		WS (m/s)		BP (mbar)	
	Value	Time	Value	Time	Value	Time	Value	Time
Maximum	1063.000	13	34.770	18	8.260	21	936.000	0
Minimum	0.000	0	15.060	7	0.522	9	931.000	17
Peak to peak	1063.000		19.710		7.738		5	
Mean	451.577		24.421		3.190		934.242	
Median	121.777		24.229		2.974		935.000	
Root Mean Square	656.065		25.428		3.810		934.243	

5.2.4 RESULTS FROM THE RESOURCES MODEL CONSIDERING GRAAF-REINET'S WEATHER VARIATIONS ON JULY 1, 2015

In this section, Graaf-Reinet's weather variations for the first 24 hours on July 1, 2015 is shown in Figure 5.9. The hourly DNI (in W/m^2) variations is plotted in the green curve of the Figure 5.9. The hourly wind speeds (in m/s) variations for 24 hours is plotted in the yellow line of the Figure 5.9. The hourly atmospheric temperture (in ℃) variations for 24 hours is plotted in the blue line of the Figure 5.9. The hourly atmospheric pressure (in mBar) variations for 24 hours is plotted in red line of the Figure 5.9.

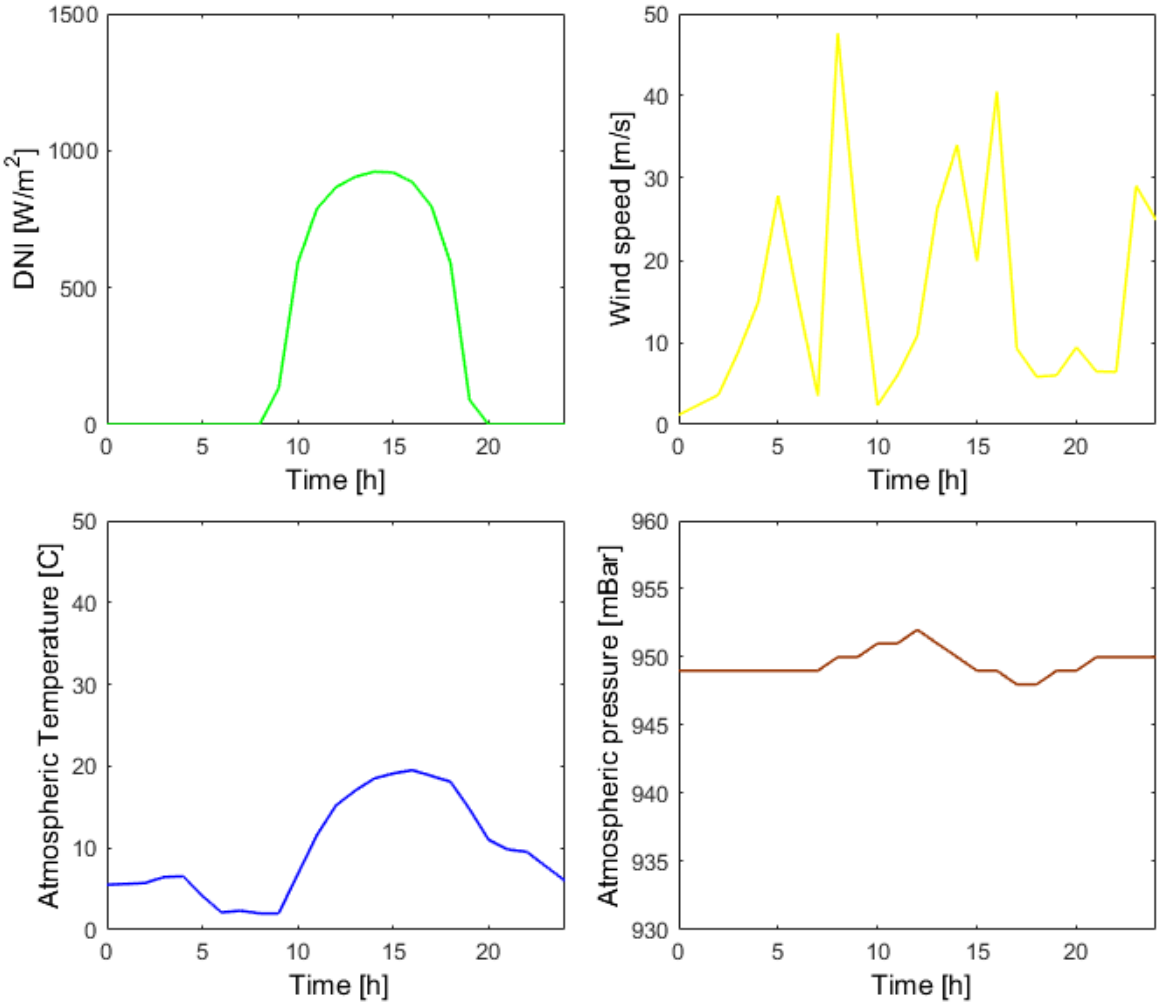

Figure 5.9 Graaf-Reinet's weather variation for the first 24 hours on July 1, 2015

Table 5.4 shows ststistics of Graaf-Reinet's weather variations for the first 24 hours on July 1, 2015.

Table 5.4 The statistical analysis of the result in Figure 5.9

	DNI (W/m^2)		Air_Temp (° C)		WS (m/s)		BP (mbar)	
	Value	Time	Value	Time	Value	Time	Value	Time
Maximum	923.000	14	19.520	16	47.630	8	952.000	12
Minimum	0.000	0	2.010	9	1.173	10	948.000	17
Peak to peak	923.016		17.510		46.456		4	
Mean	309.442		9.970		15.420		949.560	
Median	0.000		8.674		11.105		949.000	
Root Mean Square	495.210		11.608		18.934		949.560	

5.2.5 RESULTS FROM THE RESOURCES MODEL CONSIDERING VANRHYNSDORP'S WEATHER ON JANUARY 1, 2015

In this section, Vanrhynsdorp's weather variations for the first 24 hours on January 1, 2015 is shown in Figure 5.10. The variations in hourly DNI (in W/m^2), wind speeds (in m/s), atmospheric temperture (in ℃), atmospheric pressure (in mBar) variations for 24 hours is plotted with the same axes and colours convection as section 5.2.1 to 5.2.3.

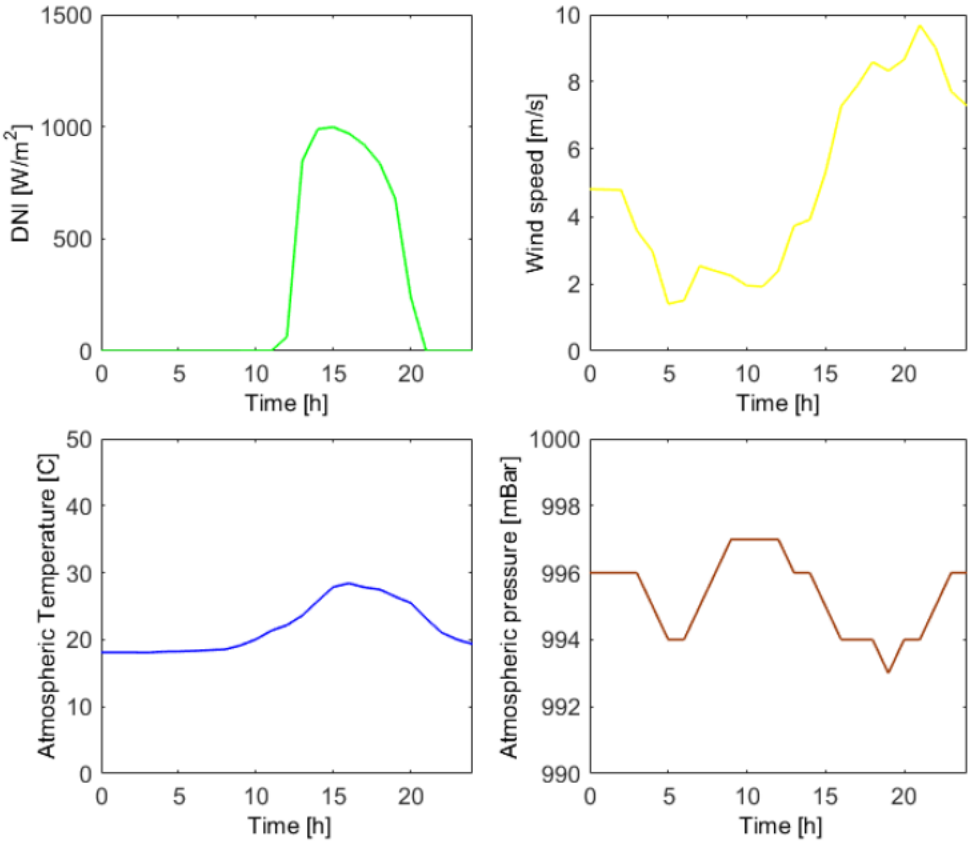

Figure 5.10 Vanrhynsdorp's weather variation for the first 24 hours on Jan 1, 2015

Table 5.5 shows the statistical values of Vanrhynsdorp's weather variations for the first 24 hours on January 1, 2015.

Table 5.5 The statistical analysis of the result in Figure 5.10

	DNI (W/m^2)		Air_Temp (° C)		WS (m/s)		BP (mbar)	
	Value	Time	Value	Time	Value	Time	Value	Time
Maximum	998.234	15	28.420	16	4.690	21	997.000	9
Minimum	0.000	0	18.060	9	1.389	5	993.000	0
Peak to peak	998.234		10.360		8.292		4	
Mean	270.589		21.829		4.943		995.298	
Median	0.350		20.553		4.445		995.500	
Root Mean Square	479.046		21.138		5.634		995.298	

5.2.6 RESULTS FROM THE RESOURCES MODEL CONSIDERING VANRHYNSDORP'S ON JULY 1, 2015

In this section, Vanrhynsdorp's weather variations for the first 24 hours on July 1, 2015 is shown in Figure 5.11. The variations in hourly DNI (in W/m^2), wind speeds (in m/s), atmospheric temperture (in℃), atmospheric pressure (in mBar) variations for 24 hours is plotted with the same axes and colours convection as section 5.2.1 to 5.2.3.

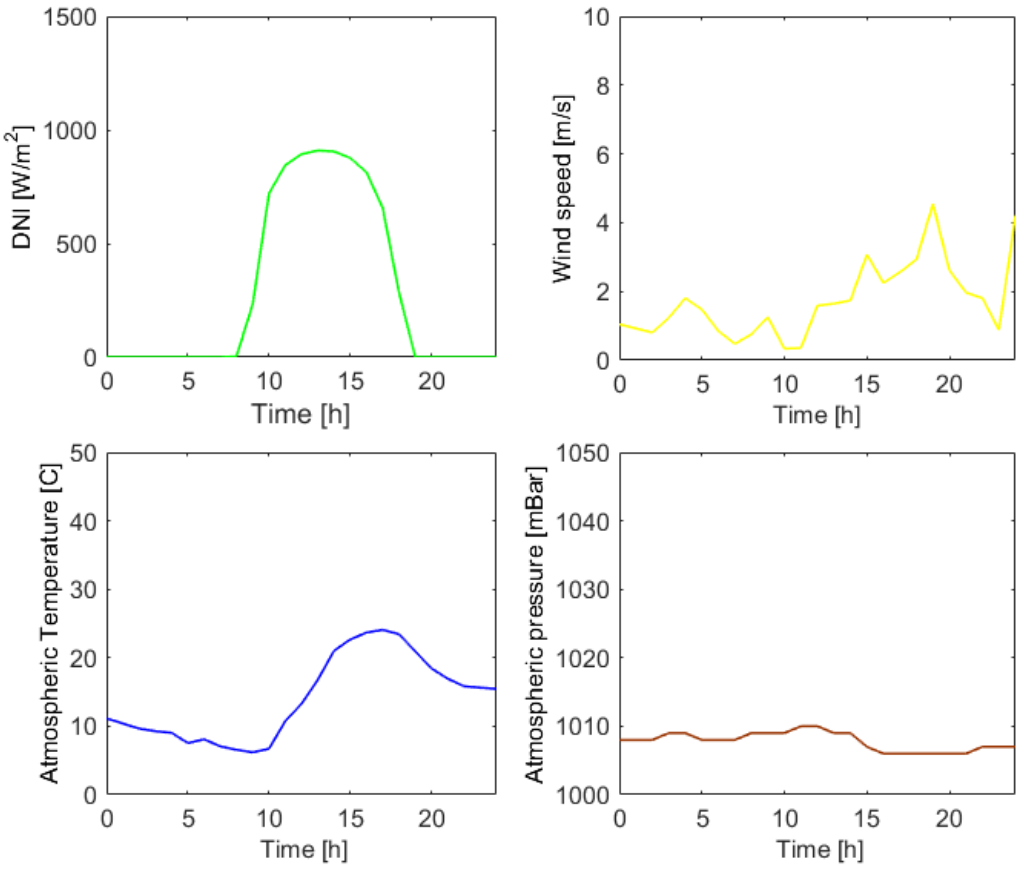

Figure 5.11 Vanrhynsdorp's weather variation for the first 24 hours on July 2015

Table 5.6 shows the statistics of Vanrhynsdorp's weather variations for the first 24 hours on July 1, 2015.

Table 5.6 The statistical analysis of the result in Figure 5.11

	DNI (W/m^2)		Air_Temp (° C)		WS (m/s)		BP (mbar)	
	Value	Time	Value	Time	Value	Time	Value	Time
Maximum	909.530	15	24.070	17	4.547	19	1010.000	11
Minimum	0.000	0	6.187	9	0.336	10	1006.000	16
Peak to peak	909.530		17.883		4.211		4	
Mean	293.977		14.066		1.700		1008.000	
Median	0.000		13.270		1.587		1008.000	
Root Mean Square	479.315		15.302		1.960		1008.000	

The results presented in section 5.2 for the resources are those of the crucial part of STORC power plant input parameter. The model allows the use of data for any location and date of preference, depending on the availability of data.

5.3 THERMAL COLLECTOR MODEL

This part of the report presents the Matlab Simulink model for collector and results

5.3.1 SIMULINK BLOCK FOR THE COLLECTOR

The collector model requires an input parameter from the resources model output. The other inputs to the collector are: the geometry and the thermo-physical properties of the collector unit, which determines the output parameter that includes the collector efficiency, heat gain and heat loss from the collector unit and the fluid exit temperature in the collector receiver HCE. Figures 5.12 and 5.13 show some important parts of the collector model.

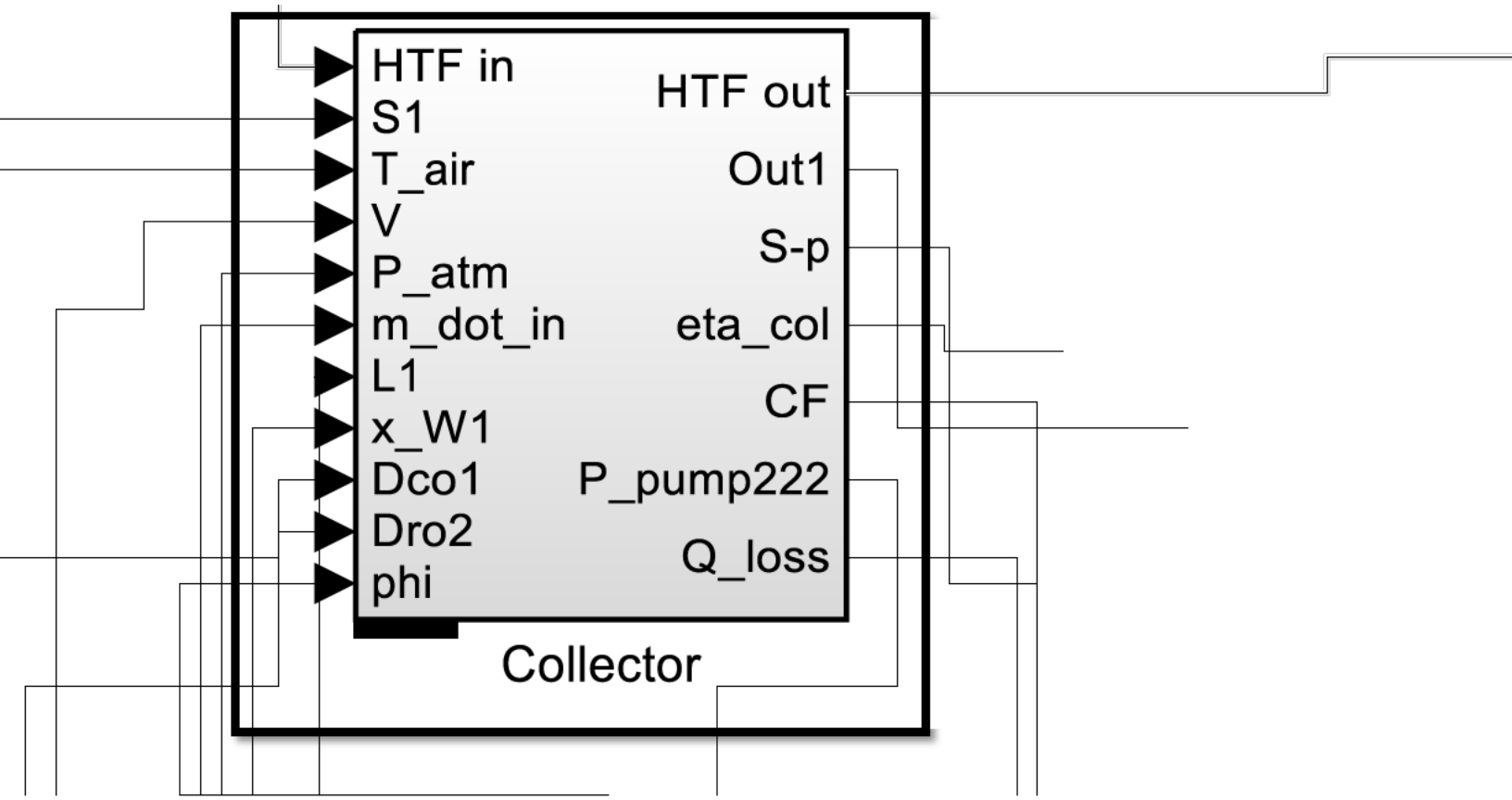

Figure 5.12 Main subsystem block for the collector

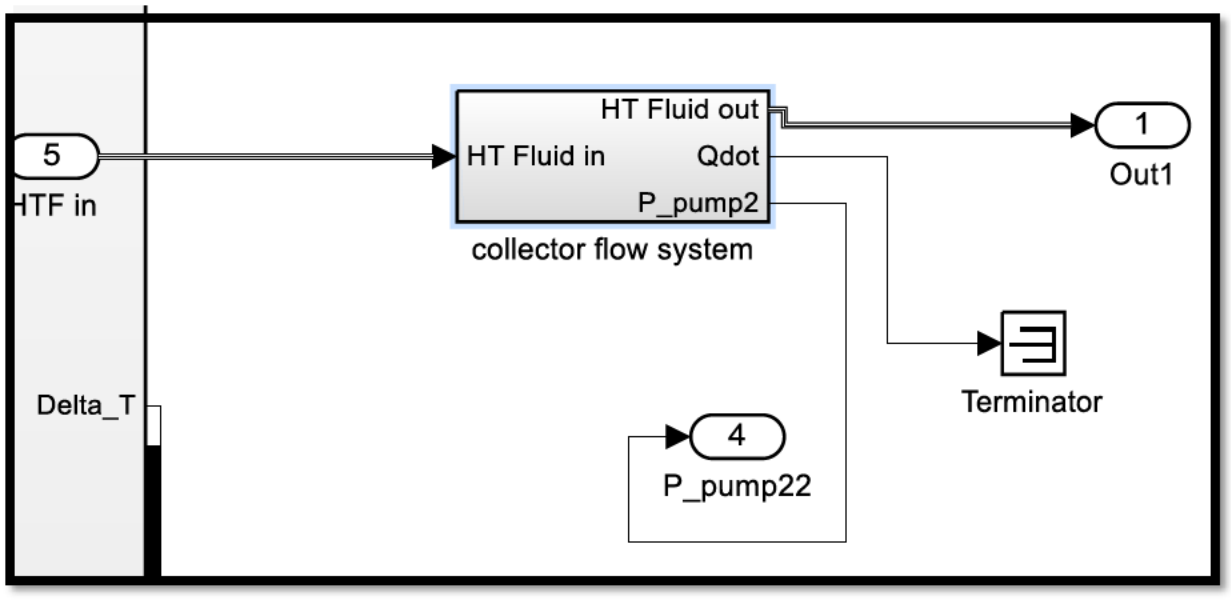

Figure 5.13 Model determines the flow properties at different state in the collector

5.3.2 RESULTS FROM THE SIMULINK BLOCKS FOR COLLECTORS

- The most important output variable are considered for three cases. The first case will consider the variation for this important output variables and was plotted for 24 hours of the day.
- The second case is the variation of the output with the dimension and HTF in the collector system. Last will be the variations of the parameters relative the location of interest.

The thermal efficiency of the collector with a collector length of 10 m, aperture width of 2.5 m, glass cover diameter of 0.09 m and receiver outside diameter of 0.06 m and other characteristics for the preheated HTF, are plotted in Figure 5.14. The plot shows that the efficiency is directly proportional to the DNI input to the system. This curve of DNI follows a similar trend to that of the DNI per location.

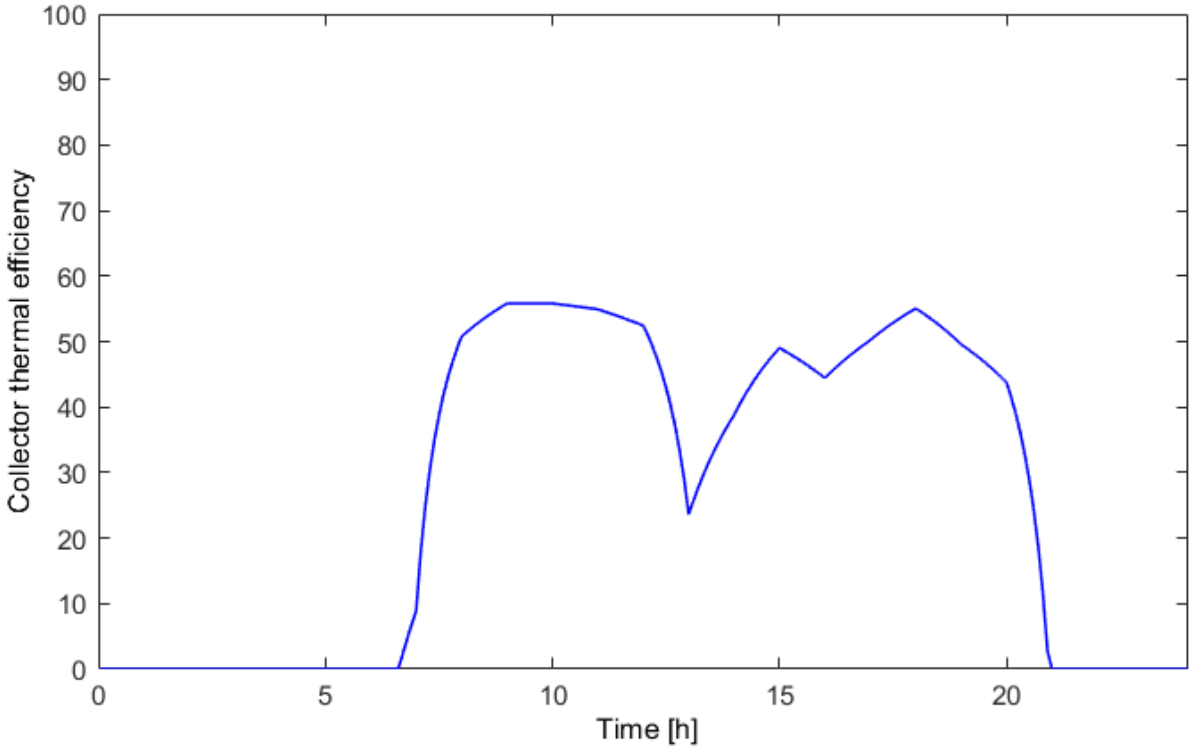

Figure 5.14 The plot of the hourly collector efficiency over a day on the 1st of January 2015 for Bloemfontein without the effect of optical efficiency

Figure 5.15 compares the variation in efficiency concerning the HTF. The plot shows how efficiency varies with the type of HTF in the system. The n-propane has the highest efficiency followed by the ethylene glycol and the steam is the lowest. This statistical analysis shows that the mean efficiency for ethylene glycol is 26.95 %, while that for n-propane and steam are 47.85 % and 47.268 % respectively. The mean and the root mean square values for each case (provided in Appendix B) show the significance of the effect of different HTF in the system. Although the category of the HTF fluid model has very similar physical properties, using fluid with a larger difference in physical properties will show greater difference in the efficiency curves.

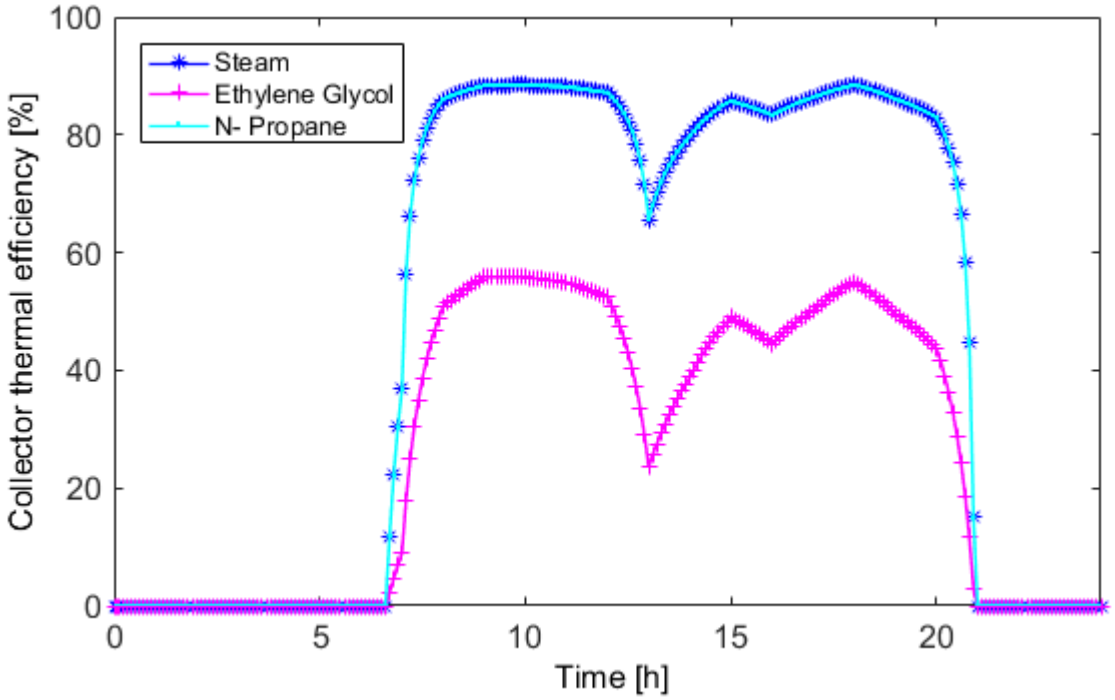

Figure 5.15 Variation in collector efficiency on the same day with different HTF in the system

Another case is that of change of heat gain over the hours of the day. It can be seen from Figure 5.16 that the variation also follows a trend over the hours of the day.

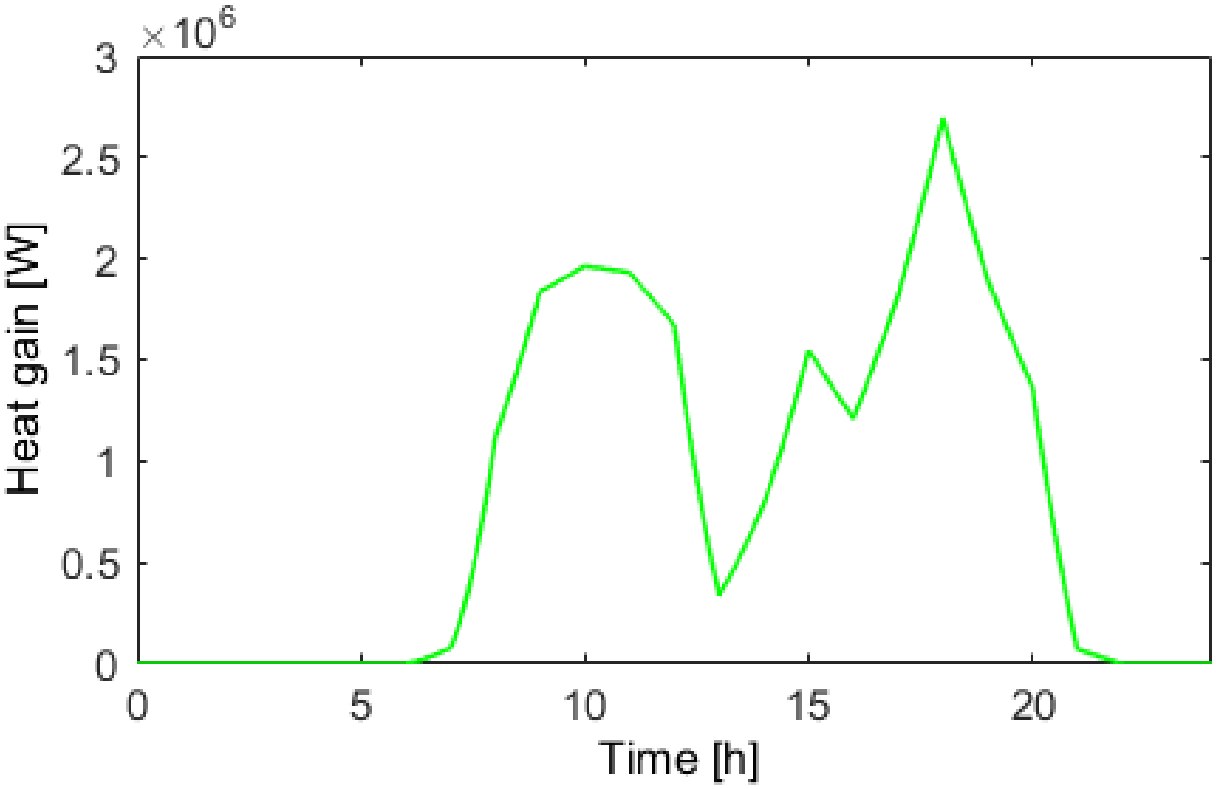

Figure 5.16 The variations of the collector heat gain over the hours of the day (chosen day was the 1st of January 2015 at Bloemfontein)

Concerning the variation of heat gain at different sites, Figure 5.17 shows the plot of heat gain still relies heavily on the DNI curve for the site. The system produces highest heat gain at Graaf-Reinet (abbreviated as GRT) followed by that of Bloemfontein (abbreviated as BFN) and is lowest at Vanrhynsdorp (abbreviated as VAN). Statistical analysis confirms this observation.

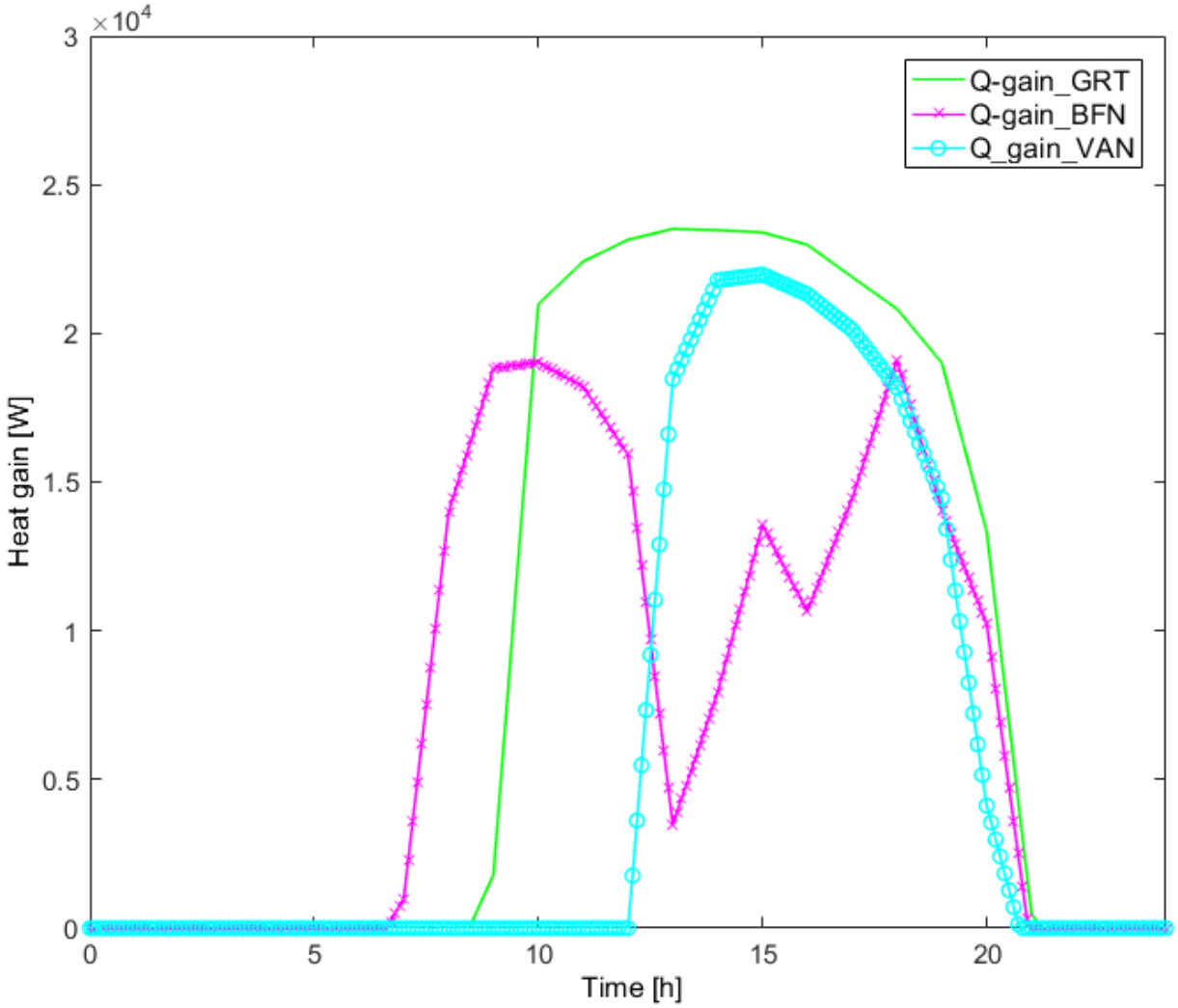

Figure 5.17 The hourly heat gain for different locations

Figures 5.18 and 5.19 also reflect the variation of heat gain with change in length and aperture width of the collector. The results obtained indicate a higher gain as sizes of the collector system increase. The result shows that the longer and wider the collector length and aperture width the higher the heat gains by the collector if all other variables are kept constant.

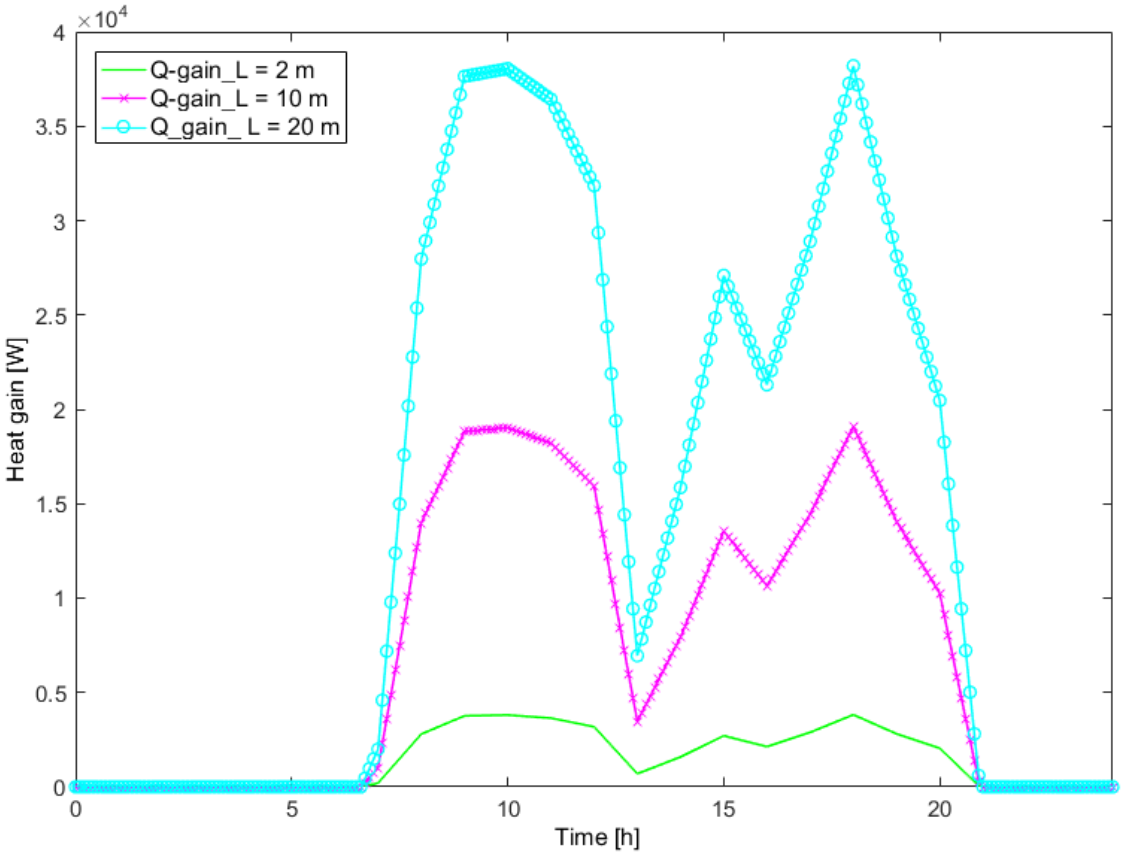

Figure 5.18 The hourly heat gain for different lengths of the collector on a chosen day of the year

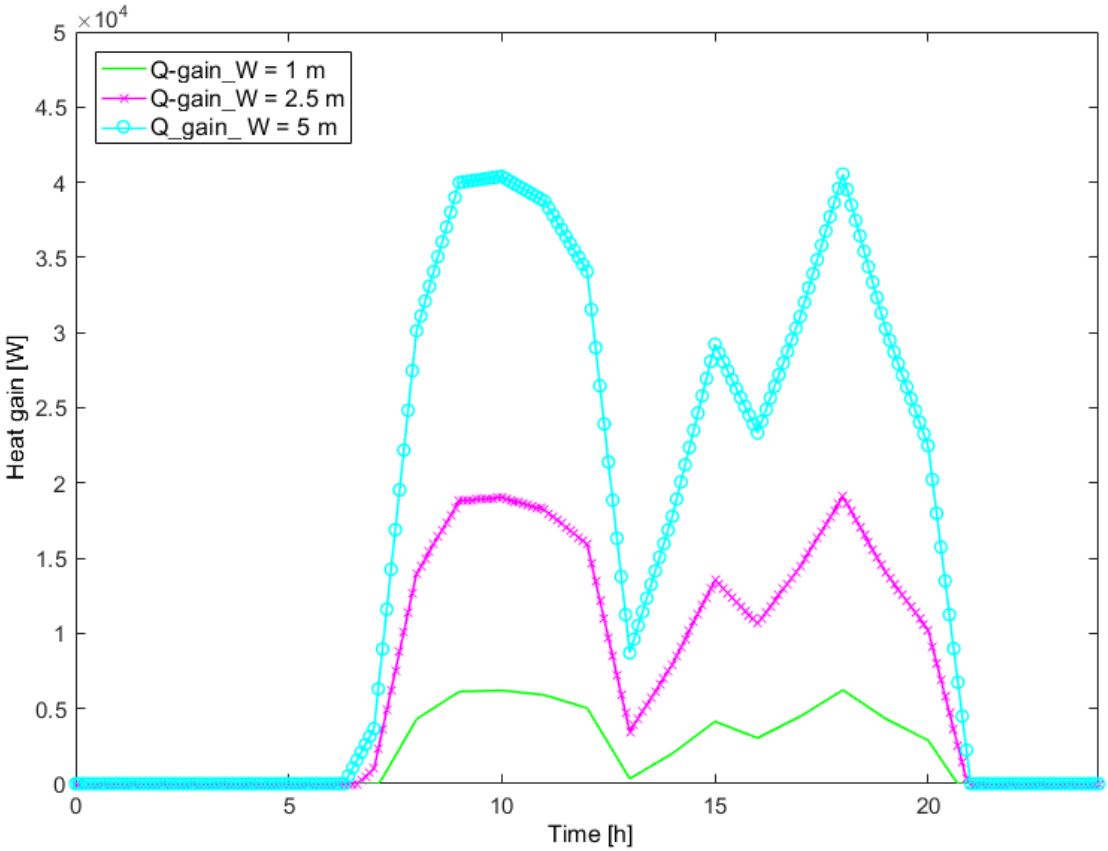

Figure 5.19 Variation of the collector heat gain with different aperture width of the collector

The last case study was that of the variation of HTF with different HTF in the system. The n-propane in the system again has the same heat gain variation, with the steam and ethylene glycol.

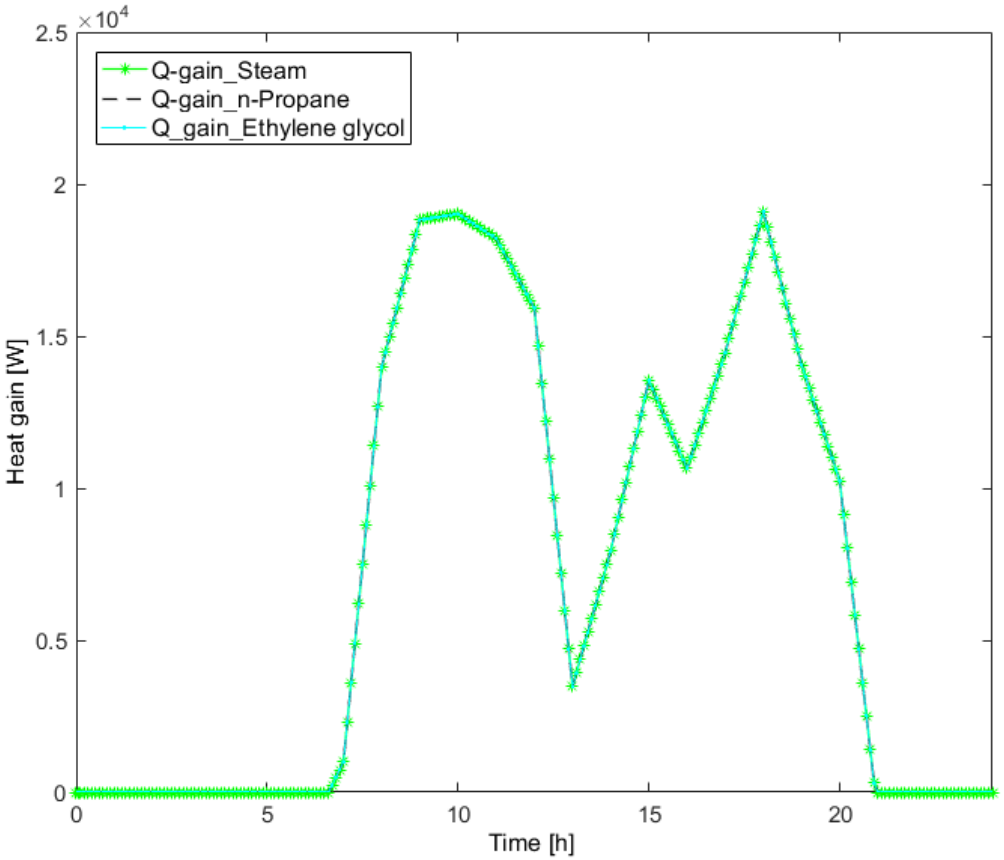

Figure 5.20 Collector heat gain with different HTF in the system

The HTF fluid exit temperature is another important output parameter of the collector. The HTF exit temperature was plotted over the hours of the day with different sizes of the collector regarding the length and aperture width. It was observed that the larger the width of the aperture, the higher the HTF exit temperature. It was also seen that the exit temperature stays almost the same with different lengths considering the one-dimensional length model. The Figures 5.21 and 5.22 confirm the observation for variation due to length and width respectively.

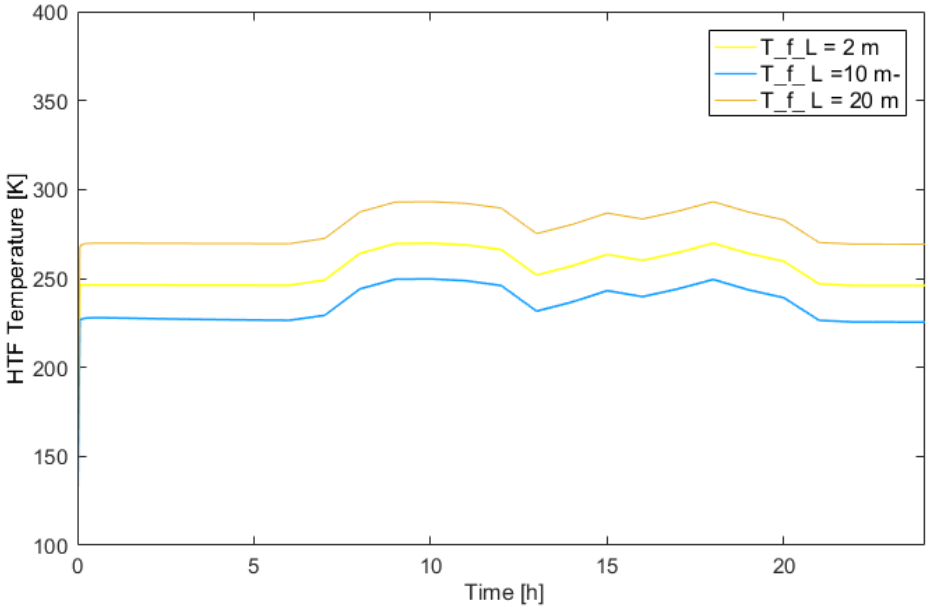

Figure 5.21 Plot of fluid exit temperature for 24 hours at different lengths of the collector

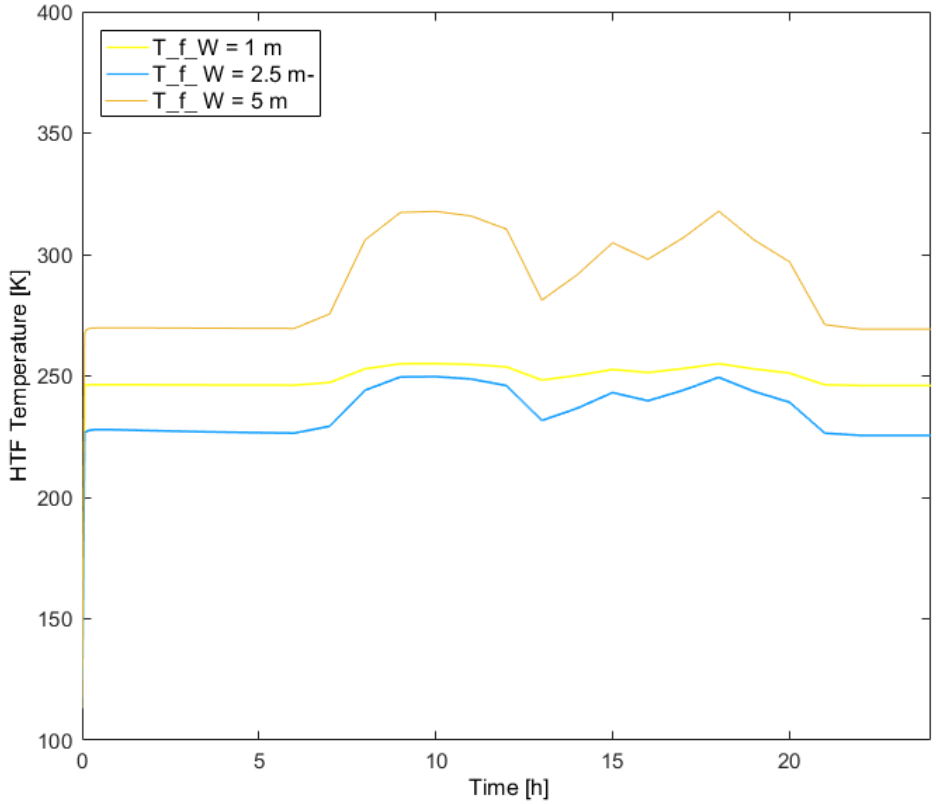

Figure 5.22 Plot of fluid exit temperature for 24 hours at different aperture widths of the collector

Heat loss for the collector was also considered for the hours of the day at different lengths of the collectors. Figure 5.23 shows the heat loss variation and has higher values during the day (12:00 to 14: 00). Figure 5.24 shows that the increase in the length of the collector leads to increase in the heat loss in the collector system.

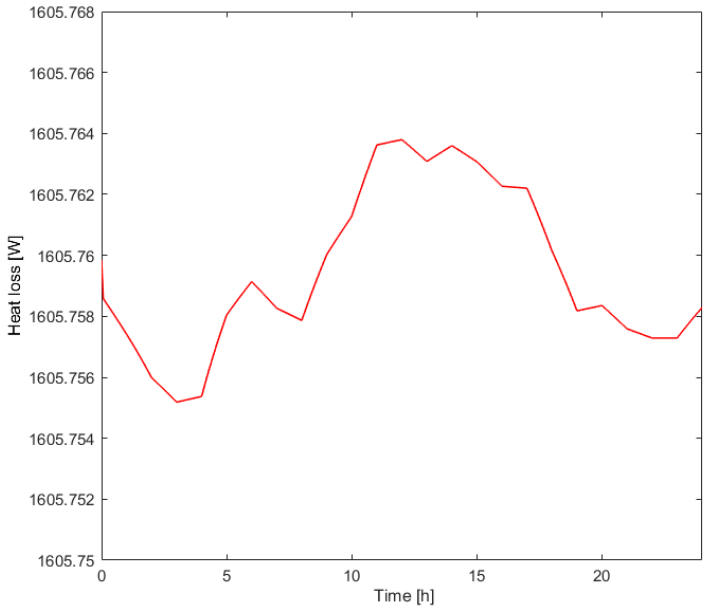

Figure 5.23 Variation of heat loss for a given a day

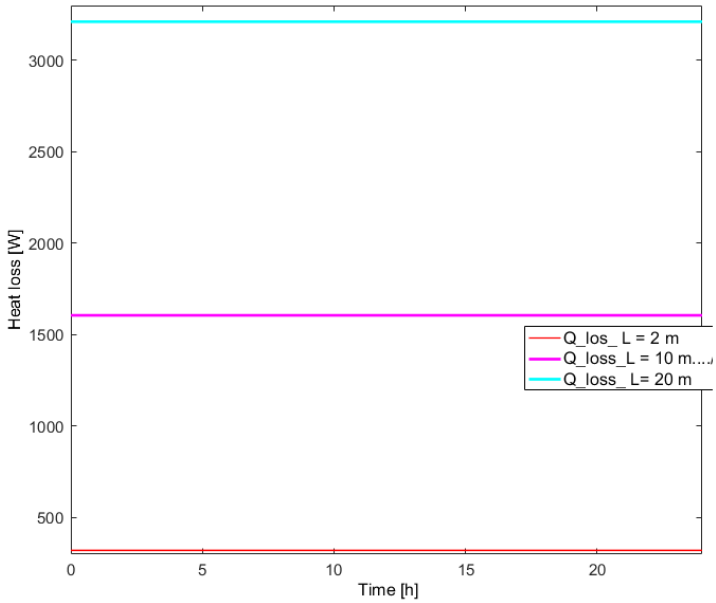

Figure 5.24 Variation of heat loss over a day at different lengths of the collector

The last consideration compares the relationship among the DNI, heat gain and energy losses in the collector. Figure 5.25 shows that the collector raises the energy level for a given loss of heat in the system.

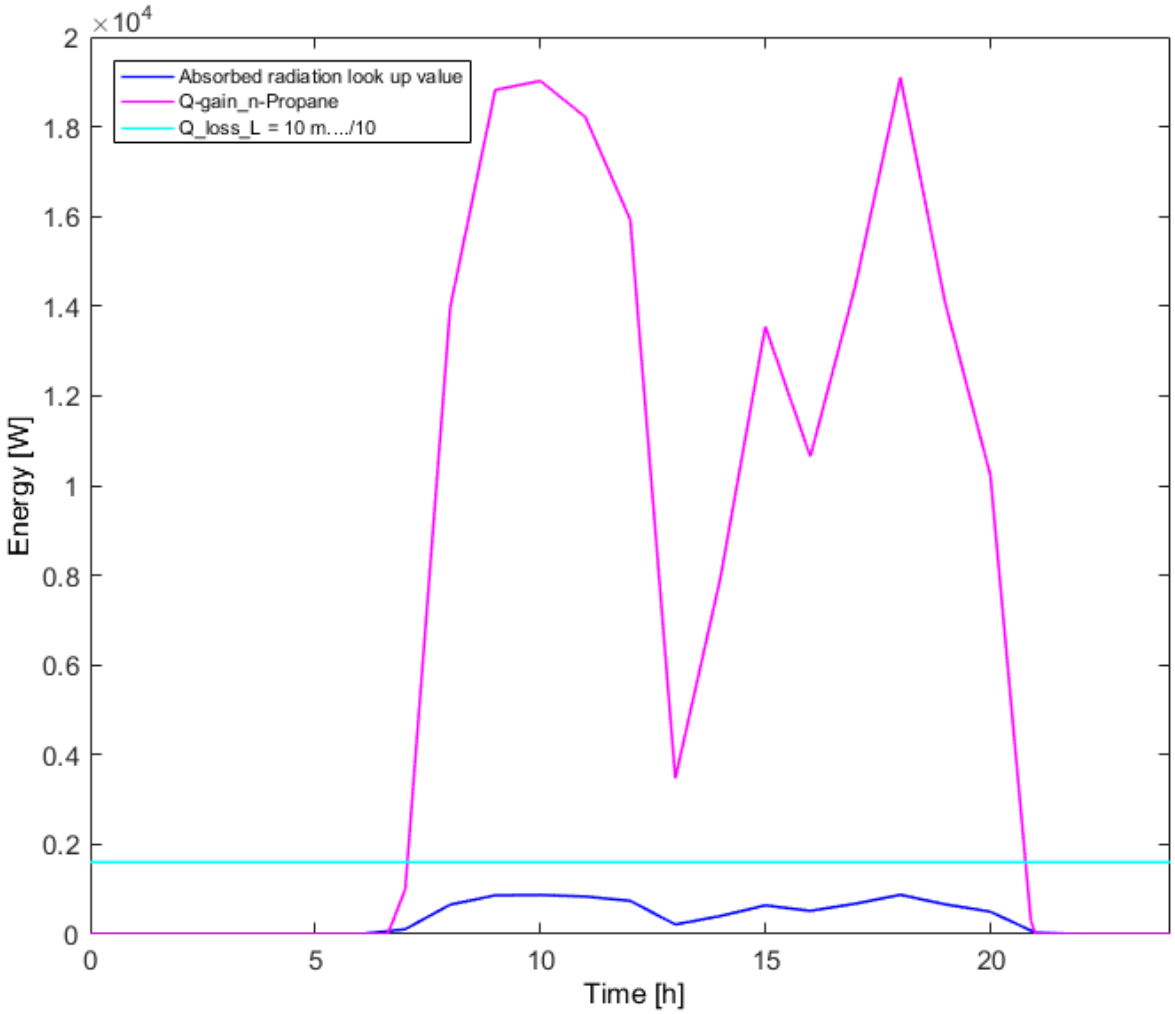

Figure 5.25 Variation of DNI, heat gain and heat loss in the system

5.4 THERMAL STORAGE MODEL

Thermal storage models on the working fluid and heat transfer fluid are utilised in the ORC and the collector part respectively. Thermolib model software in Simulink allows the change of the fluid in the system, the size of the storage and initial condition of the system.

5.4.1 SIMULINK BLOCK FOR THERMAL STORAGE

The blocks of the storage tank in Simulink are shown in Figures 5.26 and 5.27.

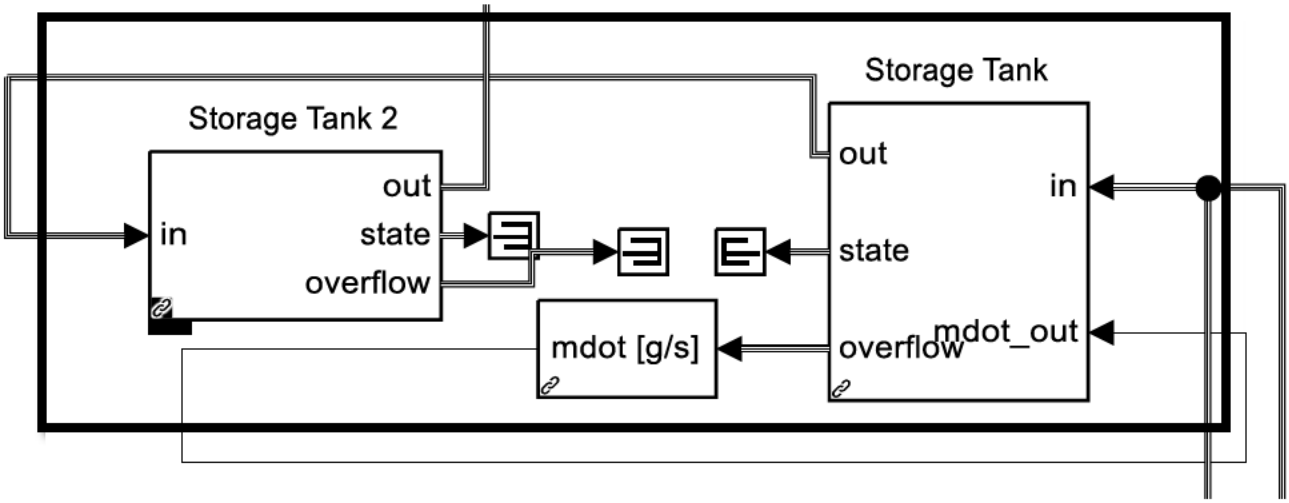

Figure 5.26 Storage tank model in the STORC power plant

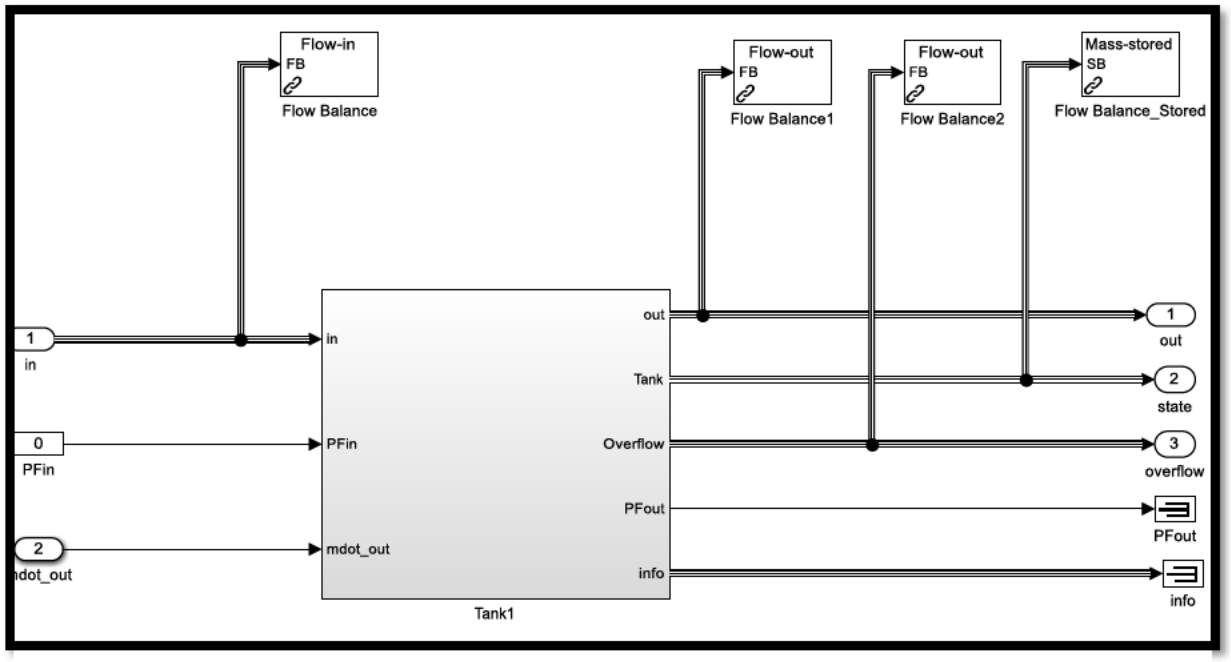

Figure 5.27 Under the mask of the storage model block

5.4.2 RESULT FOR SIMULATION OF THERMAL STORAGE

Figures 5.28 and 5.29 show the comparisons of the temperature and enthalpy before and after storage tank at a different point in the system over 24 hours of the day. It was observed that the storage tank helps to stabilise and accumulate temperature of the system.

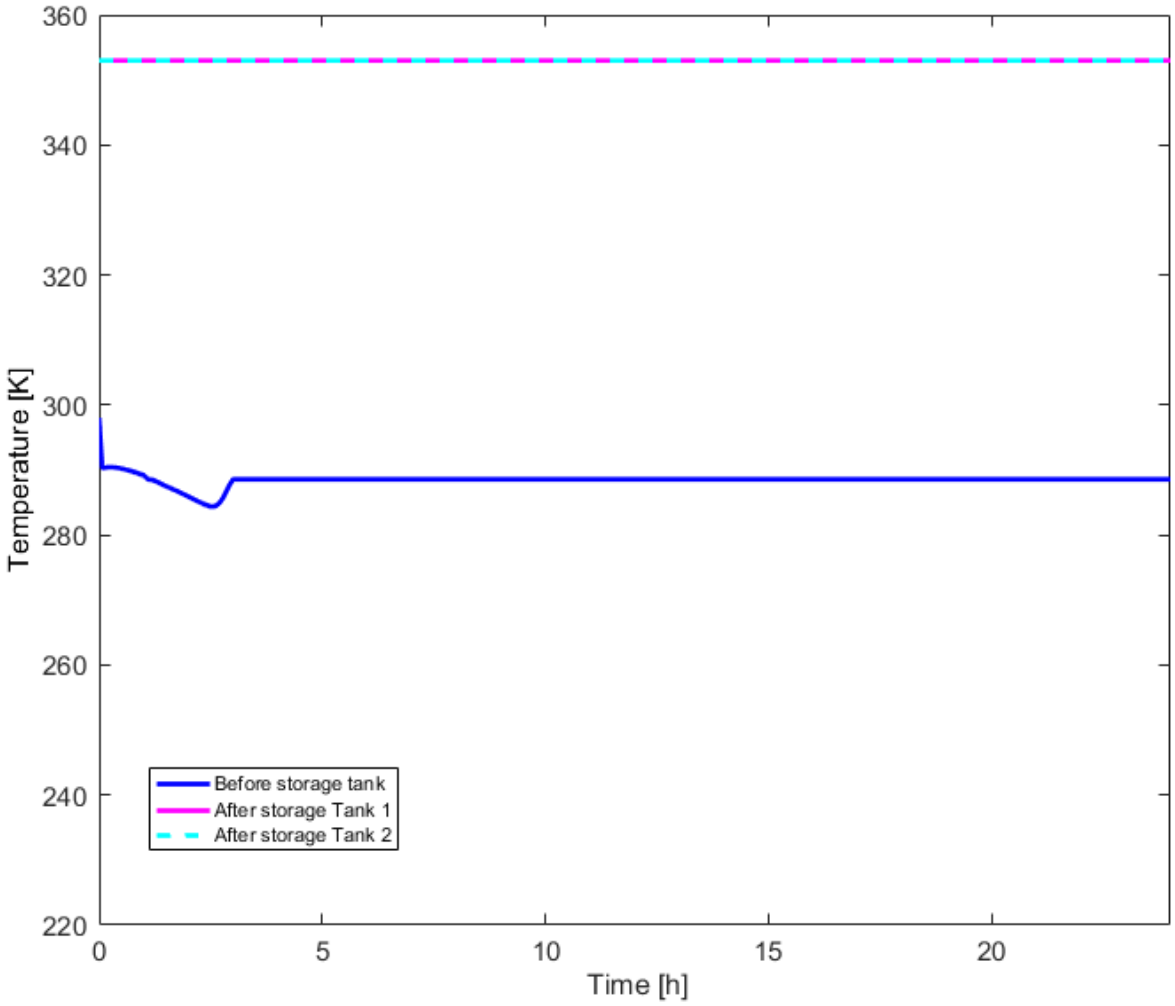

Figure 5.28 Comparisons of the temperature (in K) before it enters and after it leaves the storage tank

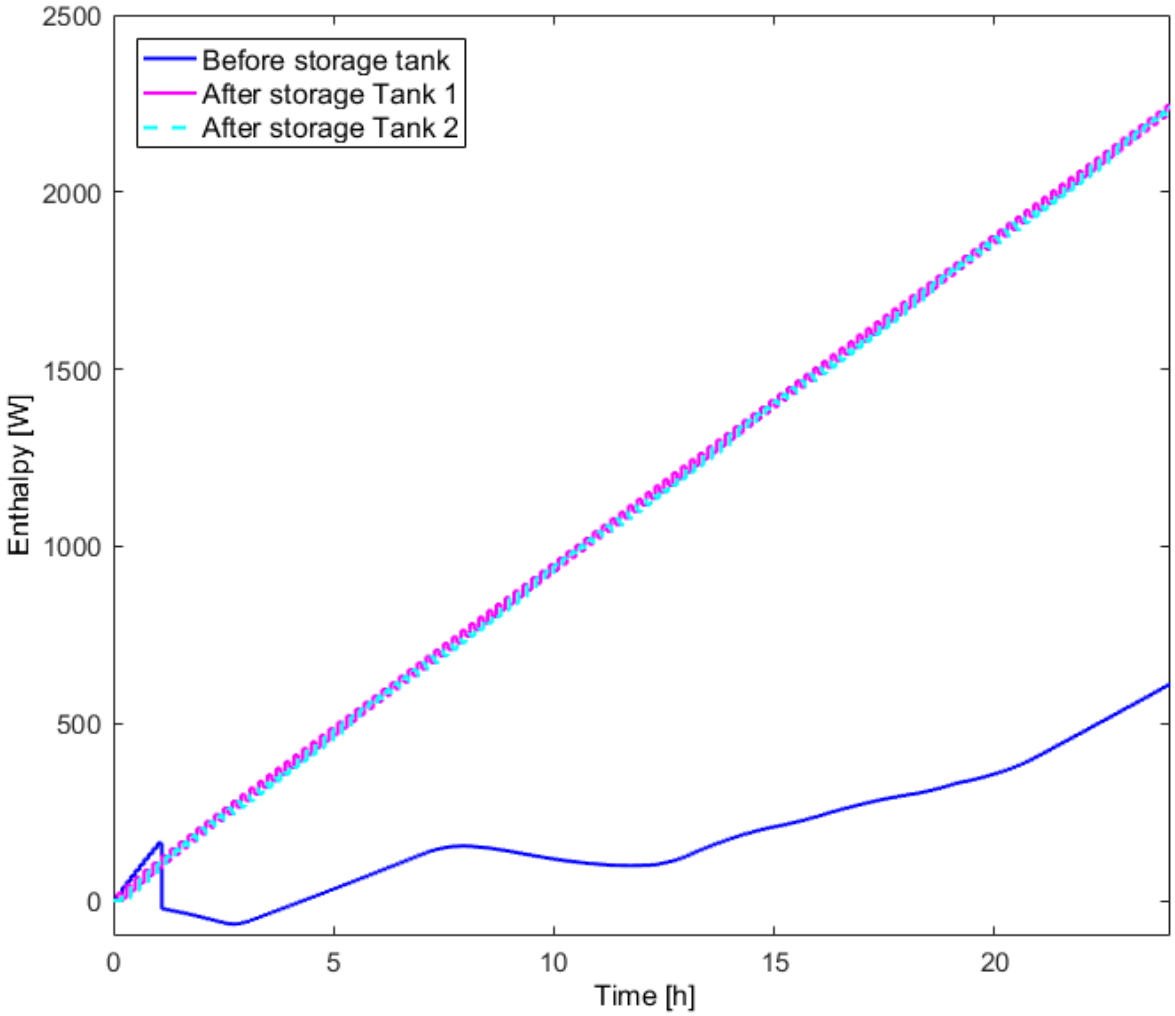

Figure 5.29 comparisons of the fluid enthalpy before it enters and after it leaves the storage tank.

5.5 ORGANIC RANKINE CYCLE MODEL

The model was also implemented with Thermolib Simulink ® library and comprised transfer of energy from evaporator to the turbines, the pump and the WF storage tank.

5.5.1 THE SIMULINK MODEL OF THE ORC PART OF THE SYSTEM

Figures 5.30, 5.31 and 5.32 show the Simulink model of the ORC part of the plant. The Simulink blocks in Figures 5.30, 5.31 and 5.32 determines the power output and thermal efficiency of the plants at the endpoint. A double stage turbine and air cooled condenser was used in the system. On the other hand, the pump and evaporator are set up for pumping and counter flow heat exchange respectively.

Figure 5.31 shows the unmasked block of the evaporator revealing the flow balance, heat exchange and energy balance blocks. The flow and power balance blocks of the turbine and the pump are also shown in Figures 5.32 and 5.33 respectively.

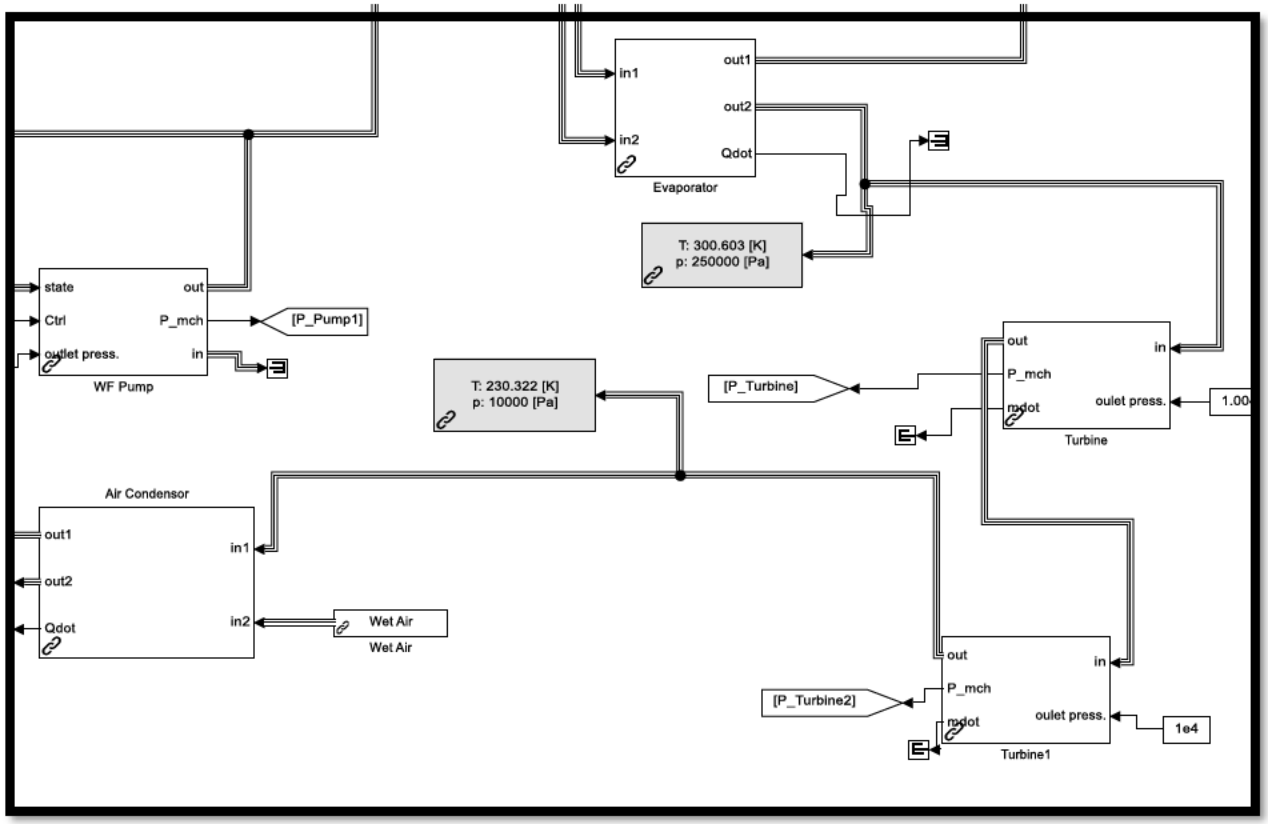

Figure 5.30 ORC part of the STORC power plant

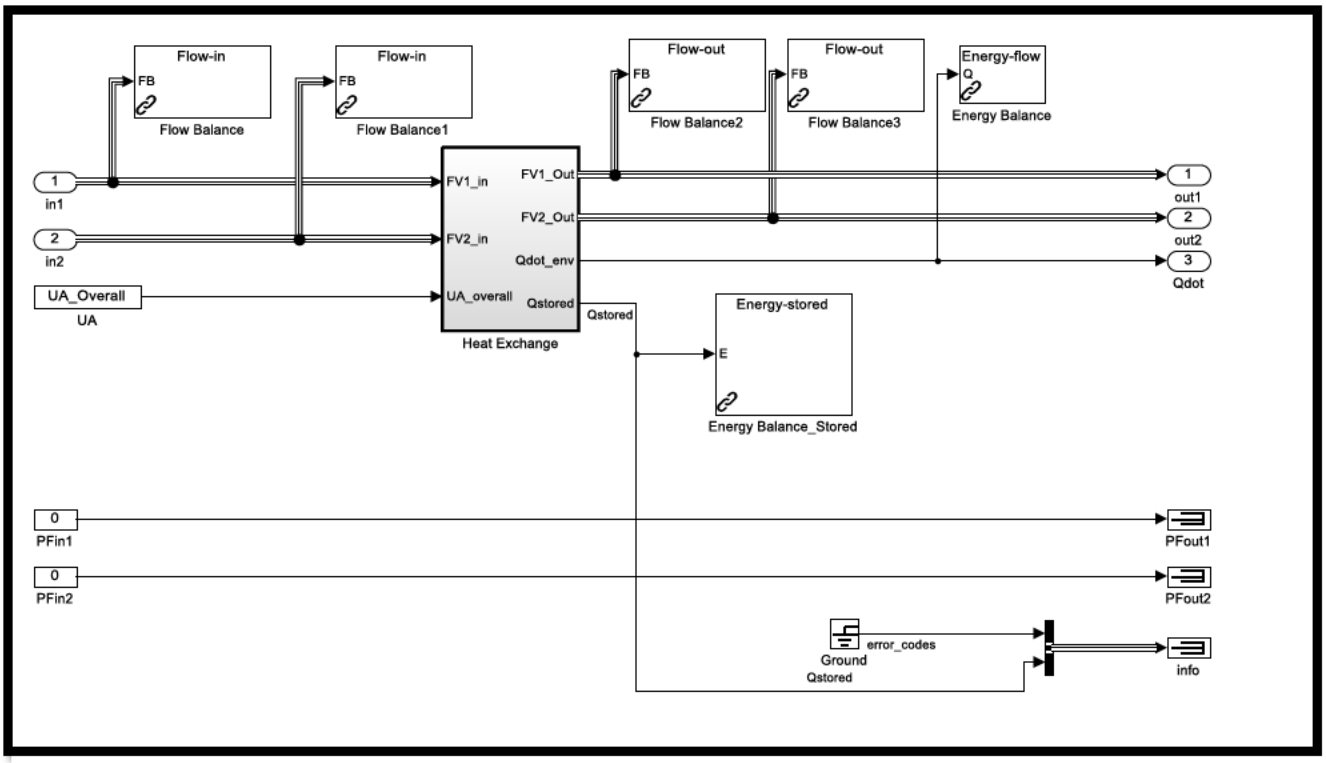

Figure 5.31 Flow, heat exchange and energy balance of the evaporator

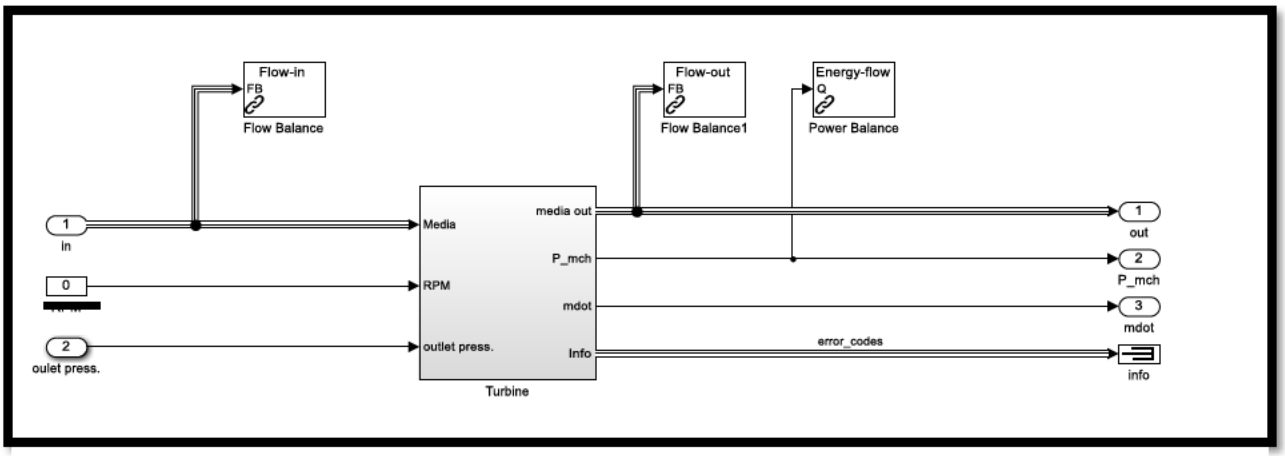

Figure 5.32 Flow and energy rate balance blocks of the turbine

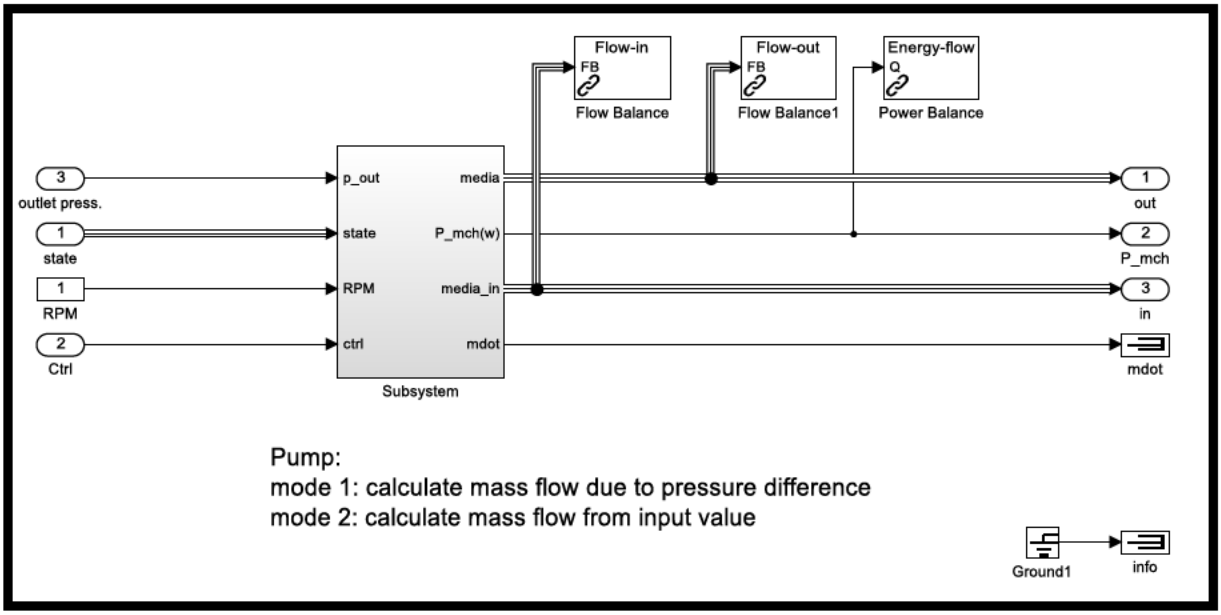

Figure 5.33 Flow and energy rate balance blocks of the pump

5.5.2 RESULT OF THE ORC SIMULATION

Figure 5.34 considers the variations for the hours and can be seen to increase.

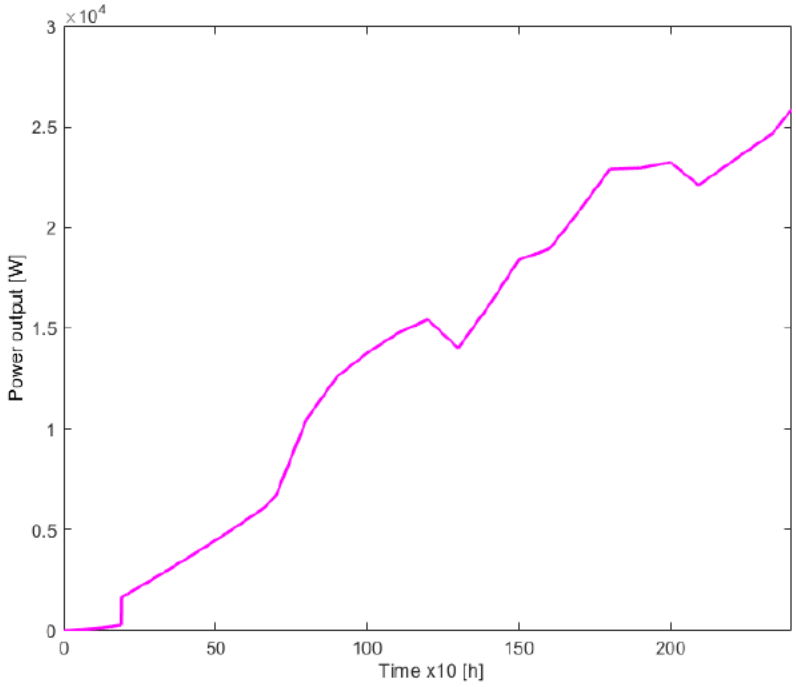

Figure 5.34 Hourly variation of the power output

Figure 5.35 presents the variation of power output with WF and HTF. The plot shows different slopes for the power output indicating how the fluid affects the output of the system.

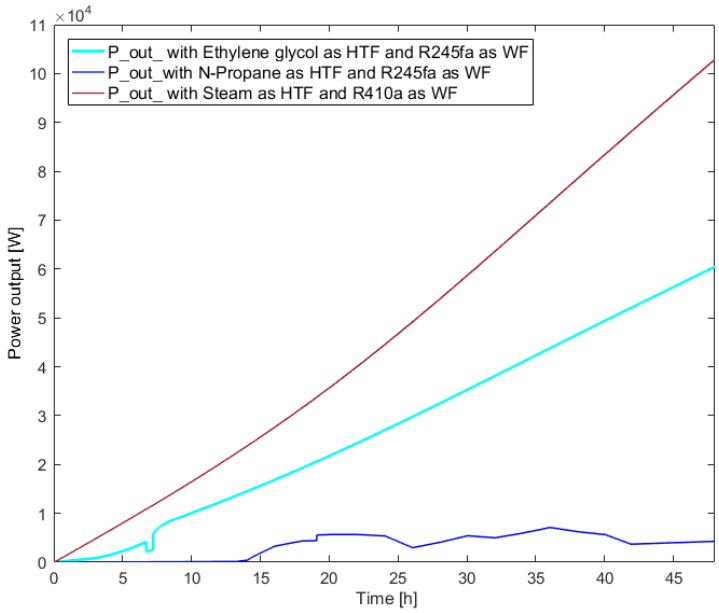

Figure 5.35 Power output for different HTF and WF in the system

The length of the collector has also affected the power output, as seen in Figure 5.36. The slope of the power output curve is steeper for lower length than for higher length, indicating the rapid increase with a shorter or smaller system.

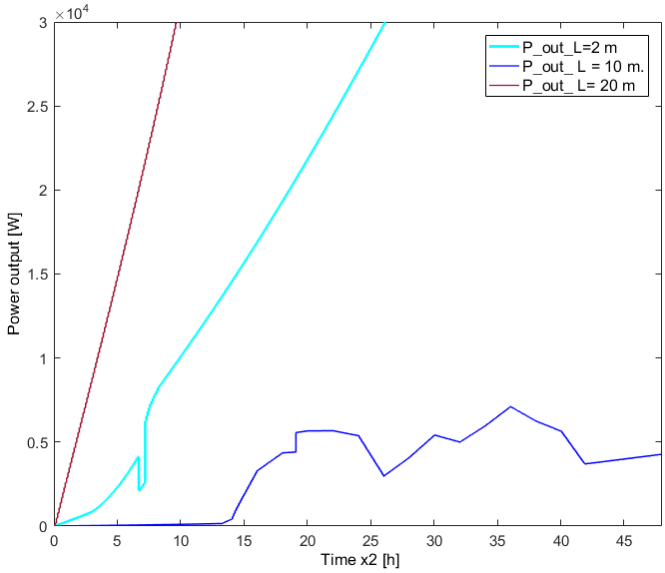

Figure 5.36 Power output with different lengths of the collector

Figure 5.37 shows the cycle efficiency plotted over 24 hours. The curve shows a constant efficiency after the system attains a steady state.

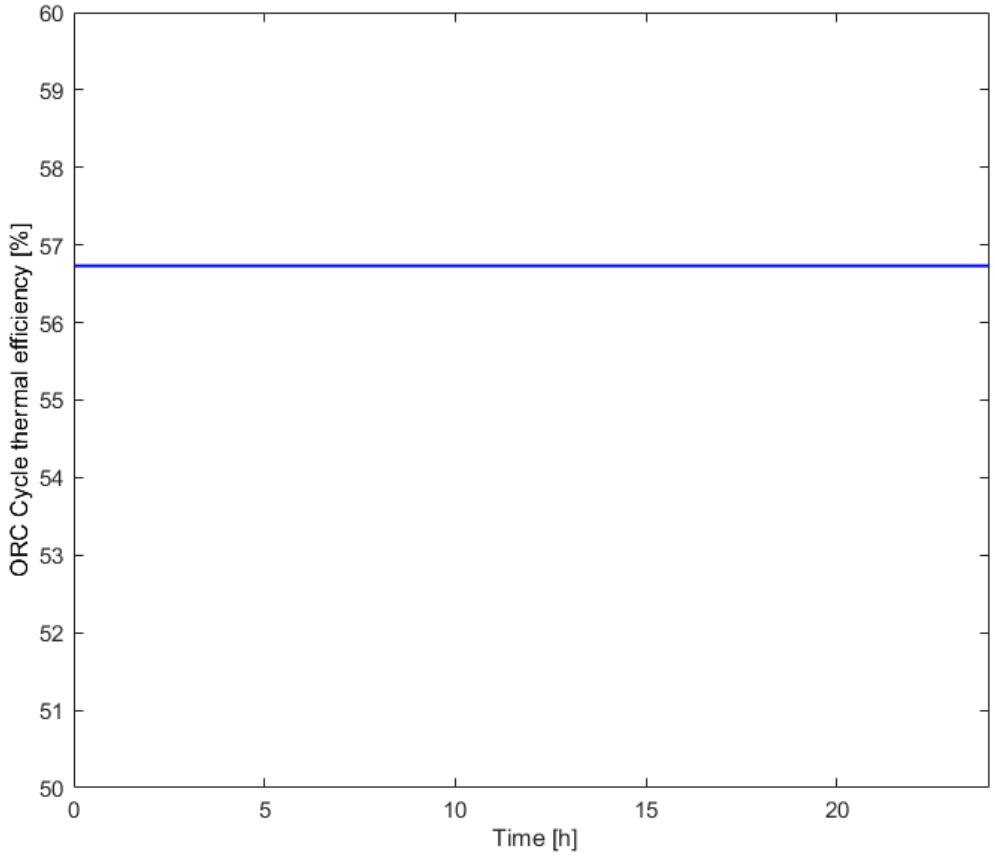

Figure 5.37 Thermal efficiency of the system for the chosen day

Figure 5.38 shows the temperature – enthalpy diagram with isobaric line map for the system's working fluid (R245fa). The figure indicates the increase in entropy for the pumping and heating element but decreases with temperature for the turbines and condensers

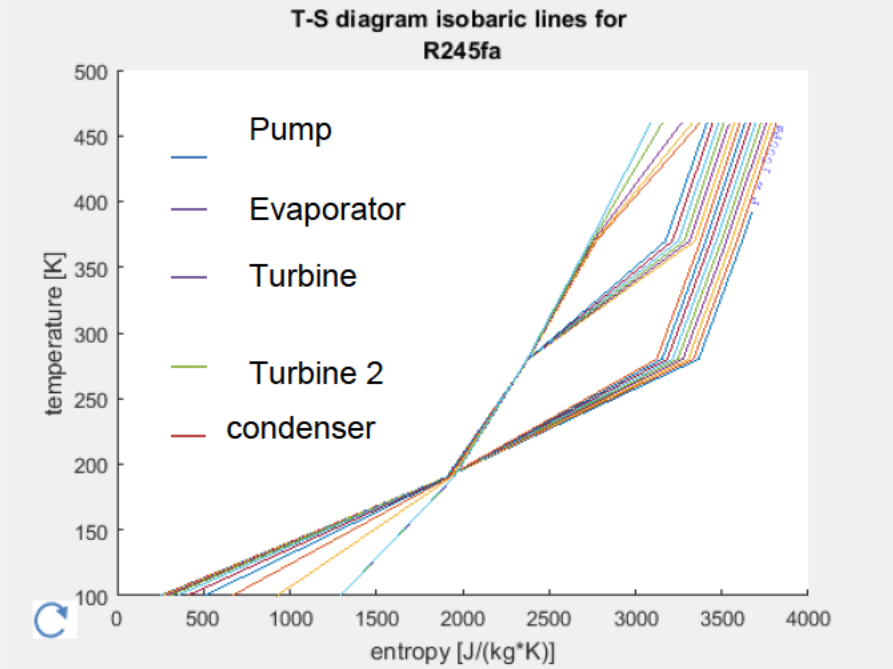

Figure 5.38 Temperature - Entropy diagram isobaric lines for the ORC system WF.

Figure 5.39 is also a plotted temperature - entropy diagram for R245fa showing the constant pressures at the entry and exit of the components of the system

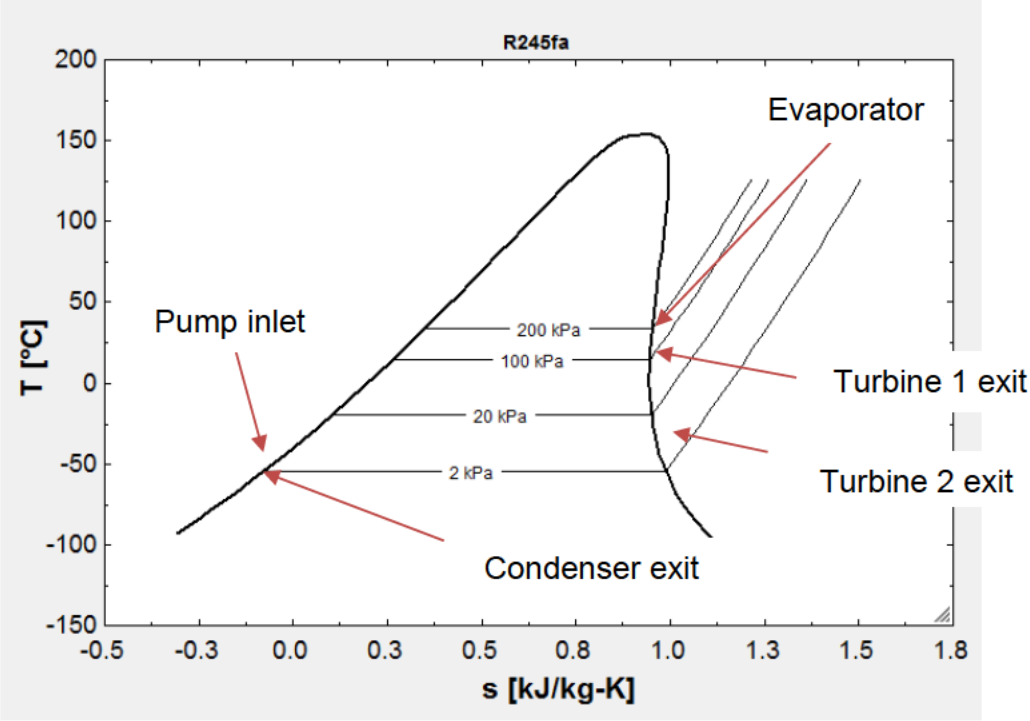

Figure 5.39 Temperature - entropy for R245fa at entry and exit of the components of the system

The pressure - enthalpy diagram was also considered as shown in Figure 5.40, and shows the increase in enthalpies at for heating devices and drops at certain pressures for cooling devices for constant temperatures at each state. The pressure also increases with pumping and drops in the turbine. The blue line represent the constant entropy at some value of enthalpies.

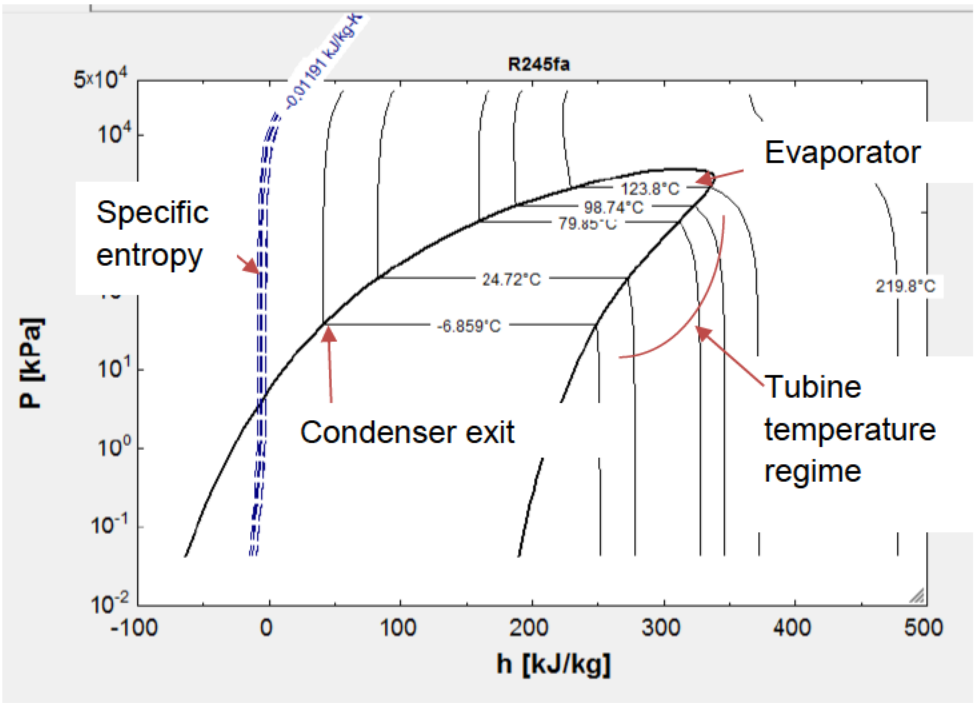

Figure 5.40 Pressure - enthalpy for R245fa at entry and exit points of the components of the system.

5.6 CONCLUSIONS FROM THE RESULTS

The Matlab Simulink ® and the Thermolib Simulink ® generated results from simulations that predict the output and performance of the STORC power plant. The model is also capable of modelling vast numbers of the parameter that includes the diameter of the receiver and glass envelope changes with the system output, the mass flow variation with the efficiency, the heat gain, heat loss and collector efficiency variations with the average HTF fluid exit temperature and other sensitive parameters.

CHAPTER 6

SIMULATION RESULTS: COMPARISON AND VALIDATION

This chapter presents the discussion and comparison of the ORC plant model. The model validity requires a reality check of the results and comparison with other existing models.

6.1 RESULTS AND VALIDITY OF ENERGY RESOURCE DATA

The weather data for the study was taken from SAURAN, as mentioned in the literature. SUARAN website was created from combined effort of various organisations. The statistics of the data used for the model allow further verification. The lookup results presented in the later part of Section 5.1.2 were validated by re-checking the data as shown in Table 6.1 against that of Table 4.1 and were found to be very accurate.

The hourly solar radiation data for South African weather is not available from the South African Weather Service. Investigation shows that this solar radiation data is not easily obtained on most databases except for the SAURAN database. Other weather elements required for the model include windspeed, atmospheric pressure and atmospheric temperature. A comparison was made below but with the weather station instrument mounted at a different location in the same place would result in some differences in the statistical values.

Table 6.1 The comparison of Bloemfontein's weather data from SAURAN with that of SAWS

	Air_Temp (° C)				WS (m/s)				BP (mbar)			
statistics	SAURAN		SAWS		SAURAN		SAWS		SAURAN		SAWS	
	Value	Time	Value	Time	Value	Time			Value	Time		
Maximum	28.750	19	29.600	13	6.756	12	6.500	14	855.000	9	863.600	7
Minimum	18.260	7	16.700	5	1.419	3	0.800	0	851.000	19	859.700	17
Peak to peak	10.490		12.900		5.337		5.700		4		3.9	
Mean	22.915		22.494		3.790		3.990		853.145		861.904	
Median	22.249		21.765		3.102		3.500		855.000		861.845	
Root Mean Square	23.193		22.976		4.102		4.374		853.146		861.905	

As seen from the statistical table, the values are not exactly the same. The discrepancy in values does not imply that data from a given database is incorrect. The discrepancies could be due to the location, altitude and direction the instrument is facing.

The data from SAWS was taken at latitude of -29.1030 °, longitude of 26.2980 ° and elevation of 1354 m, while that for SAURAN was taken at latitude: -29.1107 °, longitude 26.18503 ° and elevation of 1491 m. Both locations are in Bloemfontein but at different areas and elevations.

The SAURAN data is actually of high resolution and is reliable for use in the model.

6.2 RESULT AND VALIDATION OF SOLAR-THERMAL COLLECTORS MODEL

6.2.1 Output parameters hourly variation for the day

The result focused on the factors that change with time. As present in the literature, Forristall (2003), provided some model results from PTC. The results are not based on the South African weather but sensitivity analysis with variation in time is useful for model validation. The plotted outputs from the model and the statistical analysis were used for validation.

The EES data and the KJC test-loop data, plotted in Forristall (2003) results shows that the heat gain and outlet temperatures for the day follow a DNI curve. The results were also compared the data collection day with those of a similar plant like the AZTRAK.

Figures 6.1 and 6.2 show the plot of the heat gain and loss for different models respectively. The input parameter from the AZTRAK test was used on the present model, and the results were plotted for the different cases. The graph shows that the discrepancy between results in both cases is within 10 %. The same procedure was applied to check the other output parameters of the collector, and the maximum discrepancy was 15 %. The output from the graphical presentation of the outputs indicates that the collector model is acceptable.

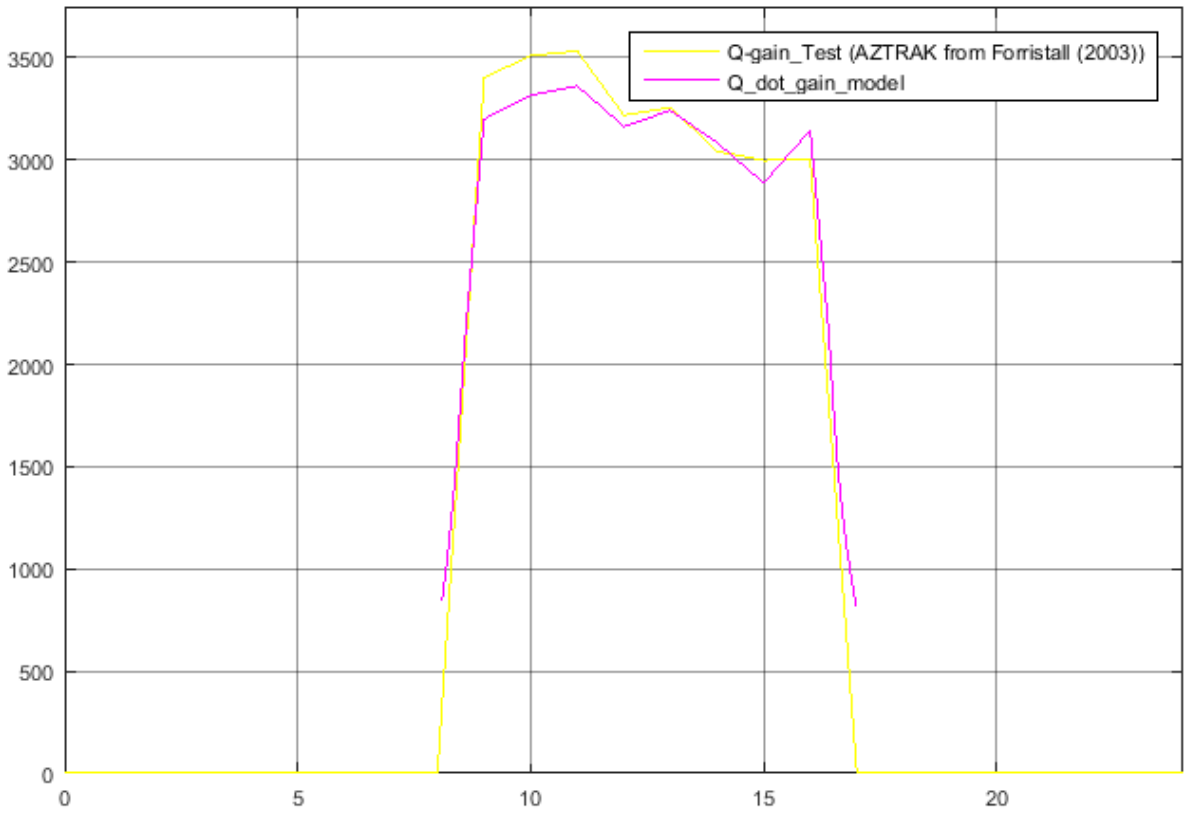

Figure 6.1 Heat gain (in Watt on Vertical axis) of the test model compared to heat gain of the present model over a day (in hours on horizontal axis)

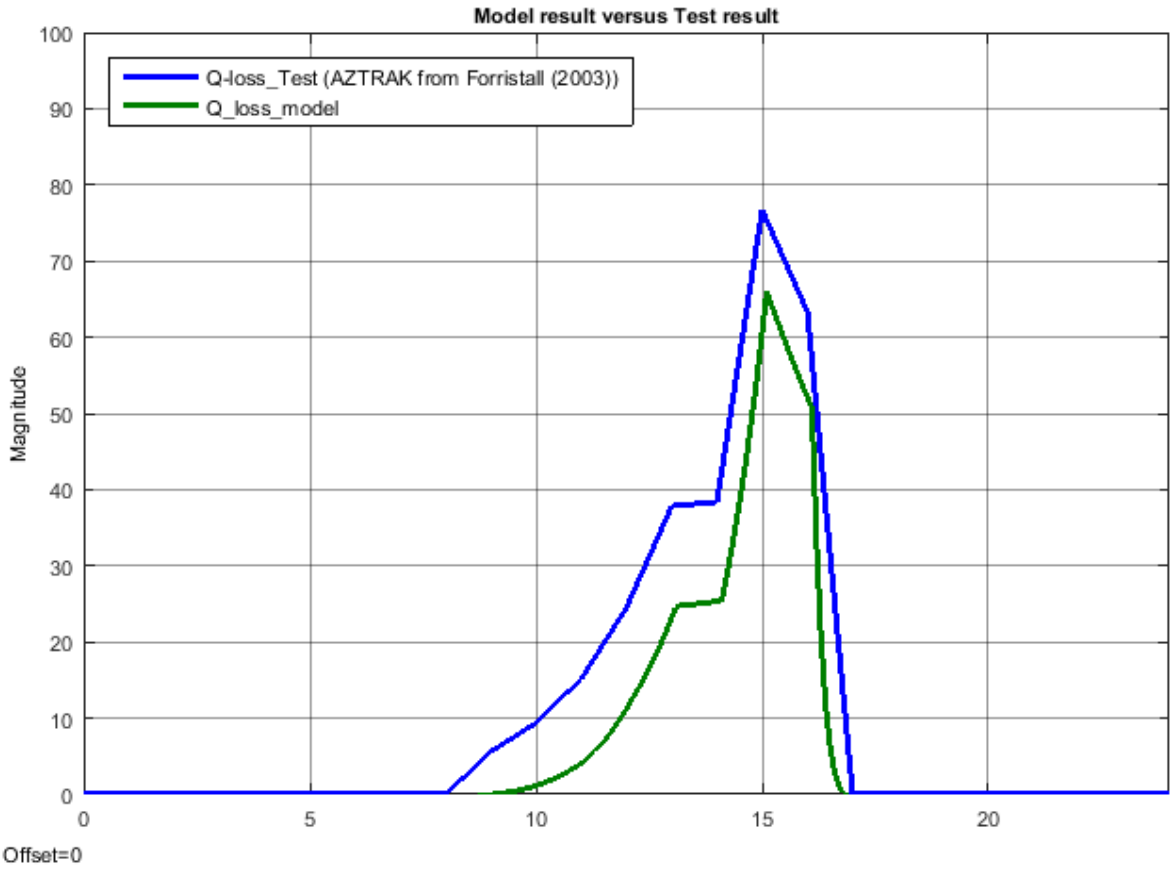

Figure 6.2 Heat loss (in Watt on vertical axis) of the test model compared to heat loss of the present model for the hours of the day (on the horizontal axis)

6.3 VALIDATION OF SOLAR-THERMAL STORAGE MODEL

The main function of the storage is to retain and stabilise temperature fluctuations. Figure 5.28 shows the storage model goal was achieved and with the appropriate heat energy and flow balance; the storage model shows a realistic result. Retention and the stability are shown regarding the temperature of fluid before entering and after leaving the storage tank. It could also be seen that the second storage tank did not affect the state of the system. From the results presented, the storage model is acceptable.

6.4 RESULT AND VALIDATION OF ORGANIC RANKINE CYCLE

6.4.1 PROPERTY DIAGRAM AND POWER OUTPUT MODEL

Based on the rapid screening analysis, the temperature-entropy diagram for a specific process were investigated. Figure 6.3 shows the temperature-entropy diagram for refrigerant R245fa in the ssytemand 6.4. The diagram property values at each state in the processes were screened, and the results correspond. This indicated that the ORC model is acceptable on a rapid screening test.

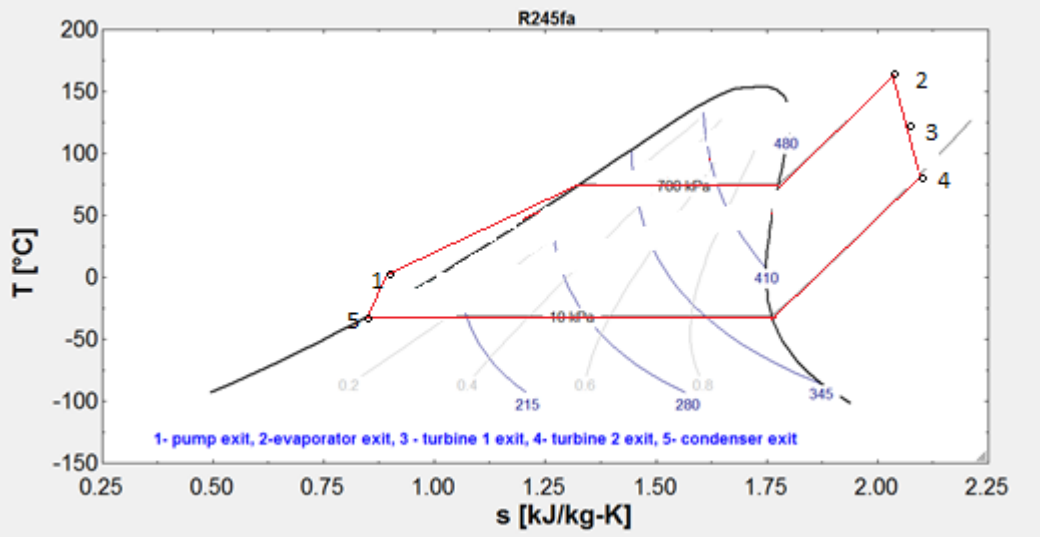

Figure 6.3 Temperature-entropy plot for a given setup

Figure 6.4 presents a rapid screening using Pressure – enthalpy diagram. The fluid properties consider the pressure and specific enthalpy are as shown for R245fa in the system.

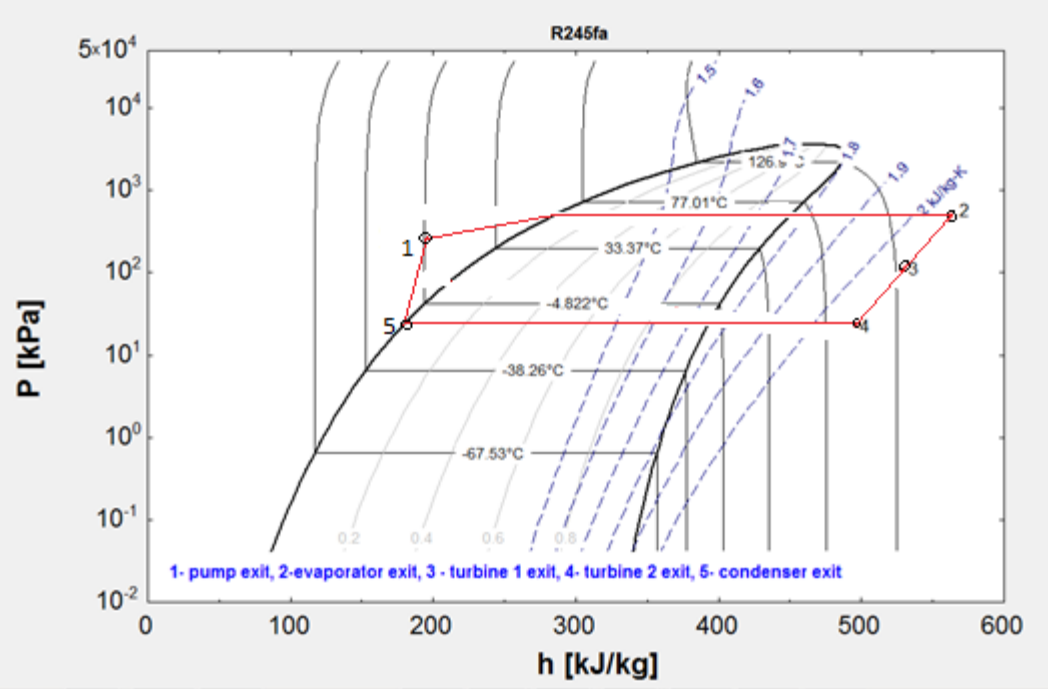

Figure 6.4 Pressure - enthalpy diagram for a chosen configuration

6.4.2 POWER OUTPUT VALIDATIONS

Data and configuration from the Lesotho plant were applied to the current model, and the results for the power output were compared. The power output data presented was only for some specific time of day. The hourly average power output data for the 11th, 12th, 15th and 16th was considered for validation as the results were not presented for all the hours of the day. The result plotted in Figure 6.5, shows that even with the estimated data, the discrepancy between result is not significant. The trend averages shows a less significant difference. Based on the little difference, the ORC model is acceptable.

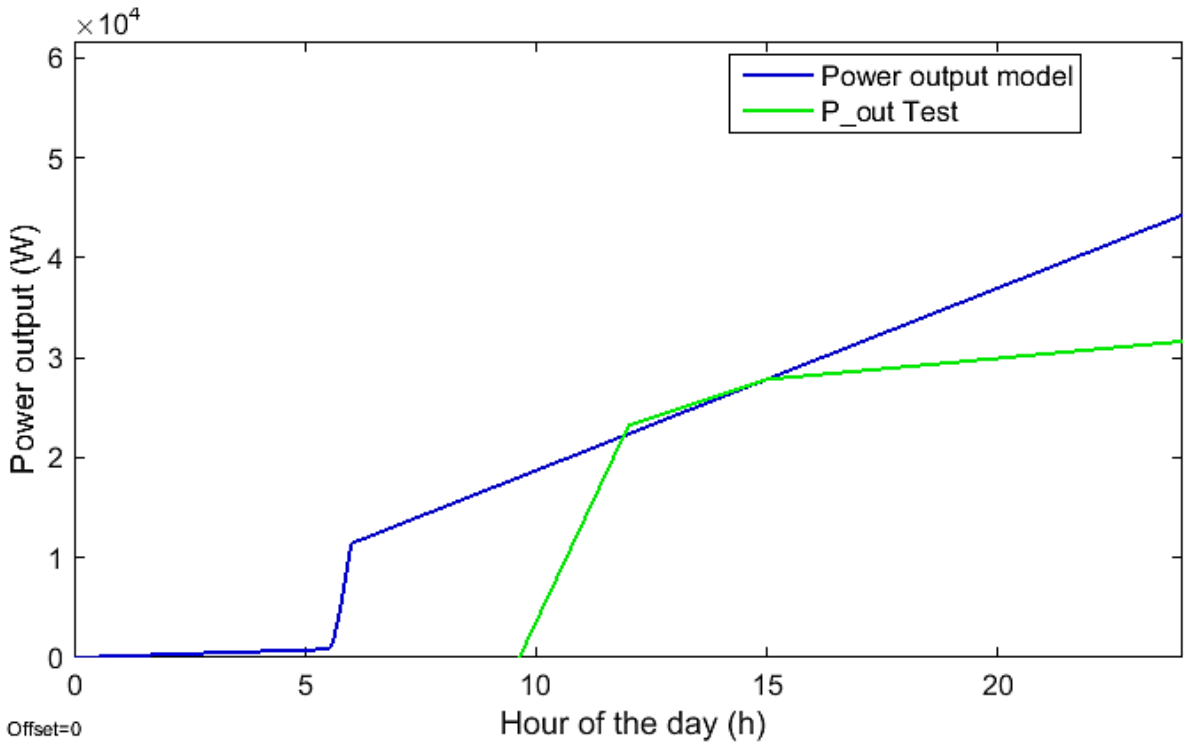

Figure 6.5 Power output comparison with SORC model

6.5 DISCUSSION OF OUTPUTS

The need for useful energy from a properly functioning STORC power plant led to the predictive modelling of the plant to limit costs in plant installation. The Solar Resources Model data were taken from a reliable source as validated, and the model could be modified for other locations globally. From the results and validations, the verified solar irradiance values presented data that could be used to predict the available solar irradiance for a particular location. The solar resources provided the required hourly outputs to the collector model.

Energy from solar irradiance needs to be converted into internal energy of a fluid (HTF) in the form of heat by increasing the heat in the fluid. The process is achieved via solar-thermal collectors. The model required values from the Resources Model and other required parameters to analyse the type of collector applicable to the plant. A one-dimensional model was developed by adopting a valid model and the principles of thermodynamics. Useful energy gain, HTF outlet temperature and collector thermal

efficiencies were determined from the model at the given input parameters. Validation was done on the variation for useful output parameters, and reasonable similarities were found when compared to other models. The main problem with the solar-thermal collector model results, was the issue to obtain all required values on validation; this is due the fact that all plants have varying configuration. Validation of the heat gain, the outlet temperature of HTF and efficiencies provided a realistic base for optimisation and prediction. The fluid from the collector system then enters the thermal storage.

As thermal energy is required for storage and stability in the power plant, the thermal storage was included in the Model. With the aid of Simulink ® Thermolib library, it was very convenient to model the storage. The results and validations also show the worth of the modelling.

Useful energy from the thermal storage is required in the ORC engine section of the plant. There are vast numbers or configurations available for ORC pertaining to various applications. A configuration was chosen based on the outcome of the screening, and the load analysis shows a positive outcome.

CHAPTER 7

CONCLUSION AND RECOMMENDATIONS

7.1 CONCLUSION

The primary aim and objective of the study were achieved. The model of the STORC power plant was designed using numerical analysis of the energy transfer involved with the technology.

Presently, there is increasing growth in the use of CSP for alternative energy technology. Modeling of the STORC power plant with considerations of the improvement in performace and cost of the technologis has highly contributed to the solution to the increasing demand for alternative energy. For the past decade now, the adoptatation of CSP technology and other alternative mean of generating clean energy improved drastically.

From this studies, the following outcome were achieved;

- Reliable tool to obtain the amount of energy resources available for a specific location of interest.
- Optimal design and operation for the PTC considering the material properties, geometric size and thermophysical considerations.
- The effect of incorporating the thermal storage in the STORC power plant performance of the plant
- Conceptual determination of the optimal configuration of the ORC units of a plant.
- Overall output of the STORC power plant with variation in sizes and configurations.

From the study results and validations, the verified solar irradiance values sourced from the database could be used for correct input parameters for the collector model. The values from SAURAN were compared to other values from different weather

databases and provided reasonable acceptance after statistical analysis. The solar-thermal collector of the model determines the useful energy gain, HTF outlet temperatures and collector thermal efficiencies and other useful parameters for analysis. It was observed that the larger the aperture and the longer the length of the collector, the higher the heat gain. Concerning storage, the correct storage capacity must be chosen to achieve the required performance. From the ORC engine model, the power output shows a realistic output could be generated from the plant. It was also found from a recent investigation that the PTCs technology is now in operation by Abengoa's in KaXu Solar One, located near the town of Pofadder in the Northern Cape Province of South Africa. Other plants are under construction and are also located the in the Northern Cape Province. The plants are the Khi Solar One, which is expected to generate around 50 MW and Xina,which has a total installed capacity of 100 MW.

The model will be useful for future maintenance and optimisation of the related plants.

The model provided reasonable up to standard accuracy. The model in Matlab Simulink ® was validated with other models and the outcomes proved the conformity of the models. The model design provided an opportunity for testing various parameters from other studies and projects. Practical and analytic prediction for implementation of plants were based on operation and sizing related to both dimensions of components and the capacity of the engine. Marching efficiencies and boundary conditions of a plant compared to another plant provided means for optimisation.

The research provides more awareness of and avenues toward exploring Concentrating Solar Power (CSP) technologies in the Engineering study. The research study area on the type of CSP technology is not only a mechanical engineering-based technology; it involves the knowledge of other fields of engineering. The model could accommodate the knowledge of Information Technology, Electrical and Electronic Engineering. The structural aspect of the plants

could be developed and modelled by researchers in the field of Civil Engineering and Building Technology.

The model is unique and powerful based on adaptability to the component choice of the plant and also allows vast configuration for the STORC power plant. With the Matlb Simulik and Thermolb, it is easier and faster for achieve the outcome for most STORC power plant of interest.

Substantial knowledge and understanding of thermodynamics as applied to alternative energy was applied and gained. There is potential for further contributions to this field of study in future.

7.2 RECOMMENDATIONS

Firstly, based on the workload involved in this type of research, it is recommended that similar studies be performed by researchers, as this would render more information on optimisation of the applicable plants. Secondly, prototyping of the plant for a niche area in future could lead to accurate and benchmarked development of STORC technology. More alternatives to the application of the technology and innovations would emerge.

Future Work

The following is recommended for future work related to this research project:

- Increase the accuracy of the models;
- Model the technology considering variations in components;
- Modelling toward other configurations of plant components;
- Prototyping of the solar-thermal ORC power plant;
- Study involving hybridization of the plant with other plants, especially upgrading existing power generation;

- Detailed transient modelling of a complete model; and
- Study of heat losses in CSP technologies.

REFERENCES

Alguacil, M., Prieto, C., Rodriguez, A. and Lohr, J. (2014). Direct Steam Generation in Parabolic Trough Collectors. *Energy Procedia*, 49, pp.21-29.

Ali Tarique, M., Dincer, I. and Zamfirescu, C. (2014). Experimental investigation of a scroll expander for an organic Rankine cycle. *International Journal of Energy Research*, 38(14), pp.1825-1834.

Allen, K. (2015). *Performance characteristics of packed bed thermal energy storage for solar thermal power plants*. Msc. University of Stellenbosch.

Al-Mohamad, A. (2004). Global, direct and diffuse solar-radiation in Syria. *Applied Energy*, 79(2), pp.191-200.

Alonso-Montesinos, J., Batlles, F. and Bosch, J. (2015). Beam, diffuse and global solar irradiance estimation with satellite imagery. *Energy Conversion and Management*, 105, pp.1205-1212.

Al-Sanea, S., Zedan, M. and Al-Ajlan, S. (2004). Adjustment factors for the ASHRAE clear-sky model based on solar-radiation measurements in Riyadh. *Applied Energy*, 79(2), pp.215-237.

Anderson, R., Bates, L., Johnson, E. and Morris, J. (2015). Packed bed thermal energy storage: A simplified experimentally validated model. *Journal of Energy Storage*, 4, pp.14-23.

Arkar, C. and Medved, S. (2005). Influence of accuracy of thermal property data of a phase change material on the result of a numerical model of a packed bed latent heat storage with spheres. *Thermochimica Acta*, 438(1-2), pp.192-201.

Astolfi, M., Romano, M., Bombarda, P. and Macchi, E. (2014). Binary ORC (organic Rankine cycles) power plants for the exploitation of medium “low-temperature geothermal sources” Part A: Thermodynamic optimisation. *Energy*, 66, pp.423-434.

Avila-Marin, A., Alvarez-Lara, M. and Fernandez-Reche, J. (2014). A Regenerative Heat Storage System for Central Receiver Technology Working with Atmospheric Air. *Energy Procedia*, 49, pp.705-714.

Bamgbopa, M. and Uzgoren, E. (2013). Numerical analysis of an organic Rankine cycle under steady and variable heat input. *Applied Energy*, 107, pp.219-228.

Bao, J. and Zhao, L. (2013). A review of working fluid and expander selections for organic Rankine cycle. *Renewable and Sustainable Energy Reviews*, 24, pp.325-342.

Benmansour, A., Hamdan, M. and Bengeuddach, A. (2006). Experimental and numerical investigation of solid particles thermal energy storage unit. *Applied Thermal Engineering*, 26(5-6), pp.513-518.

Bi, J., Huang, J., Fu, Q., Ge, J., Shi, J., Zhou, T. and Zhang, W. (2013). Field measurement of clear-sky solar irradiance in Badain Jaran Desert of Northwestern China. *Journal of Quantitative Spectroscopy and Radiative Transfer*, 122, pp.194-207.

Bindra, H., Bueno, P., Morris, J. and Shinnar, R. (2013). Thermal analysis and exergy evaluation of packed bed thermal storage systems. *Applied Thermal Engineering*, 52(2), pp.255--263.

Bindra, H., Bueno, P., Morris, J. and Shinnar, R. (2013). Thermal analysis and exergy evaluation of packed bed thermal storage systems. *Applied Thermal Engineering*, 52(2), pp.255-263.

Bird, R. and Hulstrom, R. (1981). *A Simplified Clear Sky Model for Direct and Diffuse Insolation on Horizontal Surfaces*. Cole Boulevard: Solar Energy Research Institute.

Bracco, R., Clemente, S., Micheli, D. and Reini, M. (2013). Experimental tests and modelization of a domestic-scale ORC (Organic Rankine Cycle). *Energy*, 58, pp.107-116.

Brooks, M., du Clou, S., van Niekerk, W., Gauché, P., Leonard, C., Mouzouris, M., Meyer, R., van der Westhuizen, N., Evan Dyk, E. and Vorster, F. (2015). SAURAN: A new resource for solar radiometric data in Southern Africa. *Journal of Energy in Southern Africa*, 26(1), pp.2-10.

Cheng, H., Yu, C. and Lin, S. (2014). Bi-model short-term solar irradiance prediction using support vector regressors. *Energy*, 70, pp.121-127.

Cheng, Y. (2011). Super capacitor applications for renewable energy generation and control in smart grids. pp.1131--1136.

Ciolkosz, D. (2009). SASRAD: An hourly-timestep solar radiation database for South Africa. *Journal of Energy in Southern Africa*, 20(1), p.10.

Colomer, G., Chiva, J., Lehmkuhl, O. and Oliva, A. (2014). Advanced CFD&HT Numerical Modeling of Solar Tower Receivers. *Energy Procedia*, 49, pp.50-59.

Daggubati, S. (2014). The Green Aggregates for Sustainable Development in Construction Industry. *Journal of Civil & Environmental Engineering*, 04(05).

Duffie, J. and Beckman, W. (2013). *Solar engineering of thermal processes*. Hoboken: Wiley.

Felix Regin, A., Solanki, S. and Saini, J. (2009). An analysis of a packed bed latent heat thermal energy storage system using PCM capsules: Numerical investigation. *Renewable Energy*, 34(7), pp.1765--1773.

Flamant, G., Gauthier, D., Benoit, H., Sans, J., BoissiÃ¨re, B., Ansart, R. and Hemati, M. (2014). A New Heat Transfer Fluid for Concentrating Solar Systems: Particle Flow in Tubes. *Energy Procedia*, 49, pp.617-626.

Forristall, R. (2003). *Heat Transfer Analysis and Modeling of a Parabolic Trough Solar Receiver Implemented in Engineering Equation Solver*. Springfield: National Renewable Energy Laboratory.

Gauché, P., von Backstròm, T. and Brent, A. (2013). A concentrating solar power value proposition for South Africa. *Journal of Energy in Southern Africa*, 24(1), pp.00--00.

George, R., Wilcox, S. and Anderberg, M. (2008). *National Solar Radiation Database (NSRDB) -10 km Gridded Hourly Solar Database*.

Ghadirijafarbeigloo, S., Zamzamian, A. and Yaghoubi, M. (2014). 3-D Numerical Simulation of Heat Transfer and Turbulent Flow in a Receiver Tube of Solar Parabolic Trough Concentrator with Louvered Twisted-tape Inserts. *Energy Procedia*, 49, pp.373-380.

Hefni, B. (2014). Dynamic Modeling of Concentrated Solar Power Plants with the ThermoSysPro Library (Parabolic Trough Collectors, Fresnel Reflector and Solar-Hybrid). *Energy Procedia*, 49, pp.1127-1137.

Hodge, B. (2010). *Alternative energy systems and applications*. Hoboken, NJ: Wiley.

Hsu, S., Chiang, H. and Yen, C. (2014). Experimental Investigation of the Performance of a Hermetic Screw-Expander Organic Rankine Cycle. *Energies*, 7(9), pp.6172-6185.

Huang, J., Troccoli, A. and Coppin, P. (2014). An analytical comparison of four approaches to modelling the daily variability of solar irradiance using meteorological records. *Renewable Energy*, 72, pp.195-202.

Incropera, F. (2013). *Foundations of heat transfer*. Singapore: Wiley.

Incropera, F. and DeWitt, D. (1981). *Fundamentals of heat transfer*. New York: Wiley.

Johannes, K., Fraisse, G., Achard, G. and Rusaouën, G. (2005). Comparison of solar water tank storage modelling solutions. *Solar Energy*, 79(2), pp.216-218.

Jradi, M., Li, J., Liu, H. and Riffat, S. (2014). Micro-scale ORC-based combined heat and power system using a novel scroll expander. *Int. J. Low-Carbon Tech.*, 9(2), pp.91-99.

Kaczmarczyk, T., Ihnatowicz, E. and Żywica, G. (2015). Desing and construction of the test bench for testing scroll expanders in ORC system. *Mechanik*, (7), pp.561/349-561/356.

Kalogirou, S. (2009). *Solar energy engineering*. Burlington, MA: Elsevier/Academic Press.

Kane, M., Larrain, D., Favrat, D. and Allani, Y. (2003). Small hybrid solar power system. *Energy*, 28(14), pp.1427--1443.

Karaki, W., Li, P., Van Lew, J., Valmiki, M., Chan, C. and Stephens, J. (2011). Experimental investigation of thermal storage processes in a thermocline storage tank. pp.1389--1396.

Katayama, Y. and Tamaura, Y. (2005). Development of new green - fuel production technology by combination of fossil fuel and renewable energy. *Energy*, 30(11), pp.2179-2185.

Kere, A., Goetz, V., Py, X., Olives, R., Sadiki, N. and Mercier, E. (2014). Dynamic Behavior of a Sensible-heat based Thermal Energy Storage. *Energy Procedia*, 49, pp.830-839.

Ketkar, M. and Reddy, G. (2003). MICROSOFT EXCEL-BASED NUMERICAL SOLUTION OF LINEAR, HOMOGENEOUS 1D TRANSIENT PARTIAL DIFFERENTIAL EQUATIONS. In: *Proceedings of the 2003 American Society for Engineering Education Annual Conference & Exposition*. Washington, D. C. 20036-2479: American Society for Engineering Education, pp.8.851.1 -8.851.10.

Krishna Avadhanula, V. and Lin, C. (2014). Empirical Models for a Screw Expander Based on Experimental Data from Organic Rankine Cycle System Testing. *J. Eng. Gas Turbines Power*, 136(6), p.062601.

Kumar, A. and Shukla, S. (2015). A Review on Thermal Energy Storage Unit for Solar Thermal Power Plant Application. *Energy Procedia*, 74, pp.462-469.

Le, V., Feidt, M., Kheiri, A. and Pelloux-Prayer, S. (2014). Performance optimization of low-temperature power generation by supercritical ORCs (organic Rankine cycles) using low GWP (global warming potential) working fluids. *Energy*, 67, pp.513-526.

Lemos, J., Neves-Silva, R. and Igreja, J. (n.d.). *Adaptive control of solar energy collector systems*.

Li, J. (2013). *Structural Optimization and Experimental Investigation of the Organic Rankine Cycle for Solar Thermal Power Generation*. Ph.D. University of Science and Technology of China, Hefei, China.

Li, P., Van Lew, J., Karaki, W., Chan, C., Stephens, J. and O'Brien, J. (n.d.). Transient Heat Transfer and Energy Transport in Packed Bed Thermal Storage Systems.

Liu, B., Chien, K. and Wang, C. (2004). Effect of working fluids on organic Rankine cycle for waste heat recovery. *Energy*, 29(8), pp.1207-1217.

Macedo-Valencia, J., Ramírez-Ávila, J., Acosta, R., Jaramillo, O. and Aguilar, J. (2014). Design, Construction and Evaluation of Parabolic Trough Collector as Demonstrative Prototype. *Energy Procedia*, 57, pp.989-998.

Madhawa Hettiarachchi, H., Golubovic, M., Worek, W. and Ikegami, Y. (2007). Optimum design criteria for an Organic Rankine cycle using low-temperature geothermal heat sources. *Energy*, 32(9), pp.1698-1706.

Maithani, R., Patil, A. and Saini, J. (2013). Investigation of Effect of Stratification on the Thermal Performance of Packed Bed Solar Air Heater. *International Journal of Energy Science (IJES)*, 3(4), p.9.

Manente, G., Toffolo, A., Lazzaretto, A. and Paci, M. (2013). An Organic Rankine Cycle off-design model for the search of the optimal control strategy. *Energy*, 58, pp.97-106.

Marcotte, P. and Manning, K. (2014). Development of an Advanced Large-aperture Parabolic Trough Collector. *Energy Procedia*, 49, pp.145-154.

Mason, A. and Reitze, E. (2014). Establishing Bankability for High Performance Cost Reducing SkyTrough Parabolic Trough Solar Collector. *Energy Procedia*, 49, pp.155-162.

Mather, D., Hollands, K. and Wright, J. (2002). Single- and multi-tank energy storage for solar heating systems: fundamentals. *Solar Energy*, 73(1), pp.3-13.

Mcmahan, A. (2006). *Design & Optimization of Organic Rankine Cycle Solar-Thermal Powerplants*. masters. University of Wisconsin-Madison.

Mendelsohn, M., Lowder, T. and Canavan, B. (2012). *Utility-Scale Concentrating Solar Power and Photovoltaic Projects: A Technology and Market Overview*. [online] NREL. Available at: http://www.nrel.gov/docs/fy12osti/51137.pdf [Accessed 7 Dec. 2014].

Meyer, R. (2013). CSP & Solar Resource Assessment. In: *CSP Today South Africa 2013*. Stellenbosch: University of Stellenbosch, p.28.

Mier-Torrecilla, M., Herrera, E. and Doblaré, M. (2014). Numerical Calculation of Wind Loads over Solar Collectors. *Energy Procedia*, 49, pp.163-173.

Mokhtaria, A., Yaghoubi, M., Kanan, P., Vadiee, A. and Hessamia, R. (2007). *Thermal and optical study of parabolic trough collectors of shiraz solar power plant. In*: *Thermal Engineering: Theory and Applications*. Amman: Engineering School, Shiraz University, Shiraz, Iran, pp.67-70.

Montero, C., Navío, R., Llorente, P., Romero, M. and Martínez, J. (2014). CRS Sales: Abengoa's Molten Salt Pilot Power Tower Plant Celebrates One Year of Uninterrupted Operation. *Energy Procedia*, 49, pp.488-497.

Moran, M., Shapiro, H., Boettner, D. and Bailey, M. (2011). *Principles of engineering thermodynamics*. Hoboken, N.J.: Wiley.

Opitz, F. and Treffinger, P. (2014). Packed bed thermal energy storage model. Generalized approach and experimental validation. *Applied Thermal Engineering*, 73(1), pp.245-252.

Orosz, M. (2012). *ThermoSolar and Photovoltaic Hybridization for Small Scale Distributed Generation: Applications for Powering Rural Health*. Ph.D. Massachusetts Institute of Technology.

Orosz, M., Mueller, A., Dechesne, B. and Hemond, H. (2013). Geometric Design of Scroll Expanders Optimized for Small Organic Rankine Cycles. *Journal of Engineering for Gas Turbines and Power*, 135(4), p.042303.

Oudkerk, J., Quoilin, S., Declaye, S., Guillaume, L., Winandy, E. and Lemort, V. (2013). Evaluation of the Energy Performance of an Organic Rankine Cycle-Based Micro Combined Heat and Power System Involving a Hermetic Scroll Expander. *J. Eng. Gas Turbines Power*, 135(4), p.042306.

Pérez-Burgos, A., Bilbao, J., de Miguel, A. and Román, R. (2014). Analysis of Solar Direct Irradiance in Spain. *Energy Procedia*, 57, pp.1070-1076.

Peterson, C. and Davidson, T. (1977). *Design and analysis of a 1 kw Rankine power cycle, employing a multi-vane expander, for use with a low temperature solar collector.* Undergraduate. Massachusetts Institute of Technology.

Piedehierro, A., Antón, M., Cazorla, A., Alados-Arboledas, L. and Olmo, F. (2014). Evaluation of enhancement events of total solar irradiance during cloudy conditions at Granada (Southeastern Spain). *Atmospheric Research*, 135-136, pp.1-7.

Pimm, A., Garvey, S. and Kantharaj, B. (2015). Economic analysis of a hybrid energy storage system based on liquid air and compressed air. *Journal of Energy Storage*, 4, pp.24-35.

Prabhu, E. (2006). Solar trough organic rankine electricity system (stores) stage 1: Power plant optimisation and economics. *National Renewable Energy Laboratory (US), Technical Report No. NREL/SR-550-39433*.

Prinn, R., Reilly, J., Sarofim, M., Wang, C. and Felzer, B. (2005). *Effects of Air Pollution Control on Climate*. Report No. 118. Cambridge.

Quoilin, S. (2007). *Experimental Study and Modelling of a Low-Temperature Rankine Cycle for Small Scale Cogeneration*. Degree. UNIVERSITY OF LIEGE.

Quoilin, S., Aumann, R., Grill, A., Schuster, A., Lemort, V. and Spliethoff, H. (2011). Dynamic modeling and optimal control strategy of waste heat recovery Organic Rankine Cycles. *Applied Energy*, 88(6), pp.2183-2190.

Rasul, M. (2013). *Thermal Power Plants - Advanced Applications*. Rijeka: InTech, pp.3-19.

Regin, A., Solanki, S. and Saini, J. (2008). Heat transfer characteristics of thermal energy storage system using PCM capsules: A review. *Renewable and Sustainable Energy Reviews*, 12(9), pp.2438-2458.

Resch, B., Sagl, G., Törnros, T., Bachmaier, A., Eggers, J., Herkel, S., Narmsara, S. and Gűndra, H. (2014). GIS-Based Planning and Modelling for

Renewable Energy: Challenges and Future Research Avenues.ISPRS International Journal of Geo-Information, 3(2), pp.662-692.

Saleh, B., Koglbauer, G., Wendland, M. And Fischer, J. (2007). Working fluids for low-temperature organic Rankine cycles. *Energy*, 32(7), pp.1210-1221.

Schuster, A., Karellas, S. and Aumann, R. (2010). Efficiency optimization potential in supercritical Organic Rankine Cycles. *Energy*, 35(2), pp.1033-1039.

Simulation toolbox for the Design and Development of Thermodynamic Systems in MATLAB®/Simulink®. (2011). EUtech Scientific Engineering GmbH.

Singh, R., Saini, R. and Saini, J. (2009). Models for Predicting Thermal Performance of Packed Bed Energy Storage System for Solar Air Heaters- A Review. *Open Fuels & Energy Science Journal*, 2, pp.47--53.

Situmbeko, S. and Inambao, F. (2013). System and component modelling of a low temperature solar thermal energy conversion cycle. *Journal of Energy in Southern Africa*, Volume 24(Number 4), p.12.

Soenke Holger, T. (2011). *Modeling and Calculation of Heat Transfer Relationships for Concentrated Solar Power Receivers*. M.Sc. University of Wisconsin - Madison.

Steinmann, W., Eck, M. and Laing, D. (2005). Solarthermal parabolic trough power plants with integrated storage capacity. *International journal of energy technology and policy*, 3(1), pp.123--336.

stginternational, (2014). *Solar ORC: How it works*. [image] Available at: http://www.stginternational.org/how-it-works.html [Accessed 23 Oct. 2014].

Stine, W. and Geyer, M. (2001). *PowerFromTheSun.net*. [online] Powerfromthesun.net. Available at: http://www.powerfromthesun.net [Accessed 24 Oct. 2014].

Strasser, M. and Selvam, R. (2014). A cost and performance comparison of packed bed and structured thermocline thermal energy storage systems. *Solar Energy*, 108, pp.390-402.

Tian, Y. and Zhao, C. (2013). A review of solar collectors and thermal energy storage in solar thermal applications. *Applied Energy*, 104, pp.538-553.

The Energy Blog. (2008). *The Energy Blog*. [online] Available at: http://Thefraserdomain.typepad.com [Accessed 8 Aug. 2012].

Tukiainen, M. (2014). *Bloemfontein, South Africa - Sunrise, sunset, dawn and dusk times for the whole year - Gaisma*. [online] Gaisma.com. Available at: http://www.gaisma.com/en/location/bloemfontein.html [Accessed 26 Dec. 2014].

Tyner, C. and Wasyluk, D. (2014). eSolar's Modular, Scalable Molten Salt Power Tower Reference Plant Design. *Energy Procedia*, 49, pp.1563-1572.

Voorthuysen, E. and Roes, R. (2014). Blue Sky Cooling for Parabolic Trough Plants. *Energy Procedia*, 49, pp.71-79.

Webbook.nist.gov. (2013). *NIST Chemistry WebBook*. [online] Available at: http://webbook.nist.gov/chemistry/ [Accessed 15 Nov. 2013].

Wei, J., Kawaguchi, Y., Hirano, S. and Takeuchi, H. (2005). Study on a PCM heat storage system for rapid heat supply. *Applied Thermal Engineering*, 25(17-18), pp.2903-2920.

Weathersa.co.za. (2016). *Forecast*. [online] Available at: http://www.weathersa.co.za/ [Accessed 28 Apr. 2016].

Winter, C., Sizmann, R. and Vant-Hull, L. (2012). *Solar Power Plants: Fundamentals, Technology, Systems, Economics* . 1st ed. Berlin: Springer-Verlag.

Wolpert, J. and Riffat, S. (1996). Solar-powered Rankine system for domestic applications. *Applied Thermal Engineering*, 16(4), pp.281--289.

Yang, M. and Yeh, R. (2015). Thermo-economic optimization of an organic Rankine cycle system for large marine diesel engine waste heat recovery. *Energy*, 82, pp.256-268.

Zavattoni, S., Gaetano, A., Barbato, M., Ambrosetti, G., Good, P., Malnati, F. and Pedretti, A. (2014). CFD Analysis of a Receiving Cavity Suitable for a Novel CSP Parabolic Trough Receiver. *Energy Procedia*, 49, pp.579-588.

Zhang, T., Stackhouse, P., Chandler, W. and Westberg, D. (2014). Application of a global-to-beam irradiance model to the NASA GEWEX SRB dataset: An extension of the NASA Surface meteorology and Solar Energy datasets. *Solar Energy*, 110, pp.117-131.

ZHANG, Y. (2015). Performance Study on Single-screw Expander in Organic Rankine Cycle System. *Journal of Mechanical Engineering*, 51(16), p.156.

ADDENDUM A

FEW LAYOUT BLOCKS AND PROPERTIES OF MATLAB SIMULINK ® MODEL BLOCKS

A.1 MAIN SYSTEM LAYOUT OF THE STORC POWER PLANT

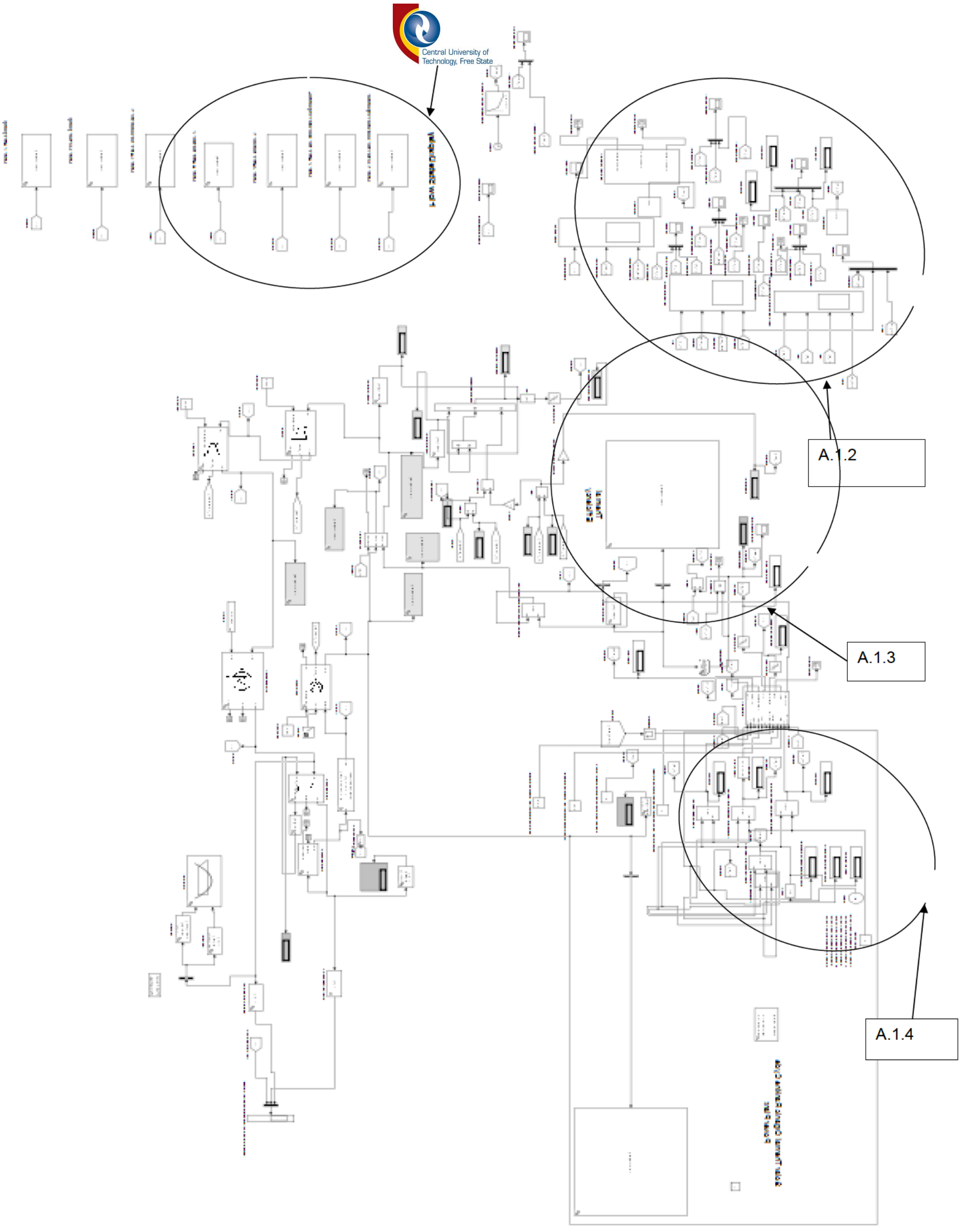

Figure A 1 Main system layout of the STORC power plant

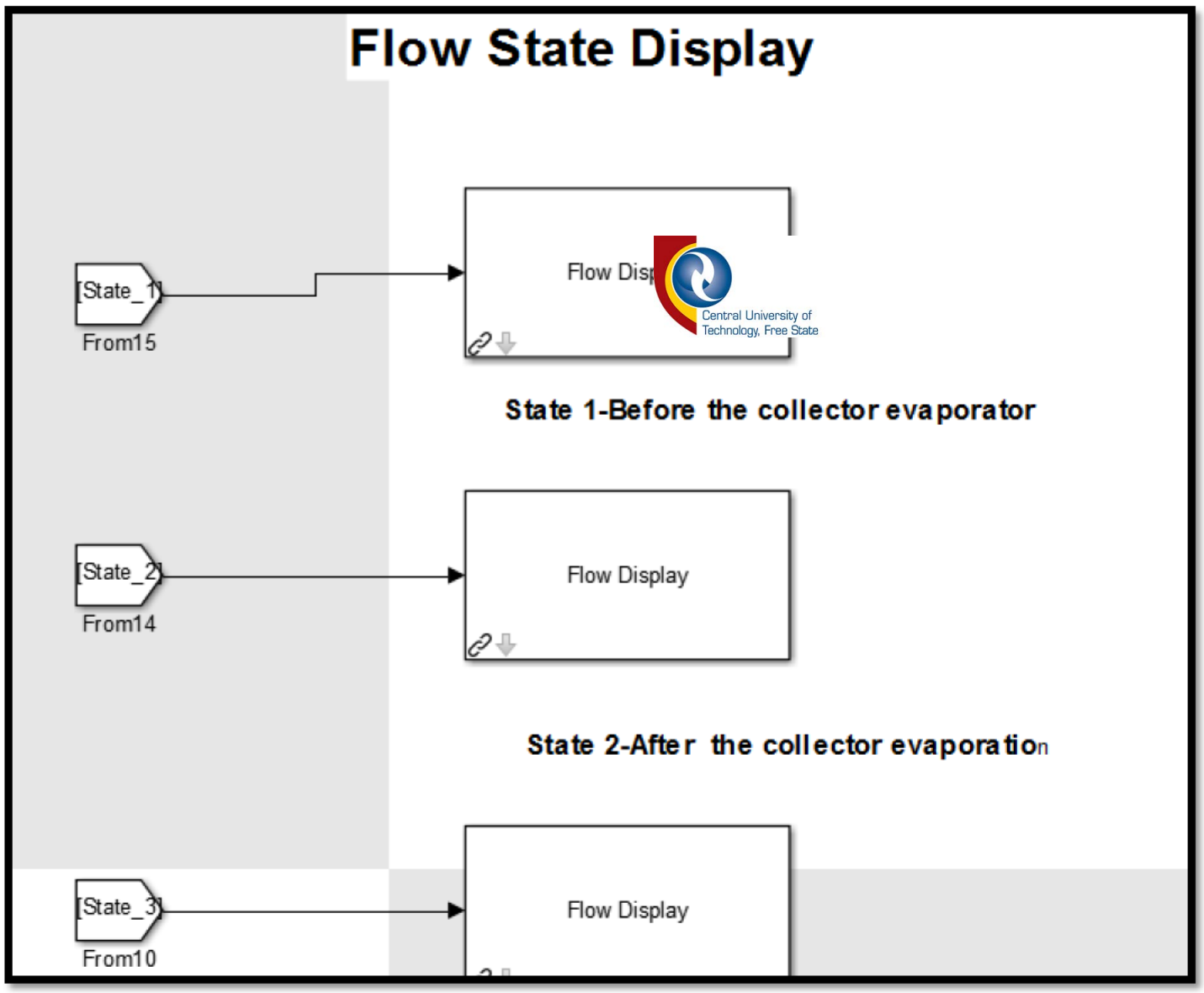

Figure A.1.1. Zoomed part (from figure A 1) of the layout showing the flow state display.

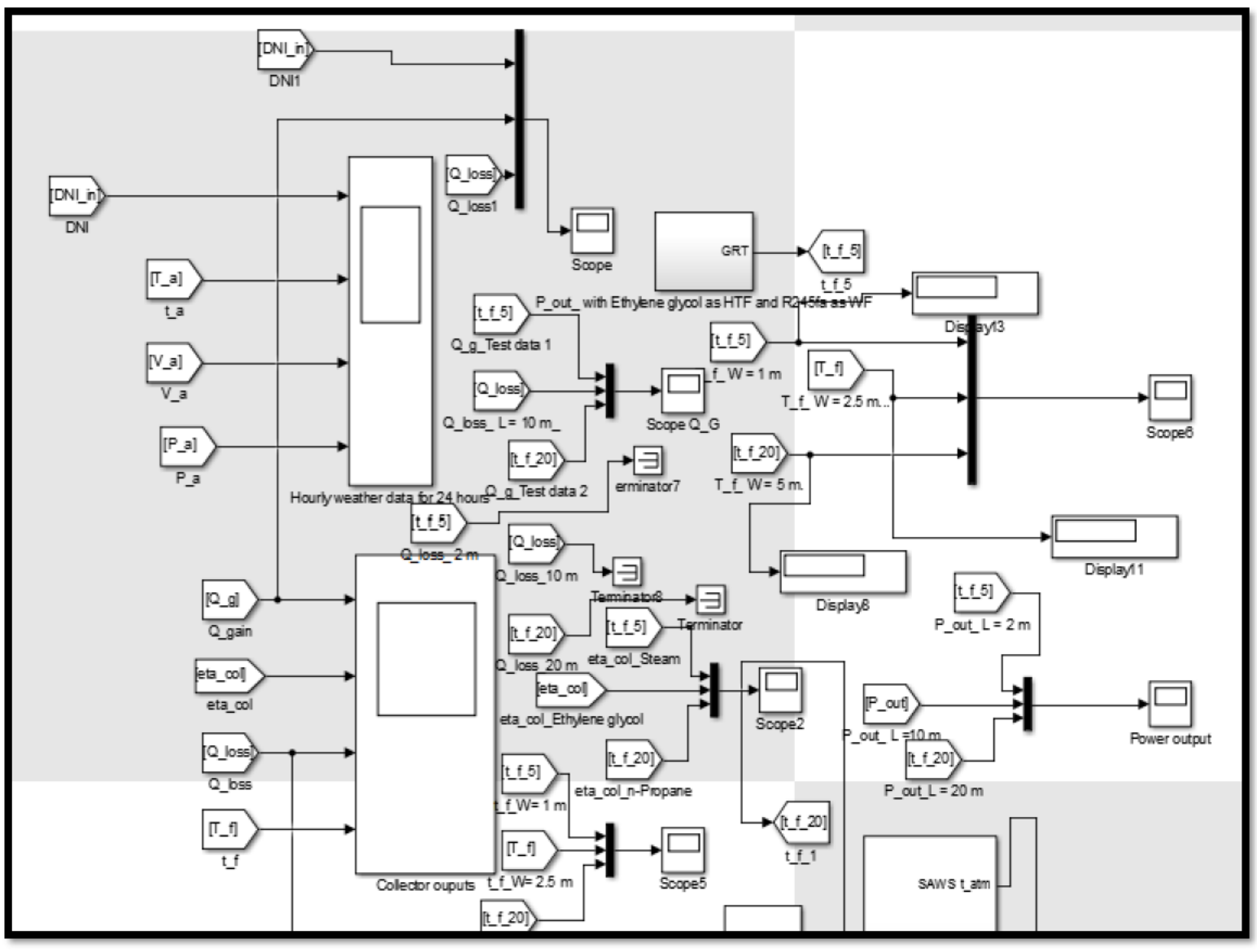

Figure A.1.2. Zoomed part (from figure A 1) of the layout showing the solar resources area.

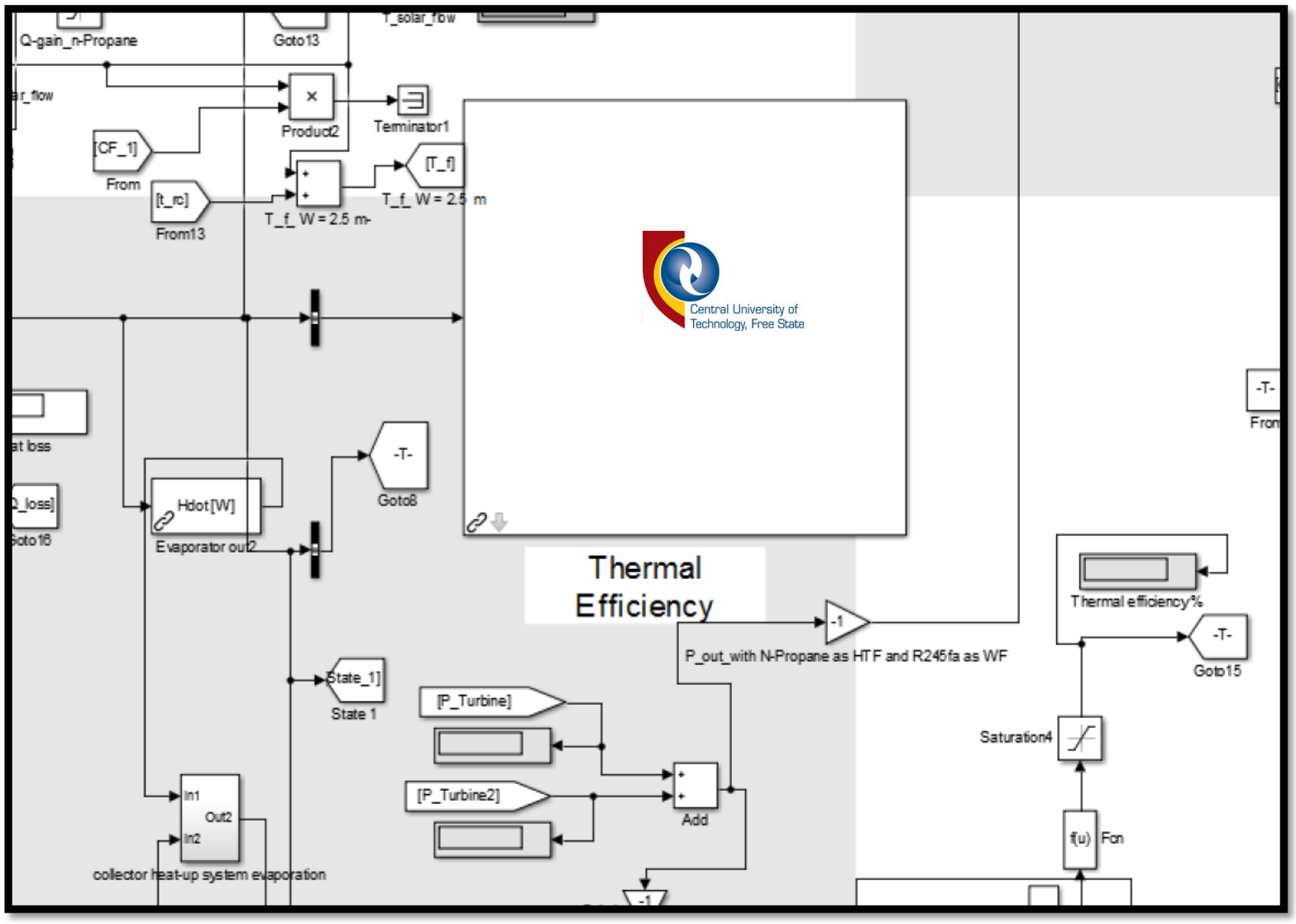

Figure A.1.3. Zoomed part (from figure A 1) of the layout showing the outputs.

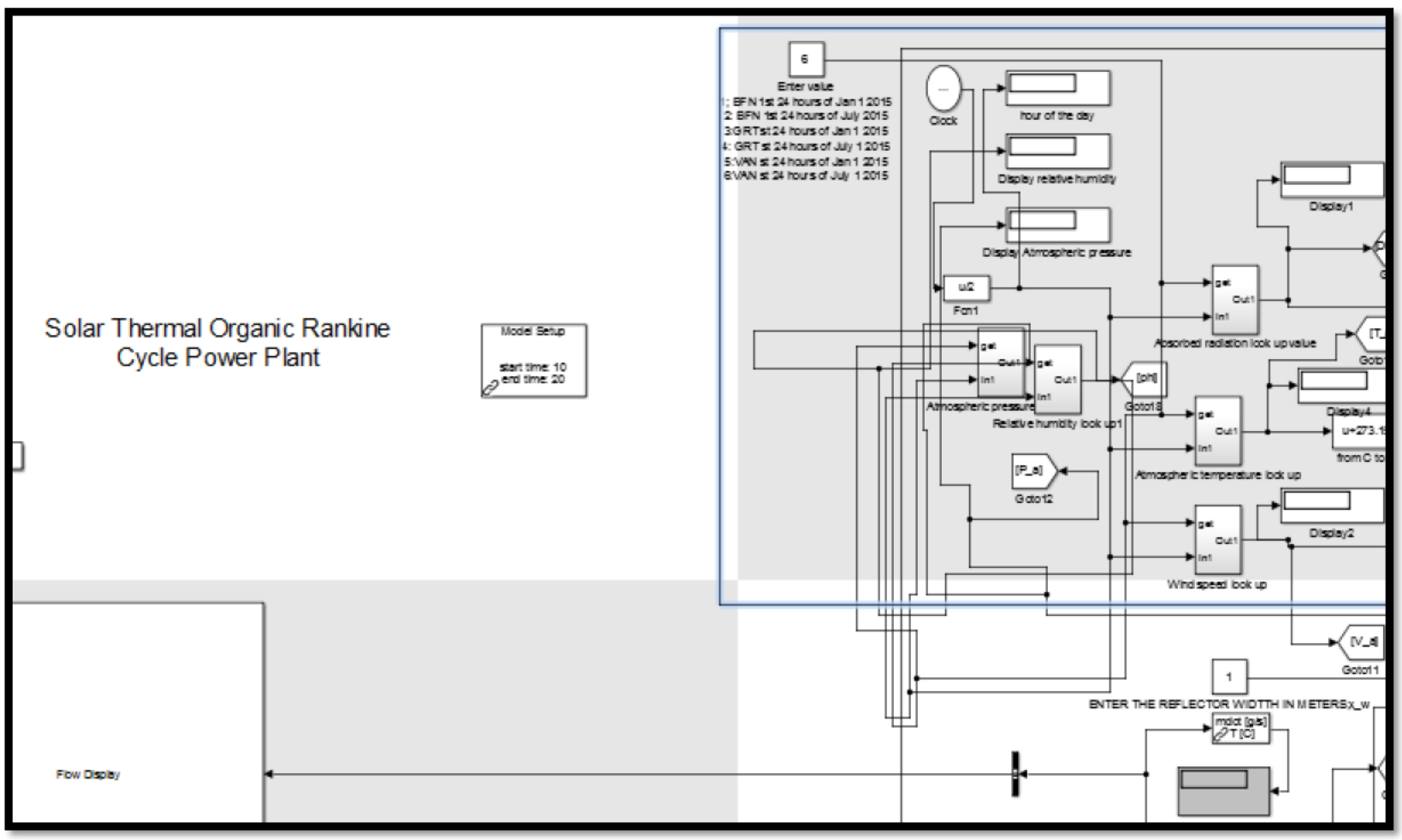

Figure A.1.4. Zoomed part ((from figure A 1) of the layout showing the input area.

A 2 INPUT BLOCK FOR THE DATA REQUIRED

A 2 Input block for the data required

Name	Port	Defined In Blk
get	1	Enter value 1; BFN 1st 24 hours of Jan 1 2015 2: BFN 1st 24 hours of July 2015 3:GRT st 24 hours of Jan 1 2015 4: GRT st 24 hours of July 1 2015 5:VAN st 24 hours of Jan 1 2015 6:VAN st 24 hours of July 1 2015
In1	2	Fcn1

A 1 COLLECTOR MODEL SUBSYSTEM 1

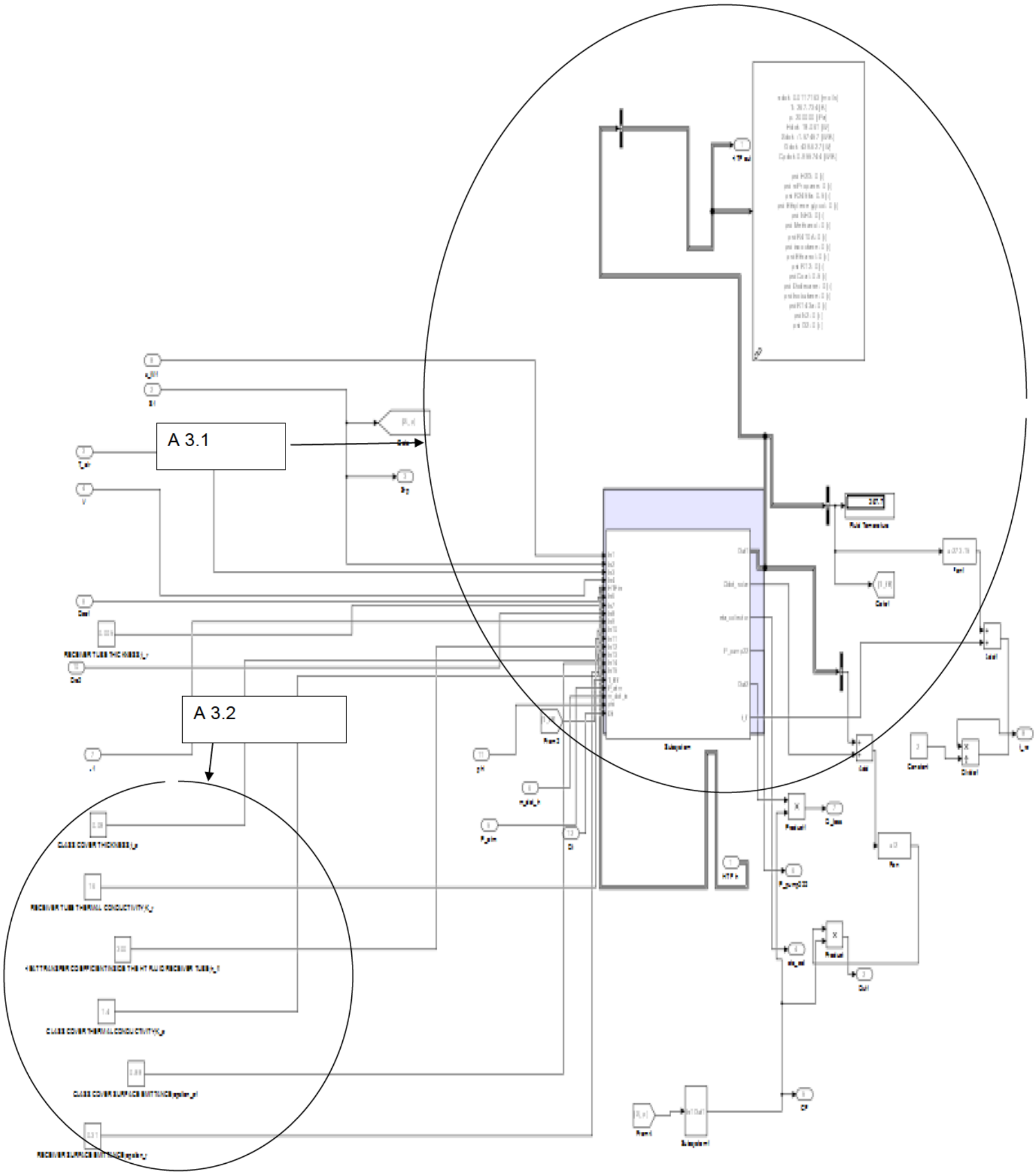

Figure A 3 Collector model subsystem 1

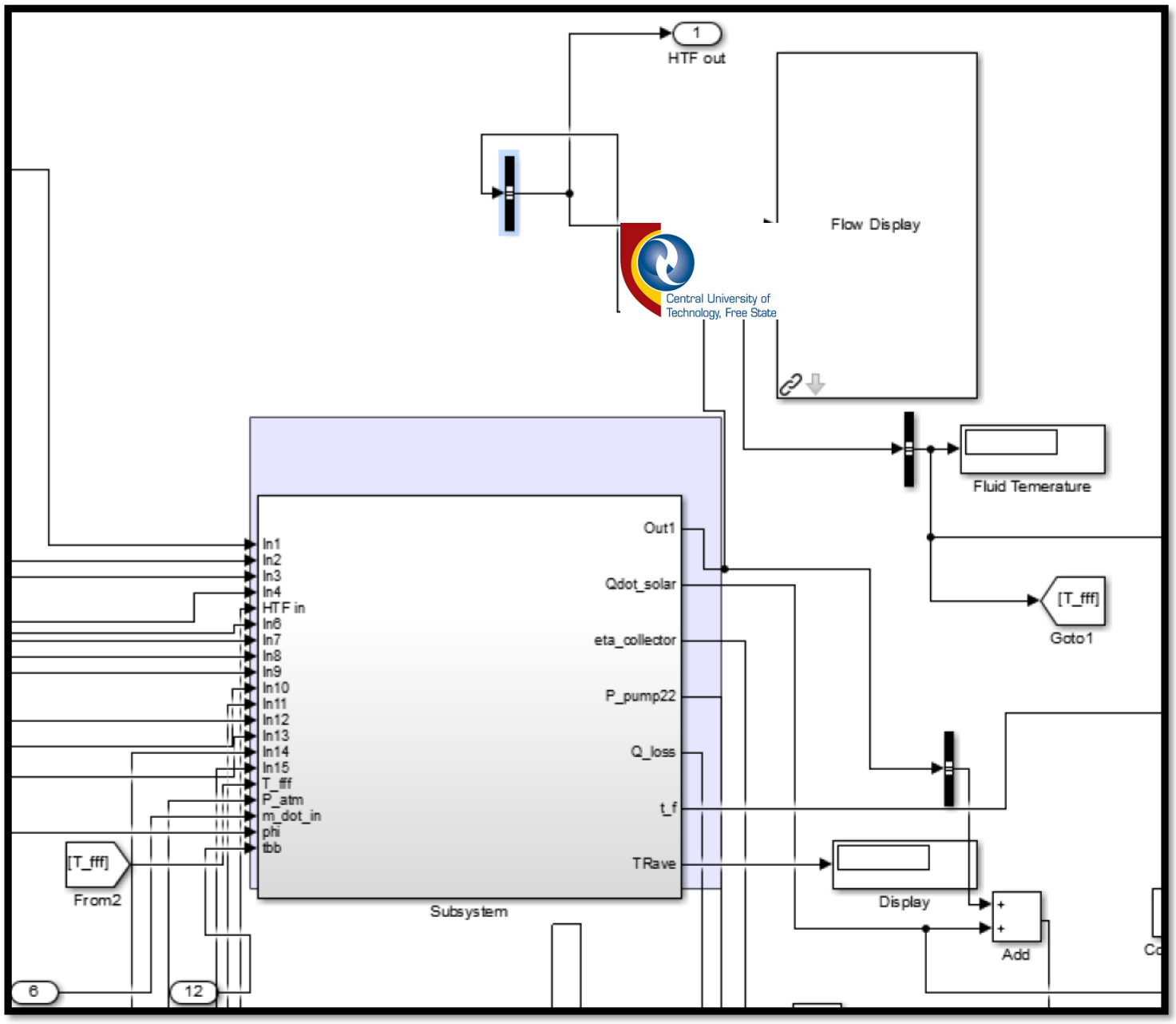

Figure A 3.1 Zoomed view (from Figure A 3) to show some parameter blocks of the collector model

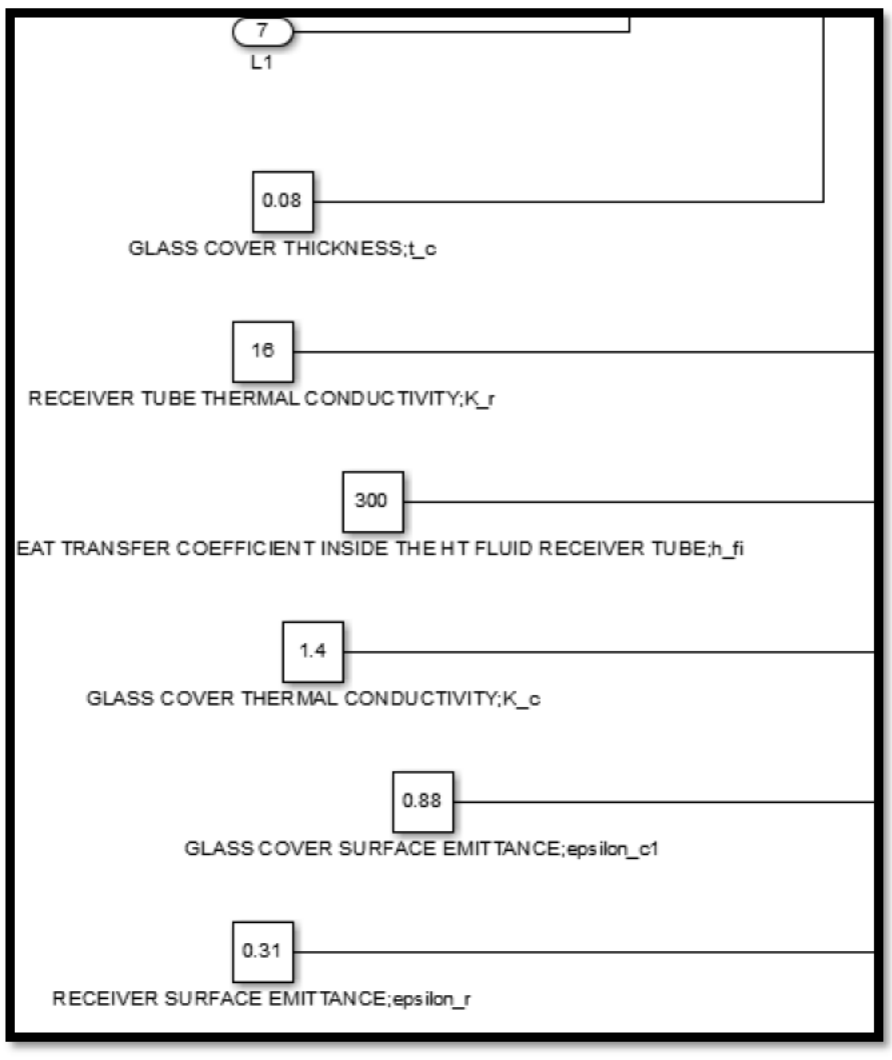

Figure A 3.2 Zoomed view (from Figure A 3) to show some input blocks of the collector model

A 4 INPUT PARAMETERS CONSTANT BLOCK PROPERTIES

A 4 Input parameters constant block properties

Name	Value	Out Data Type Str	Lock Scale	Sample Time	Frame Period
Constant		Inherit: Inherit from 'Constant value'	off	inf	inf
GLASS COVER SURFACE EMITTANCE;epsilon_c1	0.88	Inherit: Inherit from 'Constant value'	off	inf	inf
GLASS COVER THERMAL CONDUCTIVITY;K_c	1.4	Inherit: Inherit from 'Constant value'	off	inf	inf
GLASS COVER THICKNESS;t_c	0.08	Inherit: Inherit from 'Constant value'	off	inf	inf
HEAT TRANSFER COEFFICIENT INSIDE THE HT FLUID RECEIVER TUBE;h_fi	300	Inherit: Inherit from 'Constant value'	off	inf	inf
RECEIVER SURFACE EMITTANCE;epsilon_r	0.31	Inherit: Inherit from 'Constant value'	off	inf	inf
RECEIVER TUBE THERMAL CONDUCTIVITY;K_r	16	Inherit: Inherit from 'Constant value'	off	inf	inf
RECEIVER TUBE THICKNESS;t_r	0.005	Inherit: Inherit from 'Constant value'	off	inf	inf

A 5 COLLECTOR MODEL SUBSYSTEM 2

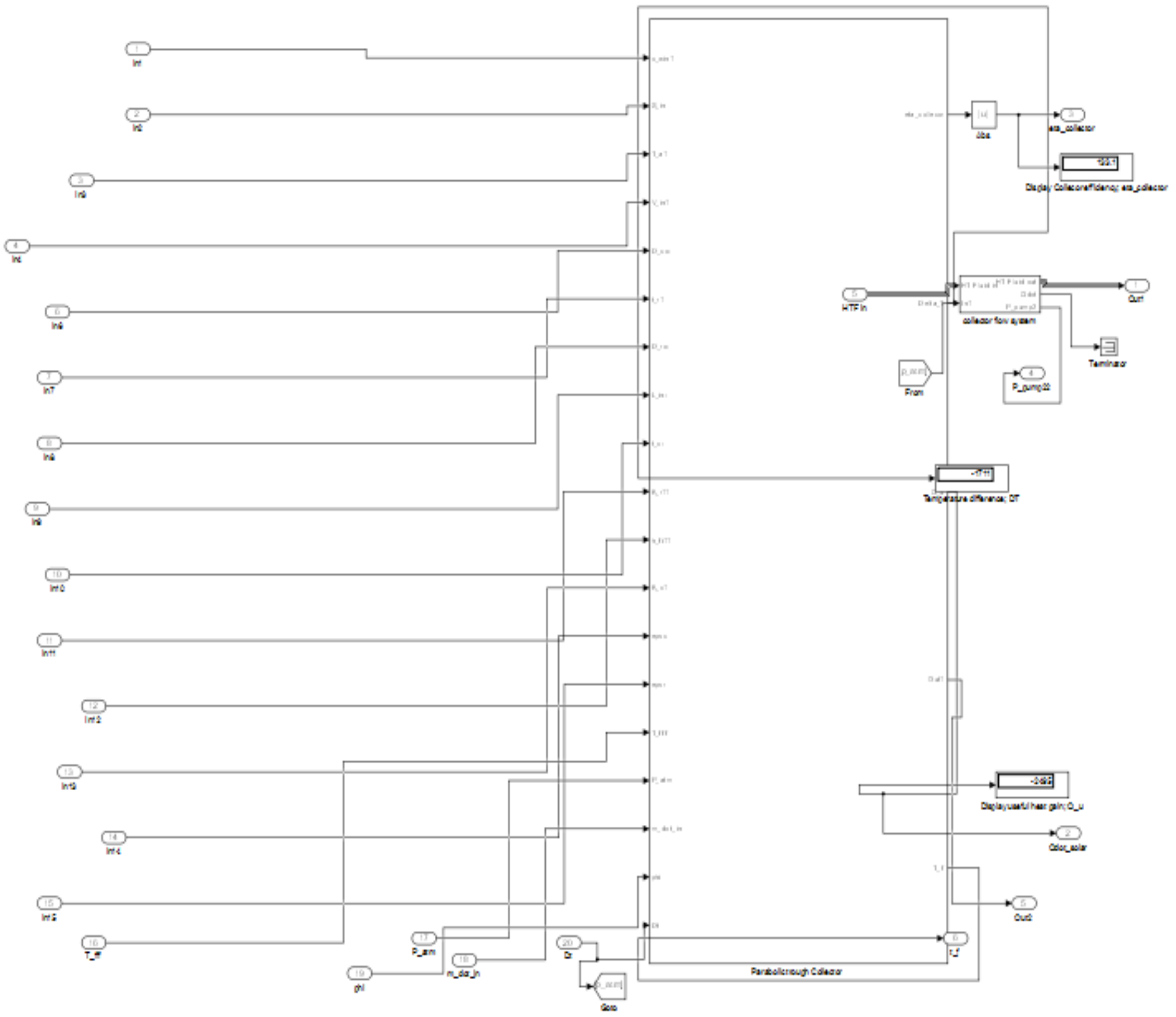

Figure A 5 collector model subsystem 2

A 6 DISPLAY COLLECTOR OUTPUT BLOCK PROPERTIES

A 6 Display collector output block properties

Name	Format	Decimation	Floating
Display Collecor efficiency; eta_collector	short	1	off
Display useful heat gain; Q_u	short	1	off
Temperature difference; DT	short	1	off

A 7 DISPLAY BLOCK PROPERTIES

A 7 Display block properties

Name	Format	Decimation	Floating
Average temperature drop in C	short	1	off
D_co	short	1	off
Display	short	1	off
Display average receiver temperature of fluid out.	short	1	off
Display Collecor efficiency; eta_collector	short	1	off
Display glas cover temperature	short	1	off
Display glas cover temperature1	short	1	off
Display glas cover temperature2	short	1	off
Display heat loss	short	1	off
Display heat loss1	short	1	off
Display heat loss222	short	1	off
Display heat loss2222	short	1	off
Display heat loss333	short	1	off
Display heat loss5	short	1	off
Display Nisselts #	short	1	off
Display Q_lossn2	short	1	off
Display Temperature of fluid out; T_fexit	short	1	off
Display U_L	short	1	off
Display useful heat gain; Q_u	short	1	off
Display wind heat tranfer coefficient;h_w	short	1	off
Display wind heat tranfer coefficient;h_w1	short	1	off
Display1	short	1	off
Display2	short	1	off
Display3	short	1	off
Display5	short	1	off
DQloss	short	1	off
F'	short	1	off
F_R	short	1	off
Inside cover Temperature	short	1	off
Inside cover Temperature1	short	1	off
Inside cover Temperature2	short	1	off
Inside cover Temperature3	short	1	off
Inside cover Temperature4	short	1	off
Inside cover Temperature5	short	1	off
Receiver area	short	1	off
Reynolds	short	1	off

A 8 FUNCTION BLOCK PROPERTIES USED FOR THE COLLECTOR MODEL

A 8 Function block properties used for the collector model

Name	Expr
Fcn	0.4+0.54*u^0.52
Fcn1	u^4
Fcn10	log(1/u)
Fcn11	u*3.142
Fcn12	u*2
Fcn13	1/u
Fcn14	u^4

Name	Expr
Fcn15	u*2
Fcn16	u^4
Fcn17	1/u
Fcn18	(1-u)/u
Fcn19	u^4
Fcn2	0.3*u^0.6
Fcn20	u^4
Fcn21	u^4
Fcn22	u^4
Fcn23	1/u
Fcn24	(1-u)/u
Fcn25	u-273.15
Fcn3	u^4
Fcn4	u^4
Fcn5	u^4
Fcn6	u^4
Fcn7	u^4
Fcn8	1/u
Fcn9	(1-u)/u
heat capacity factor per area loss; F"	u*(1-exp(-1/u))
heat capacity factor per area loss; F"1	u/2
T in K	u*273
T_ave	u/2

A 9 COLLECTOR FLUIDS THERMOPHYSICAL INPUT BLOCKS

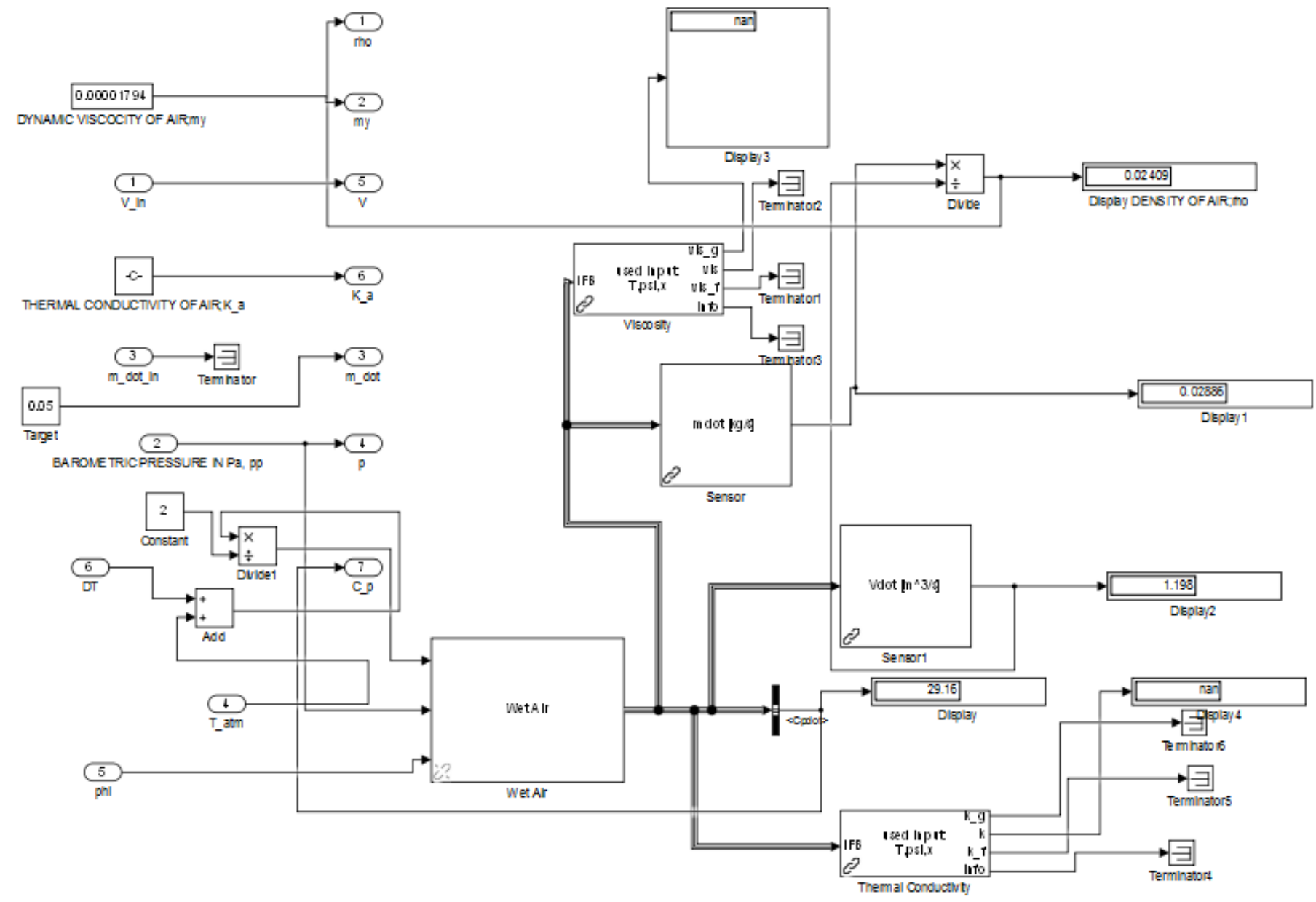

Figure A 9 Collector fluids thermophysical input blocks

A 10 COLLECTOR FLOW SYSTEM

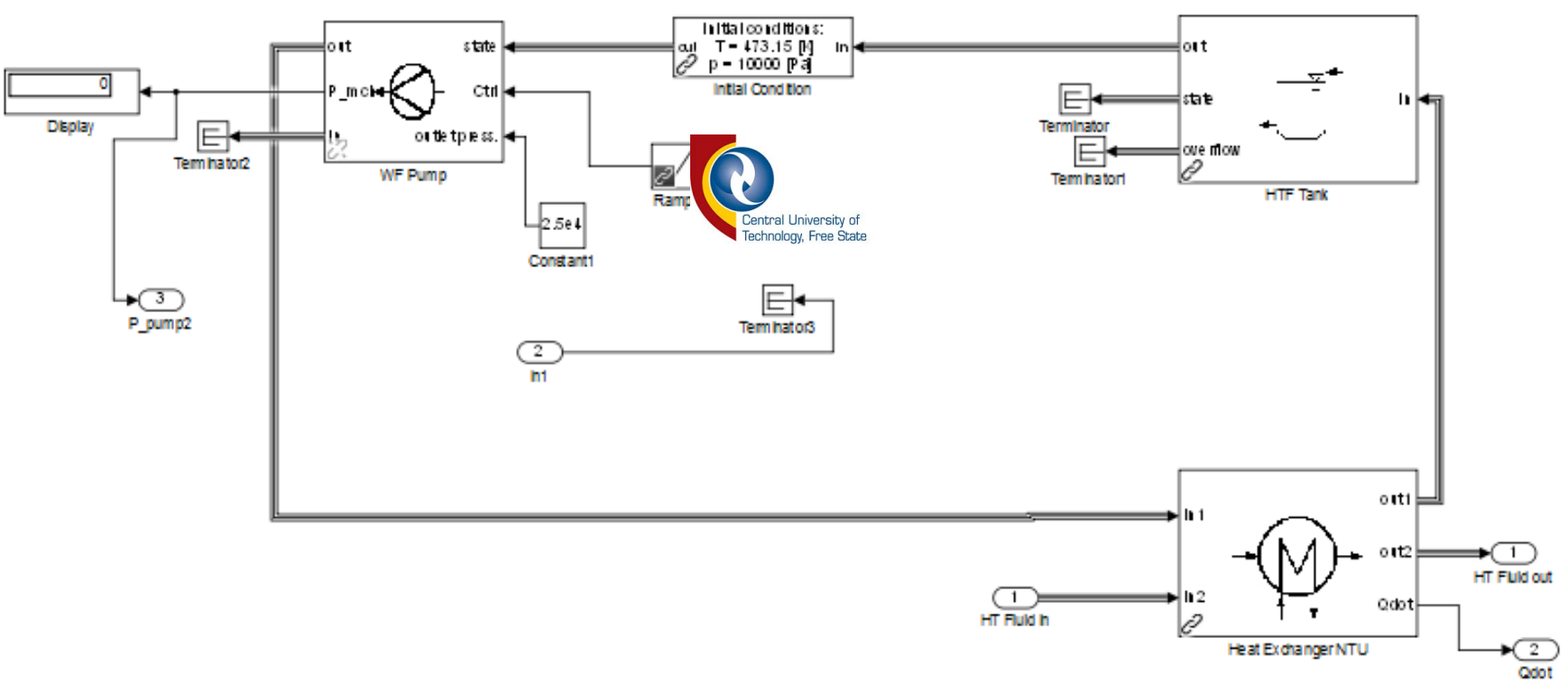

Figure A 10 Collector flow system

A 11 EVAPORATOR SYSTEM

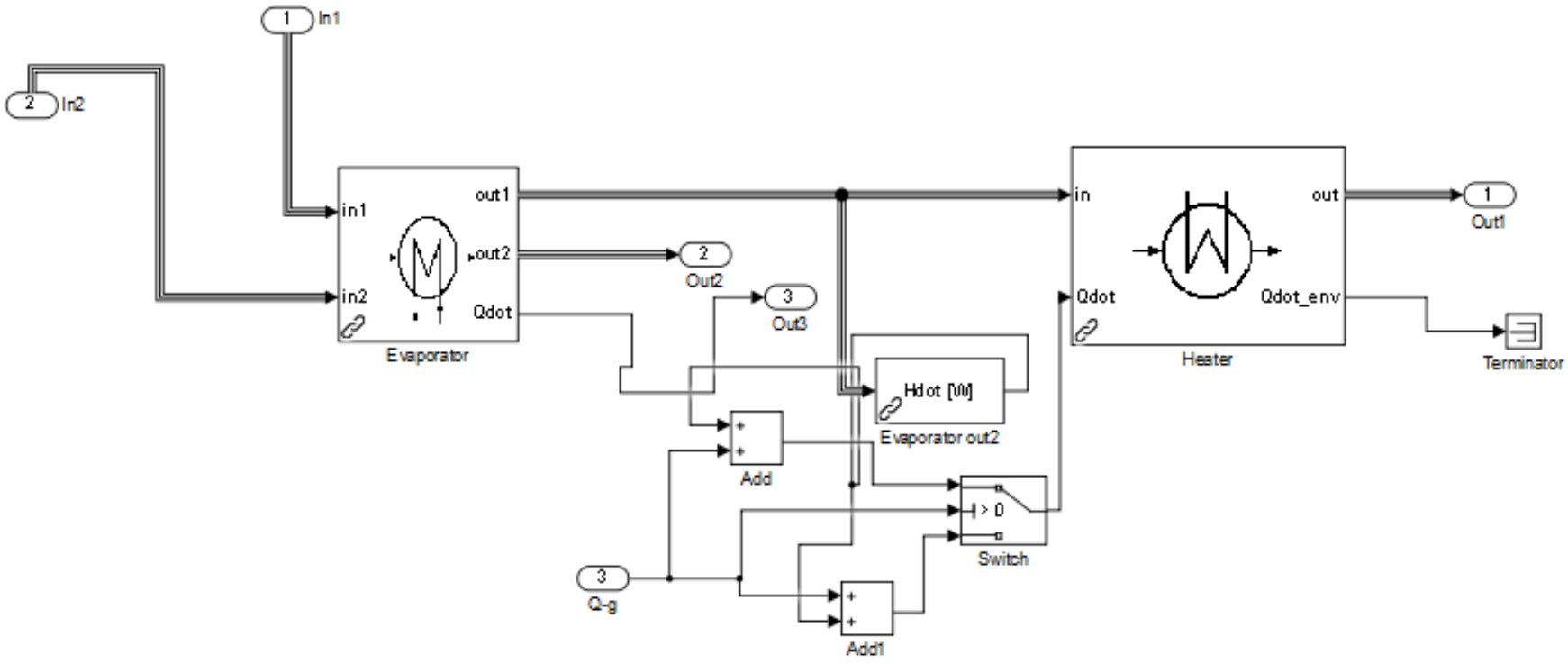

Figure A 11 Evaporator system

A 12 COLLECTOR SYSTEM THERMAL MASS

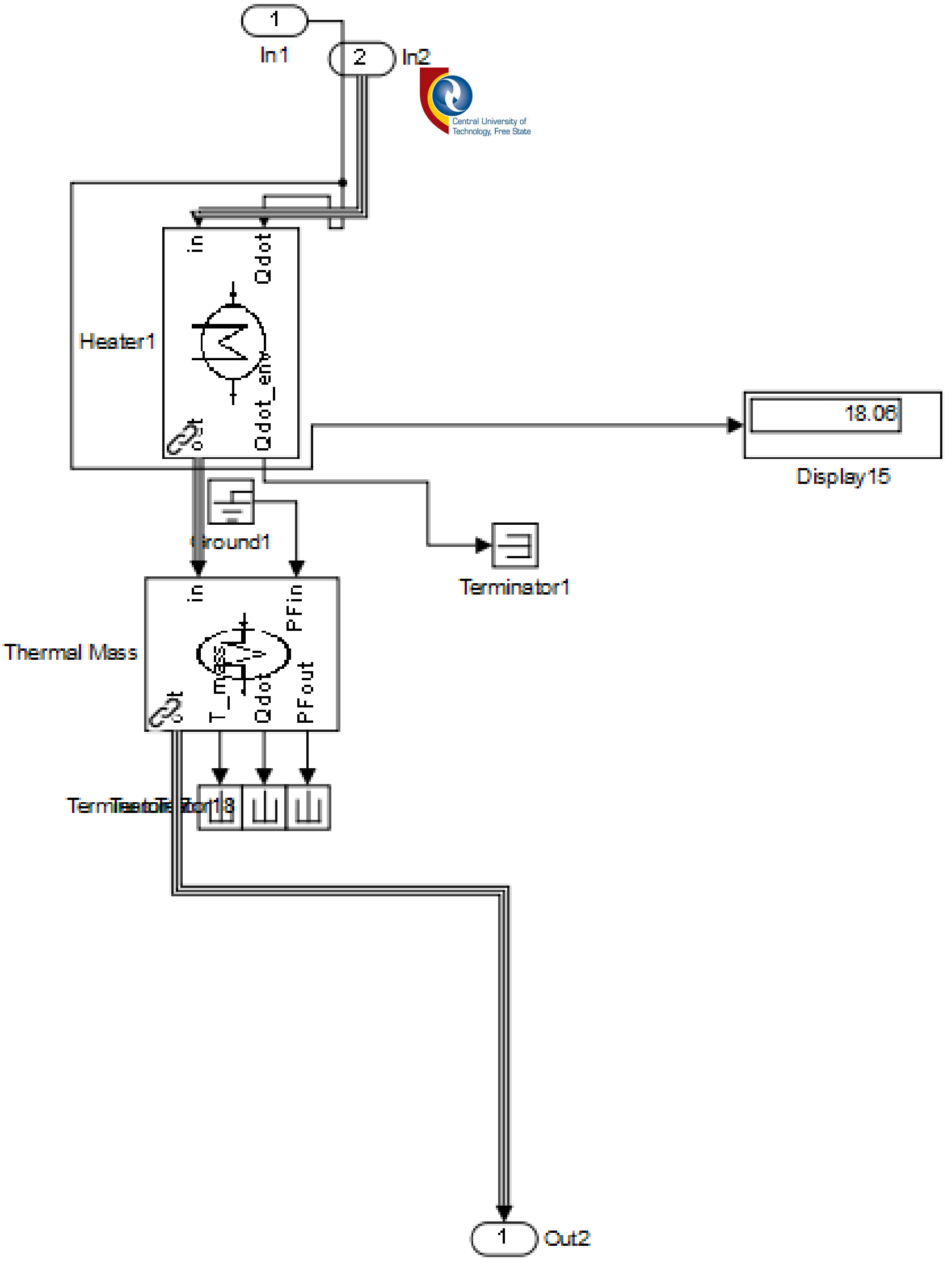

Figure A 12 collector system thermal mass

ADDENDUM B

SELECTED STATISTICS OF PLOTS IN THE RESULT ARE PRESENTED BELOW

B 1 FLUID EXIT TEMPERATURE AT DIFFERENT COLLECTOR LENGTHS FOR BFN ON JANUARY 1

Table B 1 Fluid exit temperature at different collector lengths for BFN on January 1

	5 m		10 m		20 m	
statistics	t (C)		t (C)		t (C)	
	Value	Time	Value	Time	Value	Time
Maximum	138.254	18	138.226	18	138.393	18
Minimum	113.061	0	113.063	0	113.049	0
Peak to peak						
Mean	124.96		124.186		124.245	
Median	123.236		123.221		123.274	
Root Mean Square	124.525		124.514		124.579	

B 2 COLLECTOR EFFICIENCY WITH DIFFERENT HTF FOR BFN ON JANUARY 1 (ASSUME 100% OPTICAL EFFICIENCY)

Table B 2 Collector efficiency with different HTF for BFN on January 1 (assume 100% optical efficiency)

	Steam		E-glycol		n-propane	
statistics	η_{col} (%)		η_{col} (%)		η_{col} (%)	
	Value	Time	Value	Time	Value	Time
Maximum	88.490	18	55.83	18	88.49	18
Minimum	0.000	0	0.000	0	0.000	0
Peak to peak	88.49		55.83		88.49	
Mean	47.85		26.59		47.85	
Median	76.05		33.87		76.05	
Root Mean Square	63.18		35.85		63.18	

B 3 HEAT GAIN AT DIFFERENT COLLECTOR LENGTHS FOR BFN ON JANUARY 1

Table B 3 Heat gain at different collector lengths for BFN on January 1

	2 m		10 m		20 m	
statistics	Q_g [W]		Q_g [W]		Q_g [W]	
	Value	Time	Value	Time	Value	Time
Maximum	3 820	18	19 100	18	38 200	18
Minimum	0	0	0	0	0	0
Peak to peak	3 820		19 100		38 200	
Mean	1 485		7 420		14 850	
Median	1 234		6 170		12 340	
Root Mean Square	2 092		10 045		20 910	

B 4 HEAT GAIN AT DIFFERENT COLLECTOR APERTURE WIDTHS FOR BFN ON JANUARY 1

Table B 4 Heat gain at different collector aperture widths for BFN on January 1

	1 m		2.5 m		5 m	
statistics	Q_g [W]		Q_g [W]		Q_g [W]	
	Value	Time	Value	Time	Value	Time
Maximum	6 234	18	19 100	18	40 540	18
Minimum	0	0	0	0	0	0
Peak to peak	6 234		19 100		40 540	
Mean	2 245		7 427		16 110	
Median	1 351		6 170		14 200	
Root Mean Square	3 263		10 045		22 460	

B 5 HEAT GAIN AT DIFFERENT LOCATIONS ON JAN1, 2016

Table B 5 Heat gain at different locations on January 1, 2016

	GRT		BFN		VAN	
statistics	Q_g [W]		Q_g [W]		Q_g [W]	
	Value	Time	Value	Time	Value	Time
Maximum	23 510	13	19 100	18	21 980	18
Minimum	0	0	0	0	0	0
Peak to peak	23 510		19 100		21 980	
Mean	9 779		7 427		5 777	
Root Mean Square	14 400		10 045		10 420	

B 6 HEAT GAIN WITH DIFFERENT HTF FOR BFN ON JAN1

Table B 6 Heat gain with different HTF for BFN on January 1

	Steam		E-glycol		n-propane	
statistics	Q_g [W]		Q_g [W]		Q_g [W]	
	Value	Time	Value	Time	Value	Time
Maximum	19 100	18	19 100	18	19 100	18
Minimum	0.000	0	0.000	0	0.000	0
Peak to peak	19 100		19 100		19100	
Mean	7 427		7 427		7 427	
Median	6 170		6 170		6 170	
Root Mean Square	10 045		10 045		10 045	

B 7 HEAT LOSS AT DIFFERENT COLLECTOR LENGTHS FOR BFN ON JANUARY 1

Table B 7 Heat loss at different collector lengths for BFN on January 1

	2 m		10 m		20 m	
statistics	Q_loss [W]		Q_loss [W]		Q_loss [W]	
	Value	Time	Value	Time	Value	Time
Maximum	321.200	12	1606.000	12	3212.000	12
Minimum	321.200	3	1606.000	3	3212.000	3
Peak to peak	0.008		0.009		0.008	
Mean	321.200		1606.000		3212.000	
Median	321.200		1606.000		3212.000	
Root Mean Square	321.200		1606.000		3212.000	